AD-A103 674 MODELING AND MEASUREMENT OF TURBULENT SWIRLING FLOWS THROUGH ABRUPT EXPAN..(U) ARIZONA STATE UNIV TEMPE DEPT OF MECHANICAL AND AEROSPACE ENG.. G P NEITZEL ET AL. 1/2

UNCLASSIFIED MAR 87 ASU-TR-ERC-R-86104 N00014-81-K-0420 F/G 20/4 NL

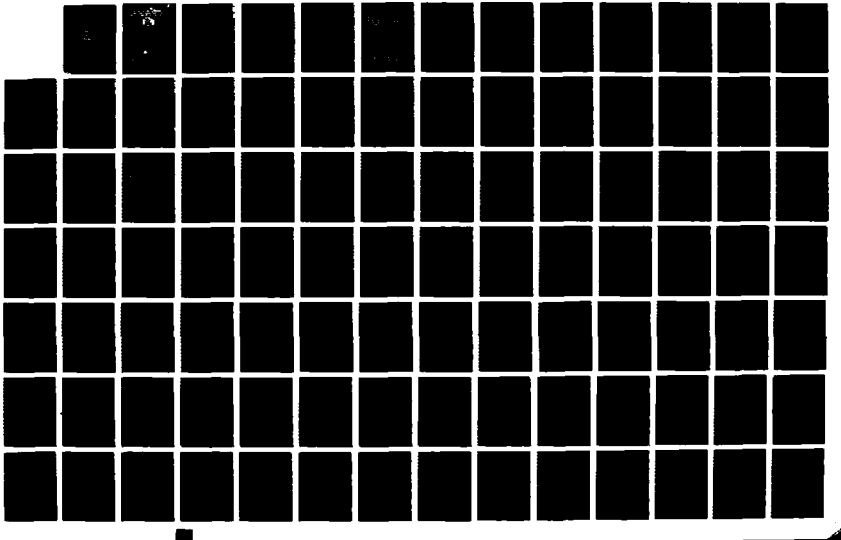

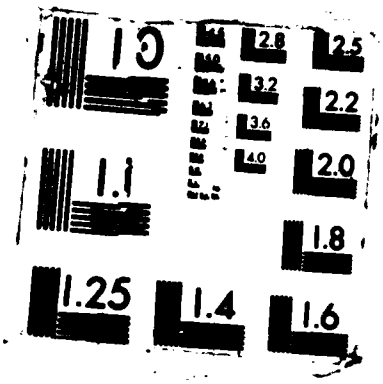
1.0
2.8
2.5
3.2
2.2
3.6
4.0
1.1
2.0
1.8
1.25
1.4
1.6

MODELING AND MEASUREMENT OF TURBULENT SWIRLING FLOWS THROUGH ABRUPT EXPANSIONS

BY
G. P. NEITZEL AND D. E. METZGER

TECHNICAL REPORT ERC-RP86104

PREPARED FOR
DEPARTMENT OF THE NAVY, OFFICE OF NAVAL RESEARCH
CONTRACT N00014-81-K-0428

MECHANICAL AND AEROSPACE ENGINEERING
ARIZONA STATE UNIVERSITY
TEMPE, ARIZONA

MARCH, 1987

MODELING AND MEASUREMENT OF TURBULENT SWIRLING FLOWS THROUGH ABRUPT EXPANSIONS

by

G.P. Neitzel and D.E. Metzger

FINAL REPORT

Prepared for

Department of the Navy, Office of Naval Research

Contract N00014-81-K-0428

Mechanical and Aerospace Engineering Department
Arizona State University

ASU Technical Report ERC-R-86104
March, 1987

PREFACE

The collection of five papers included in this report are the results of an experimental and numerical effort undertaken at Arizona State University with Office of Naval Research support under contract N00014-81-K-0428. The paper titles and where they have appeared or have been submitted are as follows:

1. "A Study of Sudden Expansion Pipe Flow Using an Algebraic-Stress Model of Turbulence," by B.K. Sultanian, G.P. Neitzel, and D.E. Metzger, AIAA Paper No. 86-1062, 1986. (Also presented at the 1986 AIAA/ASME Fluid Dynamics, Plasma Dynamics and Lasers Conference.)

2. "Comment on 'The Flowfield in a Suddenly Enlarged Combustion Chamber,'" by B.K. Sultanian, G.P. Neitzel, and D.E. Metzger, to appear, *AIAA Journal*.

3. "Turbulent Flow Prediction in a Sudden Axisymmetric Expansion," by B.K. Sultanian, G.P. Neitzel, and D.E. Metzger, in *Turbulence Measurements and Flow Modeling*, Hemisphere Publishing Corporation, New York, 655-664, 1987. (Also presented at the 1985 International Symposium on Refined Flow Modeling and Turbulence Measurements.)

4. "Heat Transfer to Turbulent Swirling Flow Through a Sudden Axisymmetric Expansion," by P.A. Dellenback, D.E. Metzger, and G.P. Neitzel, to appear, *Journal of Heat Transfer, Trans. ASME*. (Also to be presented at the 1987 ASME/AIChE National Heat Transfer Conference.)

5. "Measurements in Turbulent Swirling Flow Through an Abrupt Axisymmetric Expansion," by P.A. Dellenback, D.E. Metzger, and G.P. Neitzel, submitted to *AIAA Journal*.

The first three papers describe numerical predictions of the flowfields; paper 4 describes experimental measurements of local convective heat transfer on the tube walls downstream of expansion; and paper 5 describes detailed mean and fluctuating flowfield measurements both upstream and downstream of the expansion including precessing vortex core phenomena.

A Study of Sudden Expansion Pipe Flow Using an Algebraic-Stress Model of Turbulence

B.K. Sultanian, G.P. Neitzel, and D.E. Metzger

AIAA Paper No. 86-1062, 1986

Also presented at the 1986 AIAA/ASME Fluid Dynamics, Plasma Dynamics and Lasers Conference, Atlanta, May, 1986

AIAA'86

AIAA-86-1062

A Study of Sudden Expansion Pipe Flow Using an Algebraic Stress Model of Turbulence

B.K. Sultanian, Allison Gas Turbine Div., Indianapolis, IN; G.P. Neitzel and D.E. Metzger, Arizona State Univ., Tempe, AZ

AIAA/ASME 4th Fluid Mechanics, Plasma Dynamics and Lasers Conference

May 12-14, 1986/Atlanta, GA

A STUDY OF SUDDEN EXPANSION PIPE FLOW USING AN ALGEBRAIC STRESS MODEL OF TURBULENCE

B. K. Sultanian
Allison Gas Turbine Division*
General Motors Corporation
Indianapolis, Indiana 46206

G. P. Neitzel and D. E. Metzger
Mechanical and Aerospace Engineering
Arizona State University
Tempe, Arizona 85287

Abstract

The predictive ability of an algebraic stress model (ASM) and the Boussinesq viscosity model (BVM), or the k-ε model, is tested on a sudden expansion pipe flow against recently published measurements via laser Doppler velocimeter (LDV). Calculations are compared with the measurements on the mean axial velocity and axial turbulence intensity. While the standard model constants are used for the BVM, the additional constants that multiply the "return-to-isotropy" and "rapid" parts of the pressure-strain term in the ASM are tuned to the classical pipe flow data of Laufer. Both in the recirculation and redevelopment regions, the ASM results are in excellent agreement with the data, representing an improvement over the present BVM simulation and an earlier 2/E/FIX prediction of this flow. The ability of the ASM to successfully simulate the effects of streamline curvature and anisotropy in the turbulence field appears to be the major factor contributing to this success.

Nomenclature

c	centerline
C_1, C_2	
$C_{\varepsilon 1}$, $C_{\varepsilon 2}$	
C_μ	turbulence model constants
H	step height = $R_2 - R_1$
in	inlet
k	turbulent kinetic energy = $0.5\ \overline{u_i u_i}$
out	outlet
P	mean pressure
P	grid point (as subscript)
Q	volumetric flow rate
R_1	inside pipe radius of inlet pipe
R_2	inside pipe radius of outlet pipe
S	source term
U_i	mean-velocity component in x_i direction
u_i	fluctuating velocity component in x_i direction
u',v',w'	turbulence intensity components
x,y,r	coordinate directions
x_i	coordinates in tensor notation
x_r	reattachment length
δ	R_1/R_2
Γ	diffusion coefficient
δ_{ij}	Kronecker delta
ε	dissipation rate of k
λ	ratio of production to dissipation of k
μ	molecular viscosity
μ_t	eddy (or turbulent) viscosity = $C_\mu \rho k^2/\varepsilon$
ν_t	kinematic eddy viscosity = μ_t/ρ
ρ	fluid density
σ_k	turbulent Prandtl number for k
σ_ε	turbulent Prandtl number for ε
ϕ	general dependent variable
ϕ,(ϕ)	belonging to variable ϕ (as subscript or superscript)

1. Introduction

Engineering consideration of a sudden-expansion flow geometry dates back to 1766 and Borda's[1] original analysis. However, only in the latter half of this century has the problem received a considerable amount of interest. The main features of a pipe flow with an abrupt expansion are depicted in Figure 1, which shows the characteristics of a free-shear layer near the expansion and those of a wall boundary layer farther downstream of the reattachment. Near the expansion face, a coherent, large-scale turbulent structure plays an important role in the subsequent flow development. Although no central circulation zone exists in the absence of swirl, the existence of a large wall-bounded recirculation region makes the flow predominantly

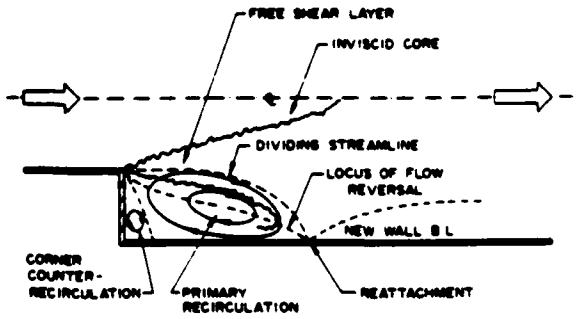

Figure 1. A sudden-expansion pipe flow structure.

*The research work reported here was conducted at Arizona State University.

elliptic in character. Based on recent LDV measurements, Stevenson[2] confirms the presence of a counter-recirculating eddy within a half step H (difference R_2-R_1 between the two pipe radii) of the expansion. Note that at the beginning of the redevelopment region the flow has many features in common with those in the far field of a free-shear layer, quite unlike conditions usually found in the entrance region of a developing pipe flow. Lipstein[3] reports that, in the range of B = 0.4 to 0.75 used in many engineering applications, the reattachment length scales properly with the step height. Perhaps the first detailed set of data on both the mean flow and the turbulence field is due to Chaturvedi.[4] However, because of the use of an intrusive probe (a hot wire) for measurement, the data are not completely reliable in the recirculation zone. Using these and other experimental results, Johnston[5] presents a useful discussion of this flow.

A flow-visualization study by Back and Roschke,[6] using dye injection, demonstrates the relative insensitivity of the reattachment length to variations in Reynolds number in the fully turbulent flow regime. Drewry[7] reports an improved flow-visualization study of the recirculation region using a surface oil-film technique. His results show that the reattachment length ranges between 7.9 and 9.2 step heights for Reynolds numbers (based on the inlet diameter) in the range of 1.3 x 10^6 to 2.2 x 10^6. The studies of Moon and Rudinger[8] and Lu[9] employ LDV. However, their data are limited to the mean axial-velocity distribution.

As to the past computational modeling of this elliptic flow, Gosman et al[10] claim to accurately calculate the reattachment length observed in the experiments of Back and Roschke[6] at large Reynolds number. Both the recirculation region and the redevelopment to normal pipe flow appear to be well predicted by Ha Minh and Chassaing.[11] Sayed and Sturgess[12] report that the reattachment length in the experiments of Chaturvedi[4] is underpredicted in their calculation by 10-15%. Moon and Rudinger[8] compare numerical results with their LDV data for the mean flow; good agreement between the two is reported. In addition, they mention that changing one of the model constants, i.e., $C_{\epsilon 2}$ = 1.70 instead of the "standard" value of 1.92, results in better agreement. Most of the results just mentioned have been obtained using the TEACH code with the standard BVM. The flow field in these cases is characterized, at the inlet, by low turbulence intensities and a nearly uniform mean axial-velocity profile, with the exception of Moon and Rudinger[8] where a fully developed inlet velocity profile is used. The outflow boundary conditions in all these cases are based on a fully developed ($\partial/\partial x$ = 0) flow assumption.

Most of the gross features in a sudden axisymmetric expansion are also shared by other fully separated internal flows such as those over single and double backward-facing steps and in confined jet mixing (ejectors). An overview of the current capabilities in predicting flows in this class are available in the proceedings of the 1980-81 AFOSR-HTTM-Stanford Conference.[13] Sindir[14] has used an ASM as one of the four models for predicting flows in backward-facing step geometries. His study shows that the relative performance of the models is region dependent. For example, the "modified" ASM has been found to produce the best predictions in the reverse flow region while exhibiting too slow a recovery rate beyond the reattachment zone.

Recently, Yang and Yu[15] reported a complete set of LDV data for an isothermal airflow in a dump-type combustor geometry. The flow field is somewhat atypical because of the presence of a high freestream turbulence level at the inlet and a contraction at the outlet. Computations of this case using BVM found that the mean axial-velocity data seriously suffer from a lack of mass conservation downstream of the expansion. Professor Yang[16] suspects that the error could be due to a shift in the blower output. A strong possibility exists, however, that a part of the error is also due to velocity bias, which is known to worsen in regions of high turbulence intensities. The importance of such a bias error in laser velocimetry is clearly demonstrated in the recent investigation of Stevenson et al.[17]

The measurements of mean axial velocity and axial turbulence intensity distribution in a sudden-expansion pipe flow have recently been reported by Stevenson et al.[18] These are very accurate LDV measurements with negligible velocity bias. The present calculations of both the mean flow and turbulence field based on the turbulence models BVM and ASM are compared with these data and their earlier prediction,[19] for the mean axial velocity distribution only, using the 2/E/FIX code of Pun and Spalding.[20]

2. Mathematical Formulation

2.1 Governing Equations with ASM and BVM

For an incompressible turbulent flow, which is statistically stationary in the mean, the conservation equations for mass (continuity equation) and momentum (Reynolds equations) may be written as follows:

$$\frac{\partial U_i}{\partial x_i} = 0 \qquad (1)$$

$$\frac{\partial}{\partial x_j}(\rho U_j U_i) = -\frac{\partial P}{\partial x_i} + \frac{\partial}{\partial x_j}\left(\mu \frac{\partial U_i}{\partial x_j} - \rho \overline{u_i u_j}\right) \qquad (2)$$

where $U_i + u_i$ is the local instantaneous velocity vector and $-\rho\,\overline{u_i u_j}$ are the Reynolds stresses. While for the BVM, the Boussinesq eddy viscosity hypothesis,

$$-\overline{u_i u_j} = \nu_t \left(\frac{\partial U_i}{\partial x_j} + \frac{\partial U_j}{\partial x_i}\right) - \frac{2}{3} k \delta_{ij}, \qquad (3)$$

is invoked, for the ASM (using Rodi's hypothesis[21]) the Reynolds stresses are expressed by the following algebraic equations:

$$\frac{\overline{u_i u_j} - \frac{2}{3} k \delta_{ij}}{k} = \frac{1 - C_2}{C_1 - 1 + \lambda} \frac{P_{ij} - \frac{2}{3} P_k \delta_{ij}}{\epsilon}, \qquad (4)$$

where $\lambda = P_k/\epsilon$, the ratio of local production of turbulent kinetic energy to its dissipation. The transport equations for k and ϵ are given by the following:

$$\frac{\partial}{\partial x_j}(U_j\, k) = \frac{\partial}{\partial x_j}\left(\frac{\nu_t}{\sigma_k}\frac{\partial k}{\partial x_j}\right) + P_k - \epsilon, \tag{5}$$

$$\frac{\partial}{\partial x_j}(U_j\, \epsilon) = \frac{\partial}{\partial x_j}\left(\frac{\nu_t}{\sigma_\epsilon}\frac{\partial \epsilon}{\partial x_j}\right) + C_{\epsilon 1}\frac{\epsilon}{k}P_k - C_{\epsilon 2}\frac{\epsilon^2}{k}, \tag{6}$$

where

$$\nu_t = \mu_t/\rho = C_\mu\, k^2/\epsilon, \tag{7}$$

and σ_k and σ_ϵ are the equivalent turbulent Prandtl numbers for k and ϵ, respectively.

Flow predictions are greatly influenced by the choice of constants that appear under any turbulence model assumption. Rather than allowing them to be used arbitrarily to fit data, they are selected with hopes of having universality. The model constants used in the BVM, as given by Launder and Spalding,[22] are now recognized as standard for most flow predictions. No such general consensus on the additional model constants C_1 and C_2 that multiply the "return-to-isotropy" term and the "rapid" part, respectively, of the pressure-strain term in the modeled Reynolds stress transport equation[23] has yet been achieved, although Launder[24] has proposed the values $C_1 = 2.2$ and $C_2 = 0.55$. With these values, the ASM results[25] show relatively poor comparison with the classical pipe flow data of Laufer.[26] Since pipe flow is the asymptotic flow in the class of applications being considered, these model constants have been recalibrated[25] to yield a satisfactory pipe flow prediction. Based on this calibration study, the values of $C_1 = 2.2$ and $C_2 = 0.70$ have been used. Figure 2 depicts the comparison of model predictions with the measurements of fully developed velocity profile in the pipe.

2.2 Boundary Conditions

For a general elliptic flow in a pipe, the computational domain has three types of boundaries: inflow, outflow, and no flow (solid pipe wall). The flow considered here permits a fully developed ($\partial/\partial x = 0$) boundary condition at the outlet. Since the BVM and ASM, in the form presented here, are not valid in the region of low turbulent Reynolds number near the wall, the wall-function approach of Launder and Spalding[22] is used. With a fully developed flow at the inlet, while the one-seventh power-law profile is assumed for the mean axial velocity, the following profiles for k_{in} and ϵ_{in} are used:

$$k_{in} = 0.0013\, U_1^2\, [1 + 4(r/R_1)^{2.5}] \tag{8}$$

$$\epsilon_{in} = C_\mu^{3/4}\, k_{in}^{3/2}/l_m \tag{9}$$

where the mixing length l_m distribution is computed from the equation

$$l_m = R_1\, [0.14 - 0.08(r/R_1)^2 - 0.06(r/R_1)^4] \tag{10}$$

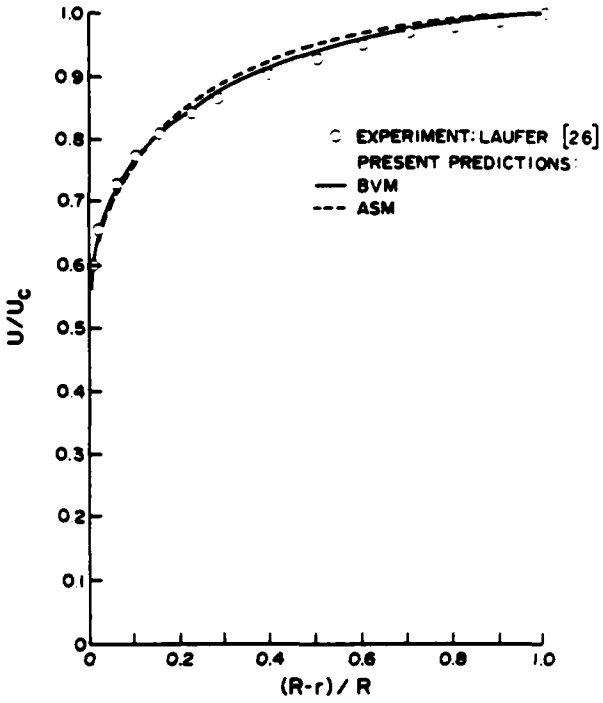

Figure 2. Comparison of calculations with measurements of Laufer[26] for a fully developed pipe flow.

3. Solution Procedure

For a common solution procedure, the governing transport equations are cast into the following common form:

$$\frac{1}{r}\left[\frac{\partial}{\partial x}(\rho U r \phi) + \frac{\partial}{\partial r}(\rho V r \phi)\right] = \frac{1}{r}\left[\frac{\partial}{\partial x}\left(r\,\Gamma_\phi\frac{\partial \phi}{\partial x}\right) + \frac{\partial}{\partial r}\left(r\,\Gamma_\phi\frac{\partial \phi}{\partial r}\right)\right] + S_\phi \tag{11}$$

where ϕ represents a general dependent variable, x and r are the axial and radial coordinates respectively with corresponding velocity components U and V, Γ_ϕ is a diffusion coefficient, and S_ϕ is the so-called source term. The latter also contains the part of the diffusion term that cannot be expressed in the form assumed in Equation (11). Finite difference equations for each ϕ are obtained by integrating Equation (11) over an appropriate control volume constructed around a grid point representing the location for ϕ. The details on deriving the discretized equations in this way are given in Ref 27. The resulting numerical scheme is based on the "hybrid" approximation for the convection terms. The SIMPLE procedure[27] is used to numerically solve these equations.

The convergence problem encountered in the use of ASM has been handled with a dual-loop iteration scheme.[25] According to this scheme, the mean flow and turbulence model variables (k and ϵ) are solved in an outer loop using Gauss-Seidel line-by-line iteration with under-relaxation. For each outer-loop iteration, the Reynolds stresses are computed from Equation (4) in an inner loop using Gauss-Seidel point iteration with under-relaxation.

4. Results

For the measurements of Stevenson, Thompson, and Gould[18] the sudden expansion ipe flow geometry consists of pipes of diameters 76.2 mm at the inlet and 152.4 mm for the expansion section with an inlet Reynolds number of 11 x 10^4. The flow is fully developed both in the inlet pipe before expansion and at the exit of the downstream pipe corresponding to x/H = 40. Although both the biased and unbiased LDV measurements for the distribution of mean axial velocity and turbulence intensity are reported for x/H values ranging from 0.33 to 15, only the unbiased data are used here for comparison with the computation. In the experiment, the reattachment is found to occur at 8.6 step heights downstream of the sudden expansion.

In an earlier calculation[19] of this flow using the 2/E/FIX computer code of Pun and Spalding,[20] the degree of agreement with data worsens as one proceeds downstream in the redevelopment region. Assuming that the measured velocity profiles are mass conserving, the computed ones are found to be deficient in this respect. In this calculation inlet conditions were specified at x/H = 0.33 (ignoring the pipe expansion geometry altogether) and uniform grid spacing was used in the axial direction, which might not properly resolve the shear-layer growth in the recirculation region. With these concerns in mind, a BVM (with its standard model constants) prediction using a 50 x 30 grid was made. The grid, shown in Figure 3, is nonuniform in the axial direction for a portion of the redevelopment region beyond which it is uniform up to the outflow boundary at x/H = 40. The results for the mean axial-velocity distribution are compared with the data and the earlier 2/E/FIX prediction in Figure 4. Although both the BVM and 2/E/FIX predictions themselves are in good agreement in the recirculation region, excellent agreement between the data and BVM prediction is seen at x/H = 15, indicating that the present computation is mass conserving as are the data.

The flow calculation with the ASM also used the grid shown in Figure 3 with boundary conditions identical to the ones used in the BVM case. The results, also shown in Figure 4, are in excellent agreement with the data for the mean axial velocity, both in the recirculation and redevelopment regions. A reattachment length of 8.5 step heights is predicted compared with the experimentally observed value of 8.6. The grid has an inherent error* of 2 x 10^{-3} and about 500 iterations are required for solution convergence according to the convergence criterion[28] used.

In the present calculations, the turbulence intensities are equated to the square root of the corresponding normal Reynolds stresses divided by the maximum mean axial velocity at the inlet. In the case of ASM, these stresses form part of the solution via Equation (4). For the BVM, however, Equation (3) is used to compute these stresses. Results for the axial turbulence intensity from both the BVM and ASM predictions are compared with the data in Figure 5. While both results are in

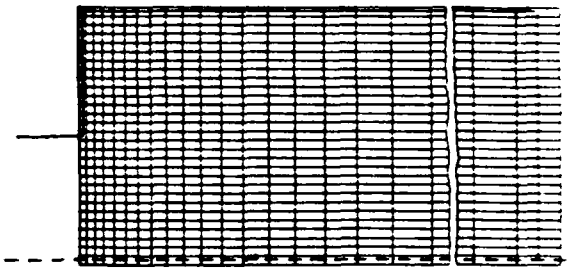

Figure 3. Grid system 50 x 30 used for computing the flow of Stevenson et al.[18] (Grid is magnified in the radial direction.)

good agreement with the data in the recirculation region, the ASM prediction is slightly better in the redevelopment region. The computational results on axial turbulence intensity distribution for the two models are summarized in Figure 6. The profiles have their maxima along the extended surface of the inlet pipe. These maxima are rather sharp near the expansion and become progressively flatter downstream.

From the results for both the mean axial velocity and the axial turbulence intensity distributions it is seen that the start of the redevelopment region is more characteristic of the far field of an axisymmetric jet than the entrance region of a conventional pipe flow. This is evident from the fact that the mean axial velocity at the center line decreases from x/H = 9 to x/H = 15 and the corresponding turbulence intensity increases over this region. In a conventional pipe-flow development, turbulence energy is produced near the wall and diffuses toward the center; whereas in a sudden expansion pipe flow just the opposite occurs in the early stages of redevelopment. These observations are also supported by the experimental investigation of Chaturvedi[4] and its discussion by Johnston.[5]

5. Discussion

The most important feature of an internal flow with separation is the recirculation region bounded by the dividing streamline and the confining wall, as shown in Figure 1. At the recent Stanford conference,[13] the performances of several turbulence models in computing the flow in a backward-facing step were compared. Most of the BVM versions were found to underpredict the reattachment length by 15-20% when compared with the experiment of Kim, Kline, and Johnston.[29] The ASM, however, predicts reattachment length within 2% of the experimental value. In addition, the detailed mean-flow results in this case are in excellent agreement with the data, especially in the recirculation region.

A very simple model is suggested in Ref 30 for predicting trends in the reattachment length data: "the shear layer reattaches when it has entrained all of the pressure gradient driven backflow." Since the pressure gradient is primarily dependent on area ratio, accurate prediction of reattachment length depends on the ability of the turbulence model to simulate the entrainment rate (or the growth rate of the shear layer). The BVM is found deficient in this respect, predicting a higher growth rate for the shear layer. The greatest weakness of all second-order turbulence models

*Inherent error = $|(Q_{in} - Q_{out})|/Q_{in}$, where Q_{in} is the known flow rate at the inlet, and Q_{out} is the computed flow rate at the outlet based on a nominal fully developed velocity profile with values at the grid points.

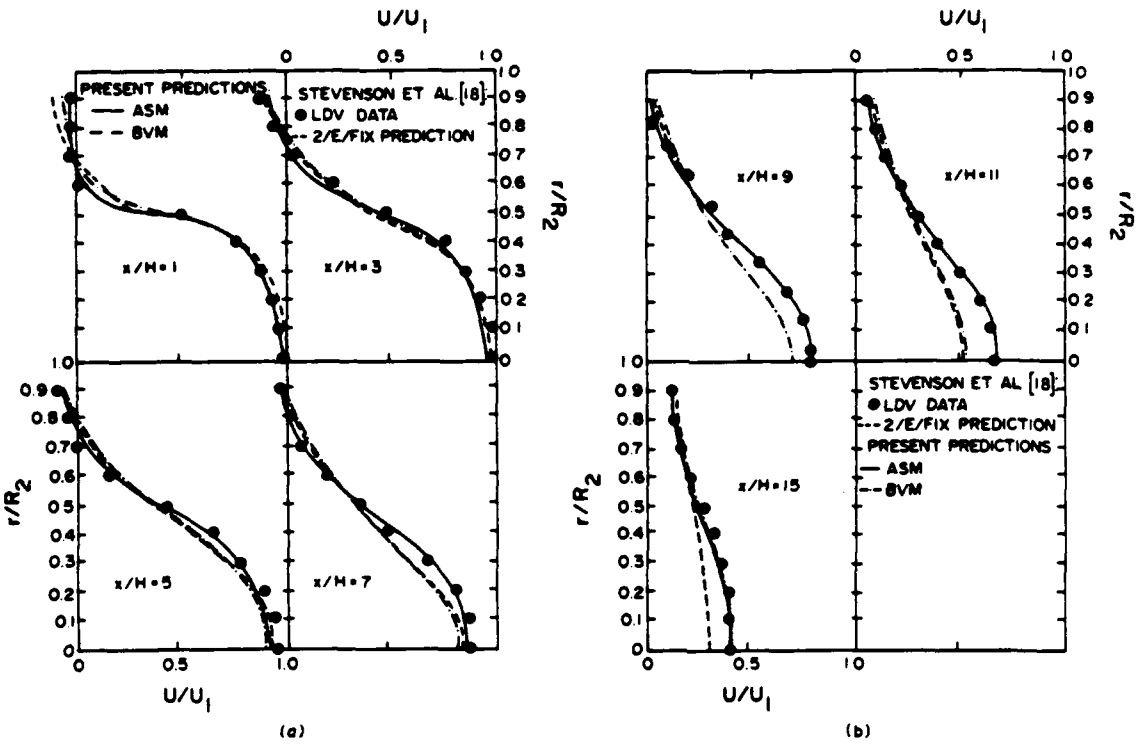

Figure 4. Comparison of computed mean axial-velocity profiles with measurements of Stevenson et al[18]: (a) recirculation region and (b) redevelopment region.

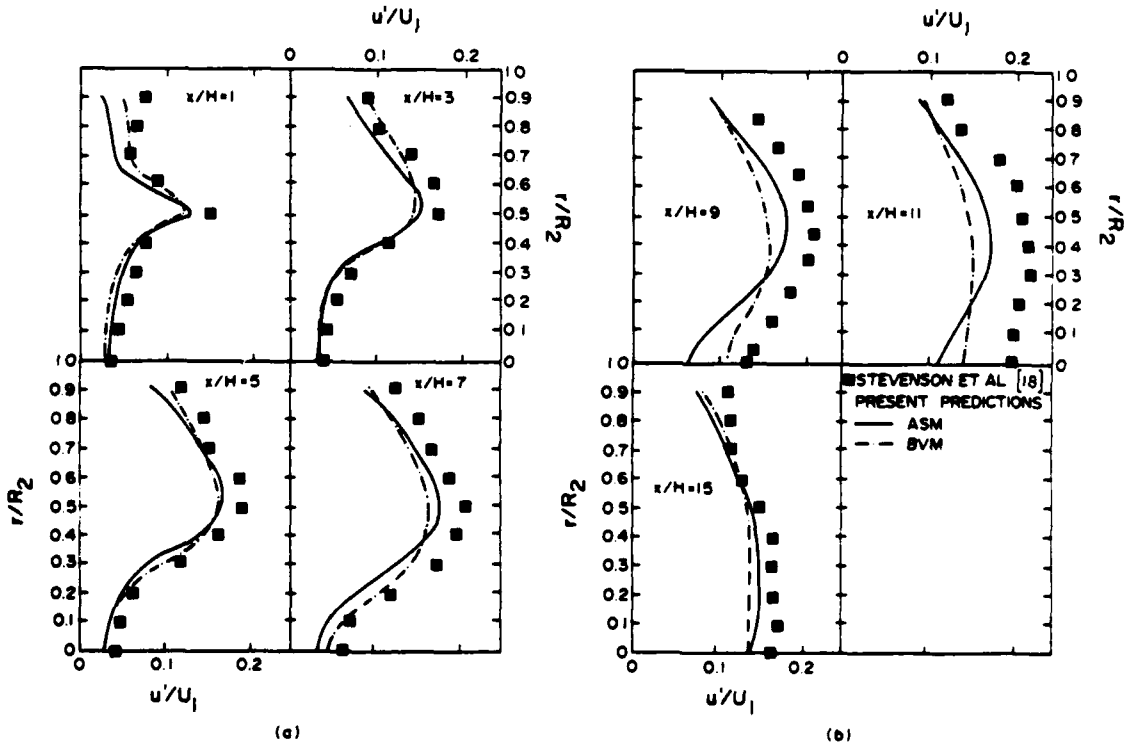

Figure 5. Comparison of computed axial turbulence intensity distribution with measurements of Stevenson et al[18]: (a) recirculation region and (b) redevelopment region.

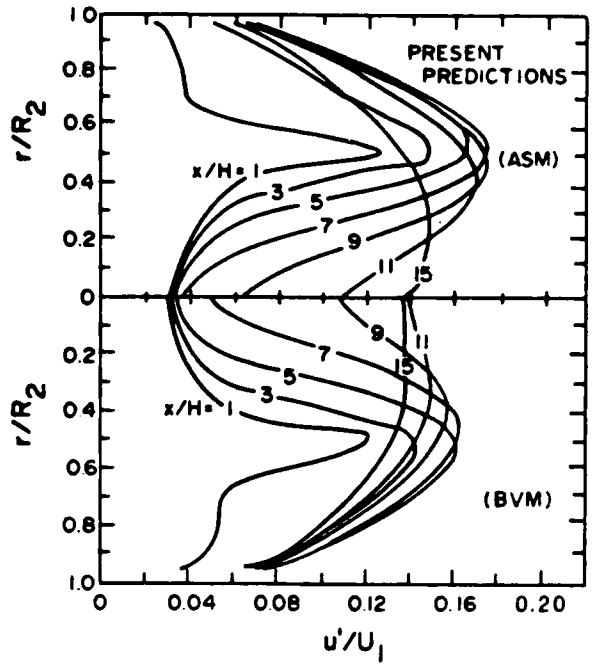

Figure 6. Distribution of axial turbulence intensity computed with BVM and ASM for the flow of Stevenson et al.[18]

using k-ε model variables is the transport equation for ε, which embraces several modeling assumptions. In addition, the BVM uses a simple eddy-viscosity hypothesis. To partly remedy these drawbacks and to capture the correct growth rate for the shear layer, the sensitivity of reattachment length to variations in the model constants $C_{\varepsilon 1}$ and $C_{\varepsilon 2}$, multiplying the production and dissipation terms, respectively in the ε-equation, has been studied. Moon and Rudinger,[8] for example, recommend changing $C_{\varepsilon 2}$ from its standard value of 1.92 to 1.70. Stevenson et al,[18] based on their numerical simulation results, report a linear correlation between the reattachment length and $C_{\varepsilon 2}$, which is of the following form:

$$C_{\varepsilon 2} = 0.059\ (x_r/H) + 2.4305 \qquad (12)$$

where x_r is the reattachment length. Our own computation, not reported here, indicates that to reproduce the experimentally observed reattachment length, $C_{\varepsilon 2} = 1.83$ should be used in BVM. Clearly, such correlations and arbitrary changes in model constants have little general validity and can at most be justified in a "postdictive" computation.

Gibson et al[31] point out that "the turbulent shear stress and intensity are reduced by streamline curvature in the plane of the mean shear when the angular momentum of the flow increases in the direction of the radius of the curvature and are increased when the angular momentum decreases with radius." According to this criterion the streamlines in the recirculation region of a pipe expansion flow possess a stabilizing curvature. Even for a thin-shear-layer prediction the utility of a linear F-factor correction is limited to flows with mild curvature. So and Mellor[32-34] are reasonably successful in simulating the effects of large curvature through the use of a pressure-strain term in the Reynolds stress equation. Although their method is open to criticism[31] due to the assumption of local equilibrium and the omission of important mean-strain effects in the modeling of pressure-strain term, the approach shares the general conclusion drawn by Castro and Bradshaw[35] that "methods based on the Reynolds-stress transport equations will be needed in complex flows." The contraction of the Reynolds stress transport equations yields the equation for k; the pressure-strain term becomes identically zero. In addition, with the eddy-viscosity assumption, the production term for k involves only the mean-strain terms. Thus, the BVM does not involve any term representing a direct interaction of turbulence with the mean flow. In this respect an important role is played by the "rapid" part in the ASM. The results for radial turbulence intensity, turbulent kinetic energy, and turbulent shear stress, shown in Figures 7 through 9, for the two models clearly bring out the superiority of ASM over BVM in successfully predicting the suppression of turbulence by stabilizing curvature in the recirculation region. Further, the strength of the recirculation eddy, as indicated by the maximum value for the stream function occurring on the locus of flow reversal, predicted by the BVM is about 5% higher than that predicted by the ASM.

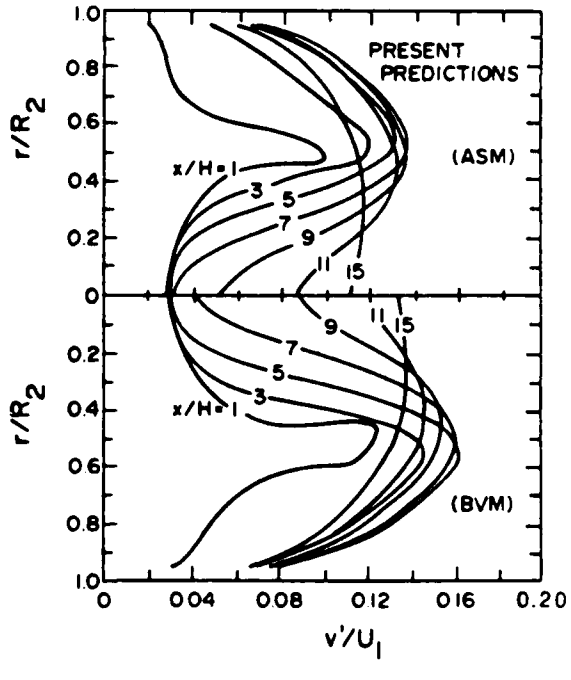

Figure 7. Distribution of radial turbulence intensity computed with BVM and ASM for the flow of Stevenson et al.[18]

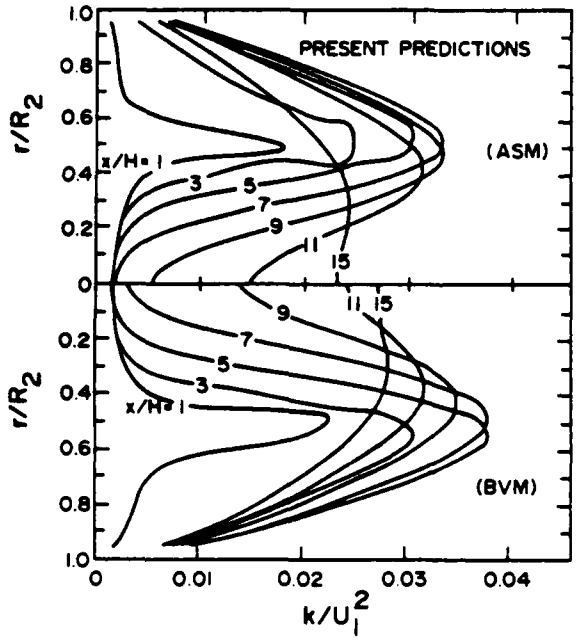

Figure 8. Distribution of turbulent kinetic energy computed with BVM and ASM for the flow of Stevenson et al.[18]

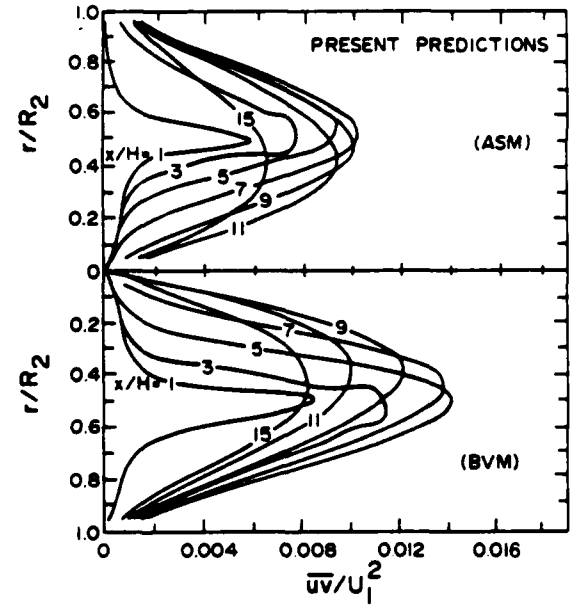

Figure 9. Distribution of Reynolds shear stress computed with BVM and ASM for the flow of Stevenson et al.[18]

6. Concluding Remarks

The predictions based on the two turbulence models BVM and ASM are compared with a recent set of LDV measurements[18] on mean axial velocity and axial turbulence intensity in a sudden expansion pipe flow.

The ASM, with its model constants tuned to a fully developed pipe flow data, yielded results in excellent agreement with the measurements in both recirculation and redevelopment regions. The agreement represents an improvement over the BVM calculation and an earlier computation of this flow using the 2/E/FIX code. A comparison of results for the turbulence field demonstrates the ability of the ASM to simulate the stabilizing effects of streamline curvature in the recirculation region, which results in relative suppression of turbulence. The modeling of the pressure-strain redistribution term in the Reynolds-stress transport equation is thought to be accountable for this mechanism, which correctly simulates the shear-layer growth and hence the reattachment length.

Acknowledgments

We wish to thank Professor D. F. Jankowski for many helpful discussions and for commenting on an earlier version of the manuscript. This work was sponsored by the Office of Naval Research under Contract No. N00014-81-K-0428.

References

1. Borda, Memoire de l'Academie royal des Sciences, Paris 1766: memoire sur l'ecoulement des fluides par les orifices des vases.
2. W. H. Stevenson, private communication, 1983.
3. N. J. Lipstein, "Low Velocity Sudden Expansion Pipe Flow," ASHRAE J, Vol 4, No. 3, 1962, pp 43-47.
4. M. C. Chaturvedi, "Flow Characteristics of Axisymmetric Expansions," ASCE, J Hydraulics Div, Vol 89, No. 61, May 1963, pp 61-92.
5. J. P. Johnston, "Internal Flows," in Topics in Applied Physics: Turbulence, (Editor: P. Bradshaw), Springer-Verlag, New York, 1978.
6. L. H. Back and E. J. Roschke, "Shear Layer Regimes and Wave Instabilities and Reattachment Lengths Downstream of an Abrupt Circular Channel Expansion," J Appl Mech, Sept 1972, pp 677-681.
7. J. E. Drewry, "Fluid Dynamic Characterization of Sudden Expansion Ramjet Combustor Flow Fields," AIAA J, Vol 16, April 1978, pp 313-319.
8. L. F. Moon and G. Rudinger, "Velocity Distribution in an Abruptly Expanding Circular Duct," J Fluids Engrg, Trans ASME, March 1977, pp 226-230.
9. C. C. Lu, "Measurements of Turbulent Flow Velocity for Sudden Expansion Cylindrical Tube Using Laser Doppler Velocimeter (LDV)," AIChE J, Vol 26, March 1980, pp 303-305.
10. A. D. Gosman, E. E. Khalil, and J. H. Whitelaw, "The Calculation of Two-Dimensional Turbulent Recirculating Flows," in Proceedings Symposium on Turbulent Shear Flows (Editors: F. Durst et al), April 1977.
11. H. Ha Minh and P. Chassaing, "Perturbations of Turbulent Pipe Flow," in Proceedings Symposium on Turbulent Shear Flows (Editors: F. Durst et al), April 1977.
12. S. A. Syed and G. J. Sturgess, "Validation Studies of Turbulence and Combustion Models for Aircraft Gas Turbine Combustors," in Momentum and Heat Transfer Processes in Recirculating Flows (Editors: B. E. Launder and J.A.C. Humphrey), ASME Winter Annual Meeting, Nov 1980.
13. J. J. Kline, B. J. Cantwell, and G. M. Lilley, The 1980-81 AFOSR-HTTM Stanford Conference on

Complex Turbulent Flows: Comparison of Computation and Experiment I, II and III, Thermosciences Division, Mechanical Engineering Department, Stanford University, Stanford, CA, 1981.

14. M. M. Sindir, Numerical Study of Turbulent Flows in Backward-Facing Step Geometries: Comparison of Four Models of Turbulence, Ph.D. Thesis, University of California, Davis, 1982.
15. B. T. Yang and M. H. Yu, "The Flow Field in a Suddenly Enlarged Combustion Chamber," AIAA J, Vol 21, No. 11, 1983, pp 92-97.
16. B. T. Yang, private communications, 1983.
17. W. H. Stevenson, H. D. Thompson, and T. C. Roesler, "Direct Measurement of Laser Velocimeter Bias Errors in a Turbulent Flow," AIAA J, Vol 20, 1982, pp 1720-1723.
18. W. H. Stevenson, H. D. Thompson, and R. D. Gould, Laser Velocimeter Measurements and Analysis in Turbulent Flows with Combustion, Part II, Report No. AFWAL-TR-82-2076 Part II, School of Mechanical Engrg, Purdue University, West Lafayette, IN, July 1983.
19. R. D. Gould, W. H. Stevenson, and H. D. Thompson, "Laser Velocimeter Measurements in a Dump Combustor," ASME Paper No. 83-HT-47.
20. W. M. Pun and D. B. Spalding, A General Computer Program for Two-Dimensional Elliptic Flows, Imperial College, Mechanical Engineering Dept, HTS/76/2, 1976.
21. W. Rodi, "A New Algebraic Relation for Calculating the Reynolds Stresses," ZAMM, Vol 56, 1976, pp 219-221.
22. B. E. Launder and D. B. Spalding, "The Numerical Calculation of Turbulent Flow," Comp Methods in Appl Mech and Engrg, Vol 3, 1974, pp 269-289.
23. B. E. Launder, G. J. Reece, and W. Rodi, "Progress in the Development of a Reynolds-Stress Turbulence Closure," J Fluid Mech, Vol 68, 1975, pp 537-566.
24. B. E. Launder, "On the Effects of Gravitational Field on the Turbulent Transport of Heat and Momentum," J Fluid Mech, Vol 68, 1975, pp 569-581.
25. B. K. Sultanian, Numerical Modeling of Turbulent Swirling Flow Downstream of an Abrupt Pipe Expansion, Ph.D. Thesis, Arizona State University, Tempe, 1984.
26. J. Laufer, The Structure of Turbulence in Fully Developed Pipe Flow, NACA Tech Report 1174, 1954.
27. S. V. Patankar, Numerical Heat Transfer and Fluid Flow, Hemisphere Publication Corporation, New York, 1980.
28. B. K. Sultanian and G. P. Weitzel, An Alternate Convergence Criterion for Internal Elliptic Flow Computations, Report No. CR-R-84029, Mechanical and Aerospace Engrg, Arizona State University, Tempe, May 1984.
29. J. Kim, S. J. Kline, and J. P. Johnston, Investigation of Separation and Reattachment of a Turbulent Shear Layer: Flow over a Backward-Facing Step, Report MD-37, Thermosciences Division, Department of Mechanical Engineering, Stanford University, 1978.
30. J. K. Eaton and J. P. Johnston, Turbulent Flow Reattachment: An Experimental Study of the Flow and Structure behind a Backward Facing Step, Report MD-39, Thermoscience Division, Mechanical Engineering Department, Stanford University, Stanford, CA, 1980.
31. M. M. Gibson, W. P. Jones, and B. A. Younis, "Calculation of Turbulent Boundary Layers on Curved Surfaces," Phys Fluids, Vol 24, No. 3, 1981, pp 386-395.
32. R.M.C. So, "A Turbulent Velocity Scale for Curved Shear Flows," J Fluid Mech, Vol 70, 1975, pp 37-57.
33. G. L. Mellor, "A Comparative Study of Curved Flow and Density-Stratified Flow," J Atmos Sci, Vol 32, July 1975, pp 1278-1282.
34. R.M.C. So and G. L. Mellor, "Turbulent Boundary Layers with Large Streamline Curvature Effects," Z Angew Math Phys, Vol 29, 1978, pp 54-74.
35. I. P. Castro and P. Bradshaw, "The Turbulence Structure of a Highly Curved Mixing Layer," J Fluid Mech, Vol 73, 1976, pp 265-304.

Comment on "The Flowfield in a Suddenly Enlarged Combustion Chamber," by B.T. Yang and M.H. Yu, *AIAA Journal*, 21, pp. 92-97, 1983

B.K. Sultanian, G.P. Weitzel, and D.E. Metzger

to appear, *AIAA Journal*

COMMENT ON "THE FLOWFIELD IN A SUDDENLY ENLARGED COMBUSTION CHAMBER"

B.K. Sultanian

Allison Gas Turbine Division*

General Motors Corporation

Indianapolis, Indiana 46206

G. P. Neitzel** and D. E. Metzger†

Mechanical and Aerospace Engineering

Arizona State University

Tempe, Arizona 85287

In an interesting paper,[1] Professor Yang and his co-worker Yu report a complete set of laser Doppler velocimeter (LDV) measurements on the mean velocities and Reynolds stresses for an isothermal airflow in a dump-type combustor geometry. A maximum error of 6.5% in the data, in terms of the flow rate at each measuring station, was claimed in the paper. The data and their projected accuracy motivated us to use them to validate our two-dimensional elliptic code STEPUP[2] for two turbulence models, the Boussinesq viscosity model (BVM), or the k-ε model, and the algebraic stress transport model. Although the flowfield is somewhat atypical because of the presence of a high freestream turbulence level at the inlet and a contraction at the outlet, computation of this flow using BVM revealed that the mean axial-velocity data seriously suffer from a lack of mass conservation downstream of the expansion. The results of this

*This investigation was conducted at Arizona State University
**Associate Professor
†Professor

calculation and a possible explanation for the error in the data are briefly discussed in the following paragraphs.

The flow geometry in this case corresponds to a dump-type combustor where, in view of a short chamber length, a fully developed outflow boundary condition does not apply. For the present elliptic computation, specification of the measured profiles at the outlet therefore becomes necessary. Two main difficulties are encountered in trying to simulate this flow: (1) the measured mean axial-velocity at the outflow boundary (x = 40 cm) yields a mass flow rate that is about 65% higher than that at the inlet, and (2) the turbulence intensity at the inlet is unusually high. As a result, the commonly assumed profiles[3] at the inflow boundary for turbulent kinetic energy k and its dissipation rate ε are found to be inadequate. In order to proceed with an attempt at simulation, the mean axial-velocity profile at the outlet was reduced uniformly to satisfy continuity. At the inlet, however, along with a nearly uniform mean axial velocity, the following profiles for k (using the centerline measurements of turbulence intensities reported near the expansion) are used:

$$k_{in} = 0.03\ U_{in}^2;\ \varepsilon_{in} = 0\ , \tag{1}$$

except at the near-wall (inlet pipe) grid point where

$$(k_{in})_p = 0.15\ U_{in}^2 \tag{2}$$

is specified. The form in Equation (2) is based on the measurements of Holladay[4] in developing pipe flow that show that the maximum value of k near the wall is about five times its value in the free stream (core flow). The inlet condition for ε,

$$(\varepsilon_{in})_p = C_\mu^{3/4}\ (k_{in})_p^{3/2}/(0.41\ y_p)\ , \tag{3}$$

is based on the existence of a thin, equilibrium wall boundary layer.

Using the numerical procedure presented elsewhere,[2] a reattachment length of six step heights (as opposed to the experimentally observed value of 4.5) results from simulation with the standard BVM. It is seen from Figure 1 that the computed mean axial-velocity profiles are in reasonable agreement with the data near the expansion while poor quantitative agreement is obtained further downstream. Results for both the axial and radial components of turbulence intensity along the chamber axis are also in satisfactory agreement with the measurements shown in Figure 2. Since the numerically determined mean axial-velocity profiles are mass conserving, the disagreement with the data downstream of the expansion indicates that the corresponding experimental profiles (in addition to the one at the outflow boundary) are also inconsistent from a continuity consideration. This is further verified by numerically integrating these experimental profiles at several of the measurement stations. The error at each station, as a percentage deviation from the inlet flow rate, is also shown in Figure 2. A value as high as 80% for this error can be seen from Figure 2, which does not agree with the reported[1] value of only 6.5%.

Professor Yang[5] suspects that the error could be due to a shift in the blower output. A strong possibility exists, however, that a part of the error is also due to velocity bias that is known to worsen in regions of high turbulence intensities. The importance of such bias error in laser velocimetry was clearly demonstrated in the recent investigation of Stevenson et al.[6] In view of these serious discrepancies in the data, no meaningful validation of a numerical procedure nor the development of an advanced turbulence model are possible.

References

1. B. T. Yang and M. H. Yu, "The Flowfield in a Suddenly Enlarged Combustion Chamber," AIAA J., Vol 21, No. 11, 1983, pp 92-97.
2. B. K. Sultanian, "Numerical Modeling of Turbulent Swirling Flow Downstream of an Abrupt Pipe Expansion," Ph.D. Thesis, Arizona State University, Tempe, 1984.
3. A. D. Gosman, E. E. Khalil, and J. H. Whitelaw, "The Calculation of Two-Dimensional Turbulent Recirculating Flows," in Proceedings Symposium on Turbulent Shear Flows, Edited by F. Durst et al, April 1977.
4. D. W. Holladay, "An Experimental Investigation of the Turbulent Flow in the Entrance Region of a Smooth Round Pipe," Ph.D. Thesis, The University of Tennessee, 1968.
5. B. T. Yang, private communications, 1983.
6. W. H. Stevenson, H. D. Thompson, and T. C. Roesler, "Direct Measurement of Laser Velocimeter Bias Errors in a Turbulent Flow," AIAA J., Vol 20, 1982, pp 1720-1723.

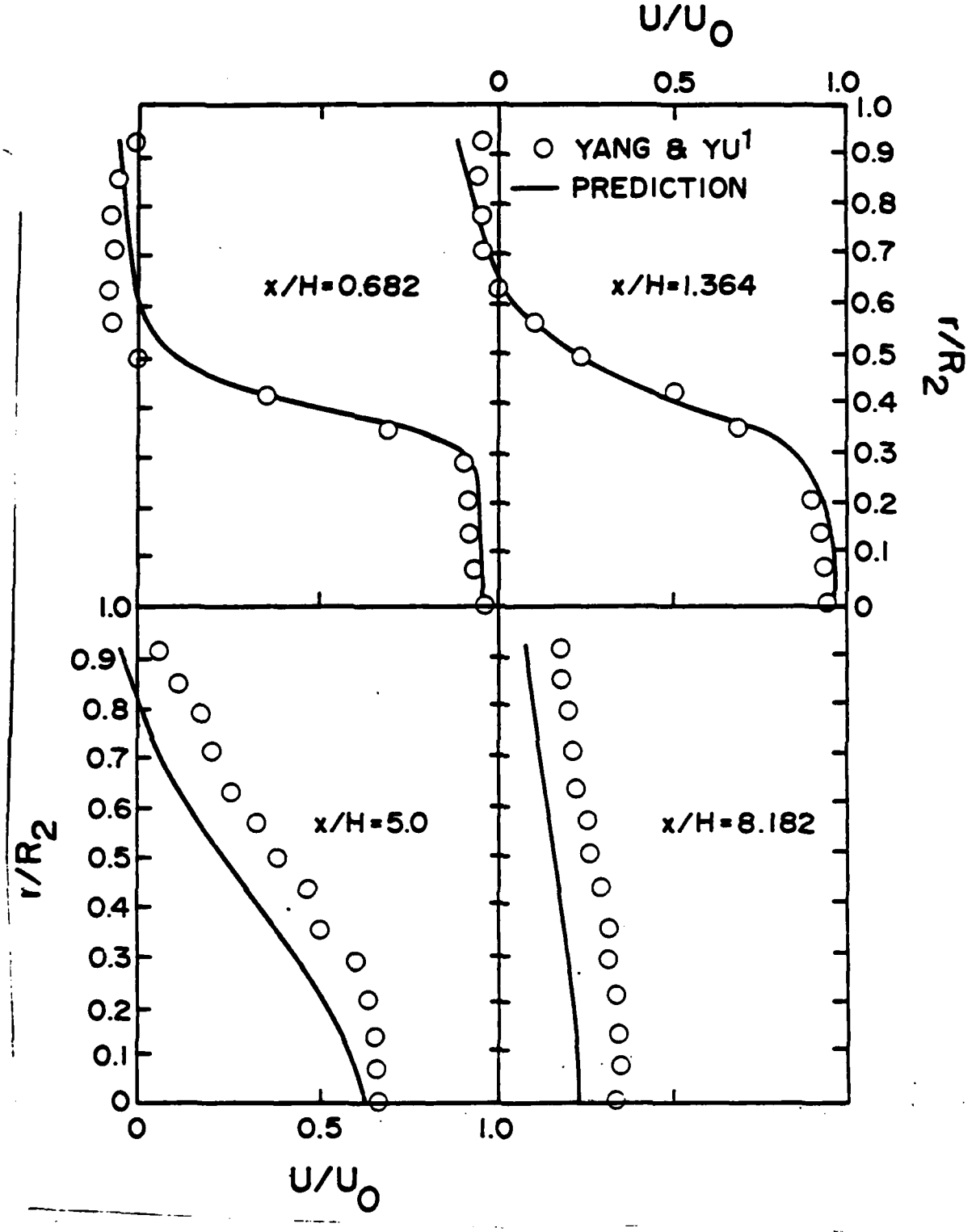

Figure 1. Comparison of calculated mean axial-velocity profiles with measurements.

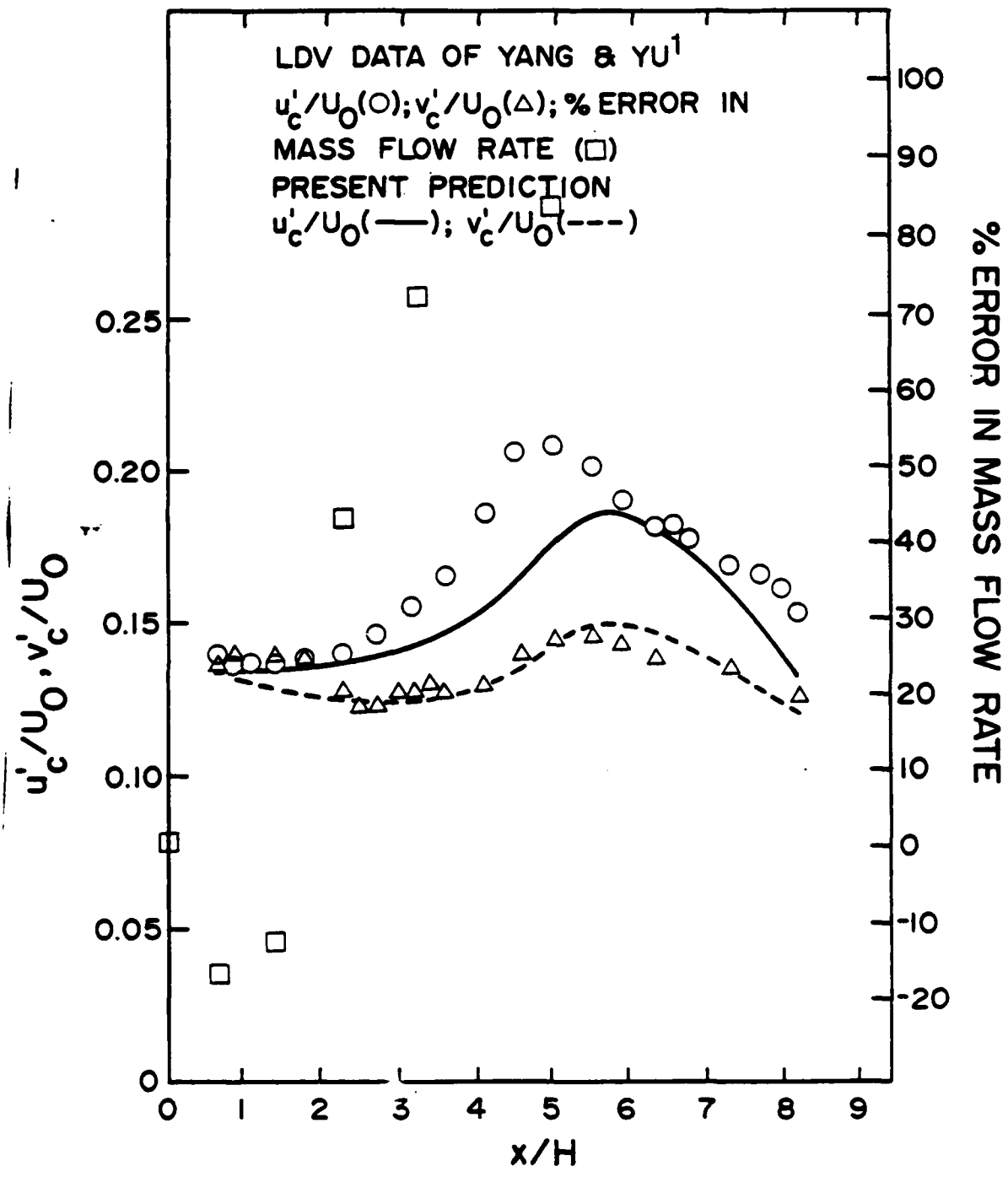

Figure 2. Comparison of calculated axial and radial turbulence intensities with measurements at the pipe centerline. Percentage error in mass flow rate computed from measured mean axial-velocity distribution.

Turbulent Flow Prediction in a Sudden Axisymmetric Expansion

B.K. Sultanian, G.P. Neitzel, and D.E. Metzger

Turbulence Measurements and Flow Modeling, Hemisphere Publishing Corporation, New York, 655-664, 1987

Also presented at the 1985 International Symposium on Refined Flow Modeling and Turbulence Measurements University of Iowa, September, 1985

Proceedings of the International Symposium on Refined Flow Modelling and Turbulence Measurements, which will be held at The University of Iowa 16-18 September 1985.

Turbulent Flow Prediction in a Sudden Axisymmetric Expansion

by

Bijay K. Sultanian

Allison Gas Turbine Division
General Motors Corporation
Indianapolis, Indiana 46206 USA

G. Paul Neitzel Darryl E. Metzger

Department of Mechanical and Aerospace Engineering
Arizona State University
Tempe, Arizona 85287 USA

SUMMARY

Refined modeling of sudden expansion pipe flows using an algebraic stress transport model (ASM) of turbulence is presented. The model has contributions from the mean flow as well as the turbulence field in its pressure-strain term, and the corresponding model constants are tuned with the classical fully-developed-pipe-flow data of Laufer. The results of computation for flows with inlet Reynolds numbers of 60,000 and 110,000 are compared with recent LDV measurements and also with the calculations using the standard Boussinesq viscosity model (BVM), alternately known as the k-ε model. The ASM, with its ability to naturally simulate the effects of streamline curvature and anisotropy in the turbulence field, is found to be superior to the BVM in predicting these flows in both recirculation and redevelopment regions.

1. Introduction

The turbulent flow in a sudden pipe expansion is an important internal flow with separation which falls in the general class of complex shear flows. Such a flow geometry is of common occurrence in industrial piping systems and those of high-technology aerospace applications with severe volume constraints. A dominant feature of the flow is the existence of a recirculation zone characterized by low mean velocities but high turbulence intensities. A typical gas turbine combustor flow field, generally three-dimensional in nature, contains one or more such recirculation regions for both flame stabilization and increased mixing of fuel and air in its primary zone.

The gross features found in a sudden axisymmetric expansion are depicted in Fig. 1. The flow structure is rather complex, combining the characteristics of a free-shear layer near the expansion and those of a wall boundary-layer farther downstream of the reattachment. The existence of a large wall-bounded recirculation region makes the flow predominantly elliptic in character. The early part of the redevelopment region, however, is quite different from the usual entrance region in a developing pipe flow.

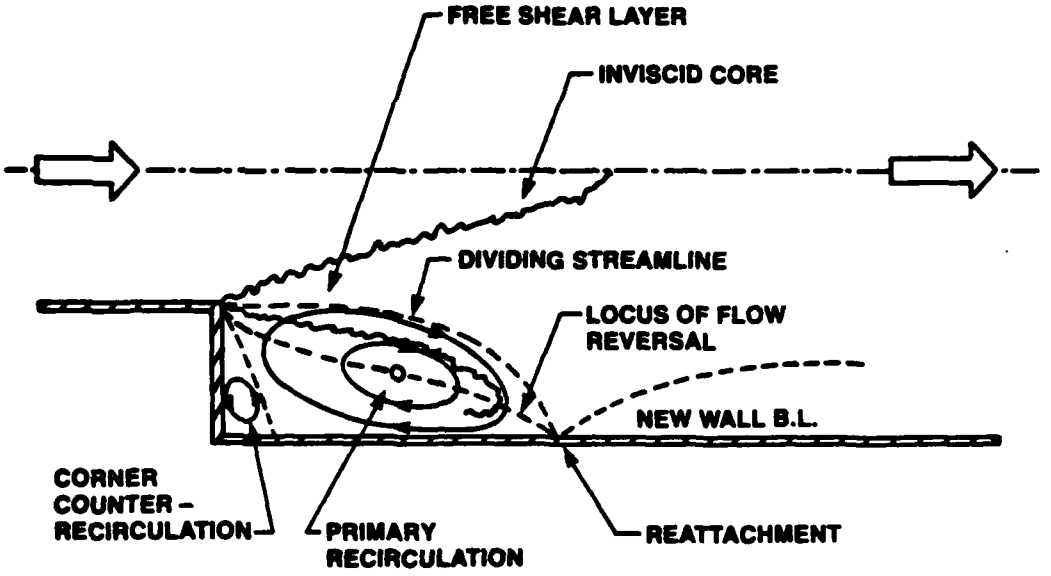

Fig. 1. Flow features in a sudden axisymmetric expansion

A number of investigations, both experimental and theoretical, of a sudden expansion pipe flow have been reviewed in Ref. (14). An overview of the current capabilities in predicting flows in this class can be had from the proceedings of the 1980-81 AFOSR-HTTM-Stanford Conference (3). The computational work reported herein, based on an algebraic stress model (ASM) and the standard Boussinesq viscosity model (BVM), uses very recent LDV data in this flow geometry for comparison.

2. Governing Equations under ASM and BVM

For an incompressible turbulent flow which is statistically stationary in the mean, the conservation equations for mass (continuity equation) and momentum (Reynolds equations) may be written as

$$\frac{\partial U_i}{\partial x_i} = 0 \tag{1}$$

$$\frac{\partial}{\partial x_j}(\rho U_j U_i) = -\frac{\partial P}{\partial x_i} + \frac{\partial}{\partial x_j}\left(\mu \frac{\partial U_i}{\partial x_j} - \rho \overline{u_i u_j}\right) \tag{2}$$

where $U_i + u_i$ is the local instantaneous velocity vector and $-\rho \overline{u_i u_j}$ are the Reynolds stresses. The ASM used here is derived from the following modeled transport equation for the Reynolds stresses presented by Launder et al. (6):

$$C_{\overline{u_i u_j}} = D_{\overline{u_i u_j}} + P_{ij} + \phi_{ij} - \epsilon_{ij} \tag{3}$$

where

(convection) $$C_{\overline{u_i u_j}} = \frac{\partial}{\partial x_\ell} (U_\ell \overline{u_i u_j}) ,$$

(diffusion) $$D_{\overline{u_i u_j}} = C_s \frac{\partial}{\partial x_\ell} (\frac{k}{\epsilon} \overline{u_\ell u_m} \frac{\partial \overline{u_i u_j}}{\partial x_\ell}) ,$$

(production) $$P_{ij} = - (\overline{u_i u_\ell} \frac{\partial U_j}{\partial x_\ell} + \overline{u_j u_\ell} \frac{\partial U_i}{\partial x_\ell}) ,$$

(pressure-strain) $$\phi_{ij} = - C_1 \frac{\epsilon}{k} (\overline{u_i u_j} - \frac{2}{3} k \delta_{ij}) - C_2 (P_{ij} - \frac{1}{3} P_{nn} \delta_{ij})$$
$$= (\phi_{ij})_1 + (\phi_{ij})_2, \text{ and}$$

(dissipation) $$\epsilon_{ij} = \frac{2}{3} \epsilon \delta_{ij} .$$

The pressure-strain term is split into two components such that $(\phi_{ij})_1$, which represents the contribution of the turbulence field alone, is modeled using the "return-to-isotropy" term of Rotta(11) and $(\phi_{ij})_2$, which results from the interaction of the mean and the fluctuating field, represents the "rapid" part whose leading term is retained here.

Invoking Rodi's hypothesis (10) results in the following algebraic equations for the Reynolds stresses:

$$\frac{\overline{u_i u_j} - \frac{2}{3} k \delta_{ij}}{k} = \frac{1 - C_2}{C_1 - 1 + \lambda} \frac{P_{ij} - \frac{2}{3} P_k \delta_{ij}}{\epsilon} \qquad (4)$$

where $P_k = P_{nn}/2$ and $\lambda = P_k/\epsilon$, the ratio of local production of turbulent kinetic energy to its dissipation.

For BVM, the Boussinesq eddy viscosity hypothesis,

$$- \overline{u_i u_j} = \nu_t (\frac{\partial U_i}{\partial x_j} + \frac{\partial U_j}{\partial x_i}) - \frac{2}{3} k \delta_{ij} \qquad (5)$$

is used. The transport equations for k and ϵ are given by

$$\frac{\partial}{\partial x_j} (U_j k) = \frac{\partial}{\partial x_j} (\frac{\nu_t}{\sigma_k} \frac{\partial k}{\partial x_j}) + P_k - \epsilon \qquad (6)$$

$$\frac{\partial}{\partial x_j} (U_j \epsilon) = \frac{\partial}{\partial x_j} (\frac{\nu_t}{\sigma_\epsilon} \frac{\partial \epsilon}{\partial x_j}) + C_{\epsilon 1} \frac{\epsilon}{k} P_k - C_{\epsilon 2} \frac{\epsilon}{k}^2 \qquad (7)$$

where

$$\nu_t = \mu_t/\rho = C_\mu k^2/\epsilon \qquad (8)$$

and σ_k and σ_ε are the equivalent turbulent Prandtl numbers for k and ε, respectively.

The model constants used in the BVM are those given by Launder and Spalding (5) which are now recognized as standard for most flow predicions. No such general consensus on the additional model constants C_1 and C_2 has yet been achieved. Presently, the values of $C_1 = 2.2$ and $C_2 = 0.70$, based on the calibration study reported in (14) against the pipe flow data of Laufer (4), are used.

3. Boundary Conditions

For a general elliptic flow in a pipe, the computational domain has three types of boundaries: inflow, outflow, and no flow (solid pipe wall). Both the flow cases considered here permit a fully-developed ($\partial/\partial x = 0$) boundary condition at the outlet. Since the BVM and ASM, in the form presented here, are not valid in the region of low turbulent Reynolds number near the wall, the wall-function approach of Launder and Spalding (5) is used here. With a fully-developed flow at the inlet, while the one-seventh power-law profile is assumed for the mean axial velocity, the following profiles for k_{in} and ε_{in} are used:

$$k_{in} = 0.0013\, U_1^2\, [1 + 4(r/R_1)^{2.5}] \tag{9}$$

$$\varepsilon_{in} = C_\mu^{3/4}\, k_{in}^{3/2}/l_m \tag{10}$$

where the mixing length l_m distribution is computed from the equation (Schlichting, 12)

$$l_m = R_1\, [0.14 - 0.08(r/R_1)^2 - 0.06\, (r/R_1)^4] \tag{11}$$

4. Solution Procedure

For a common solution procedure, the governing transport equations are cast into a common form:

$$\frac{1}{r}\left[\frac{\partial}{\partial x}(\rho U r\phi) + \frac{\partial}{\partial r}(\rho V r\phi)\right] = \frac{1}{r}\left[\frac{\partial}{\partial x}\left(r\Gamma_\phi \frac{\partial \phi}{\partial x}\right) + \frac{\partial}{\partial r}\left(r\Gamma_\phi \frac{\partial \phi}{\partial r}\right)\right] + S_\phi \tag{12}$$

where ϕ represents a general dependent variable, x and r are the axial and radial coordinates, respectively, with corresponding velocity components U and V, Γ_ϕ is a diffusion coefficient, and S_ϕ is the so-called source term. Finite difference equations for each ϕ are obtained by integrating Eq. (12) over an appropriate control volume con- structed around a grid point representing the location for ϕ. The details on deriving the discretized equations in this way are given in Ref. (7). The SIMPLE procedure of Patankar and Spalding (8) is used here to numerically solve these equations.

For the present calculations a 50 x 30 (axial x radial) non-uniform grid is used. The convergence problem encountered in the use of ASM is handled with a dual-loop iteration scheme (14). According to this scheme, the mean flow and turbulence model variables (k and ε) are solved for in an outer loop using Gauss-Seidel line-by-line iteration with under-relaxation. For each outer-loop iteration, the Reynolds

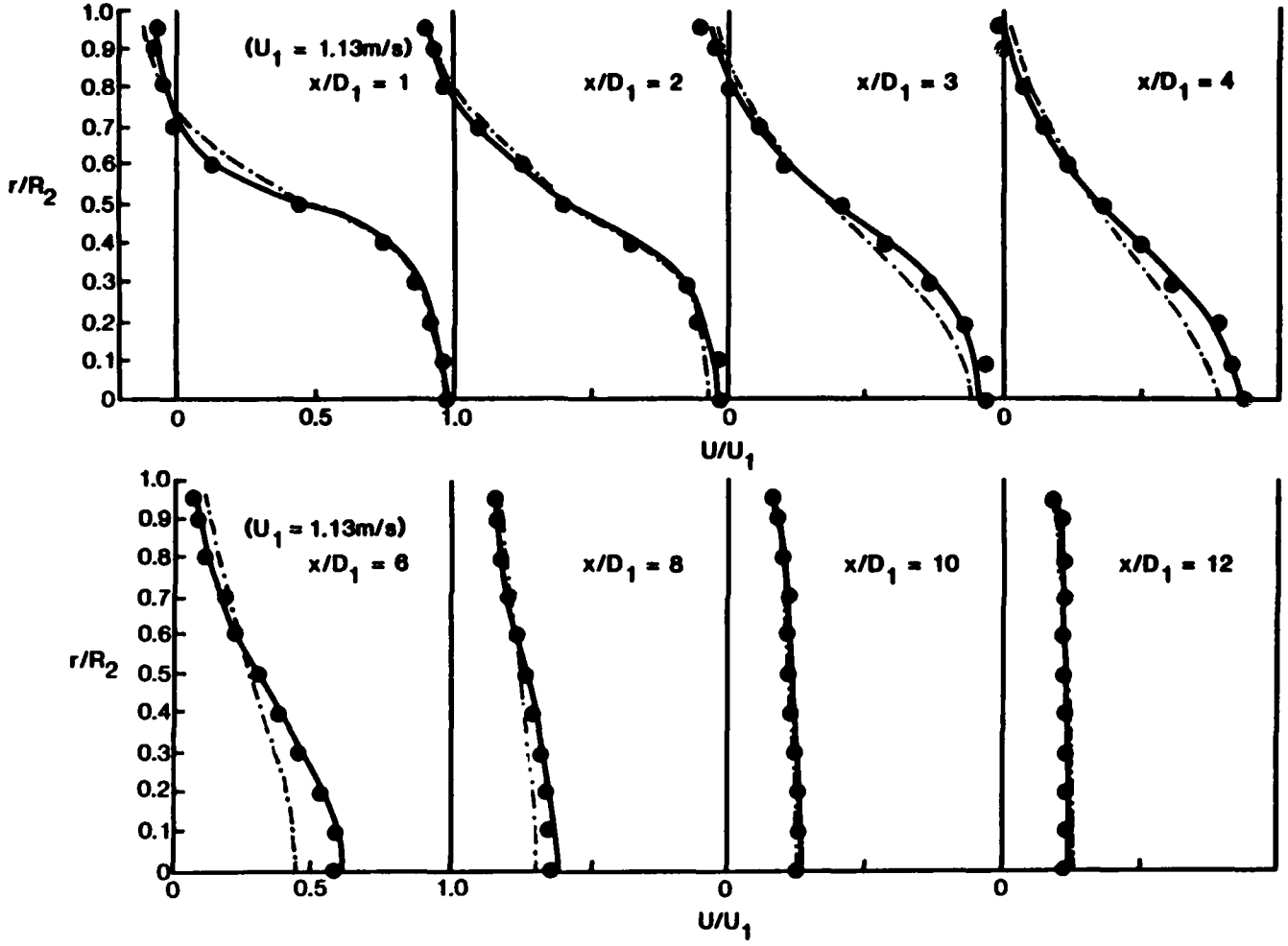

Fig. 2. Mean axial velocity profiles for Re_1 = 60,000 (● Measurement (1), — · — BVM, —— ASM)

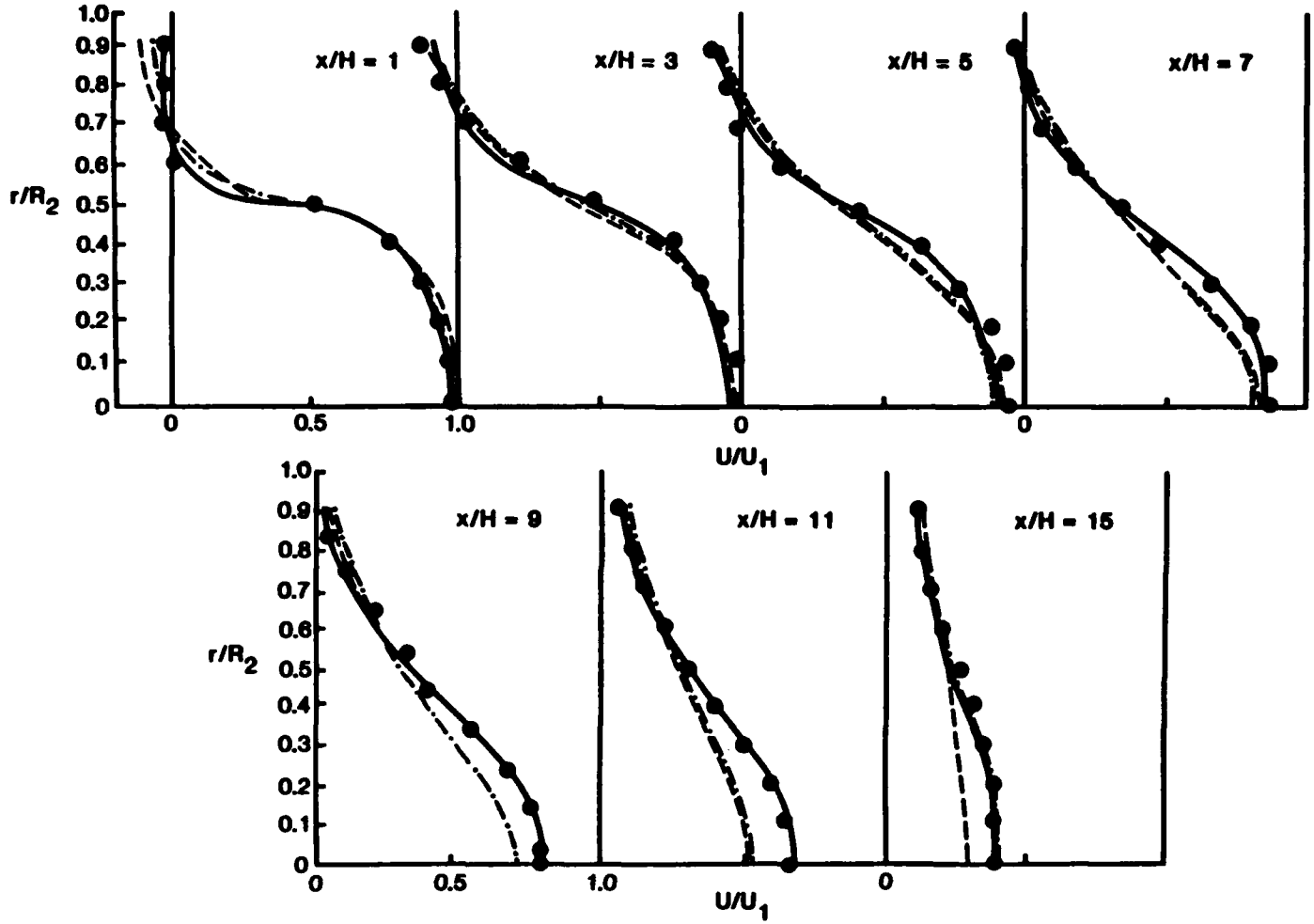

Fig. 3. Mean axial velocity profiles for Re_1 = 110,000 (● Measurement (2), — — — 2/E/FIX (2), —·— BVM, —— ASM)

stresses are computed from Eq. (4) in an inner loop using Gauss-Siedel point iteration with under-relaxation. The outer-loop iterations are terminated according to the convergence criterion based on the "inherent error" of the computational grid; details are given in Ref. (13).

5. Results and Discussion

Parameter values for the two sudden expansion pipe flows considered here for simulation are summed up in Table 1. For Re_1 = 60,000, the calculations of the mean axial velocity distribution with the two turbulence models are compared with the LDV data in Fig. 2 for both the separation (x/D_1 = 1, 2, 3, and 4) and redevelopment (x/D_1 = 6, 8, 10, and 12) regions where D_1 is the inlet pipe diameter. The reattachment length in this case corresponds to x/D_1 = 4.5. The ASM-predictions are seen to be in excellent agreement with the data in both the flow regions. The BMV-results, on the other hand, are significantly different from the experimental data over the latter half of the separation region and also in the near-redevelopment region.

Table 1. Parameter values for the simulated flows

Flow case	Fluid	R_1 (mm)	R_2 (mm)	U_1 (m/s)	Re_1	Data source
1	Water	25.4	49.3	1.13	60,000	(1)
2	Air	38.1	76.2	22.07	110,000	(2)

For the second case with Re_1 = 110,000, the air flow is fully-developed both in the inlet pipe before expansion and at the exit of the downstream pipe corresponding to x/H = 40 where H is the step height ($R_2 - R_1$). In an earlier calculation of this flow by Gould, Stevenson and Thompson (2) using the CHAMPION 2/E/FIX computer code of Pun and Spalding (9), it is found that the degree of agreement with experimental data worsens as one proceeds downstream in the redevelopment region. Since the measured velocity profiles are nearly mass conserving, the computed ones are found to be deficient in this respect which has been attributed to a possible shortcoming in the code used.

The present calculations with BVM and ASM along with the earlier 2/E/FIX prediction for the mean axial velocity are compared with the data in Fig. 3. It is seen that although both the BVM and 2/E/FIX predictions themselves are in good agreement in the recirculation region (x/H = 1, 3, 5, and 7), a better agreement between the data and BVM prediction is seen in the far-redevelopment region (x/H = 15, Fig. 3). The results obtained using the ASM, however, are seen to be in excellent agreement with the data both in the recirculation and redevelopment regions. With this model, a reattachment length of 8.5 step heights is predicted compared to the experimentally observed value of 8.6.

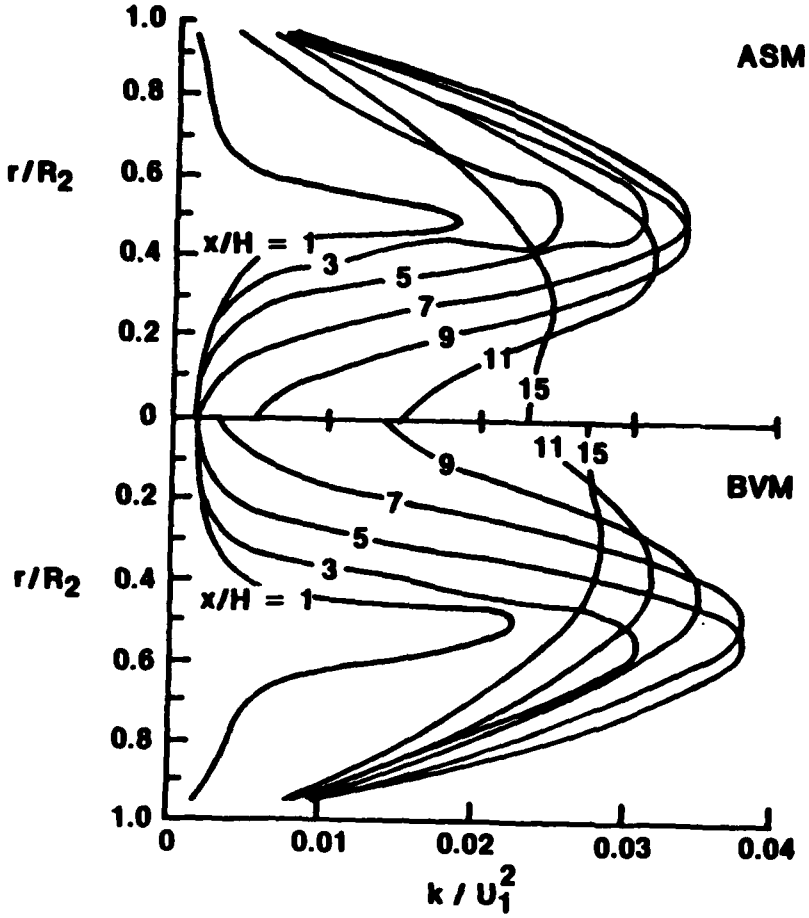

Fig. 4. BVM and ASM results for the distribution of turbulent kinetic energy

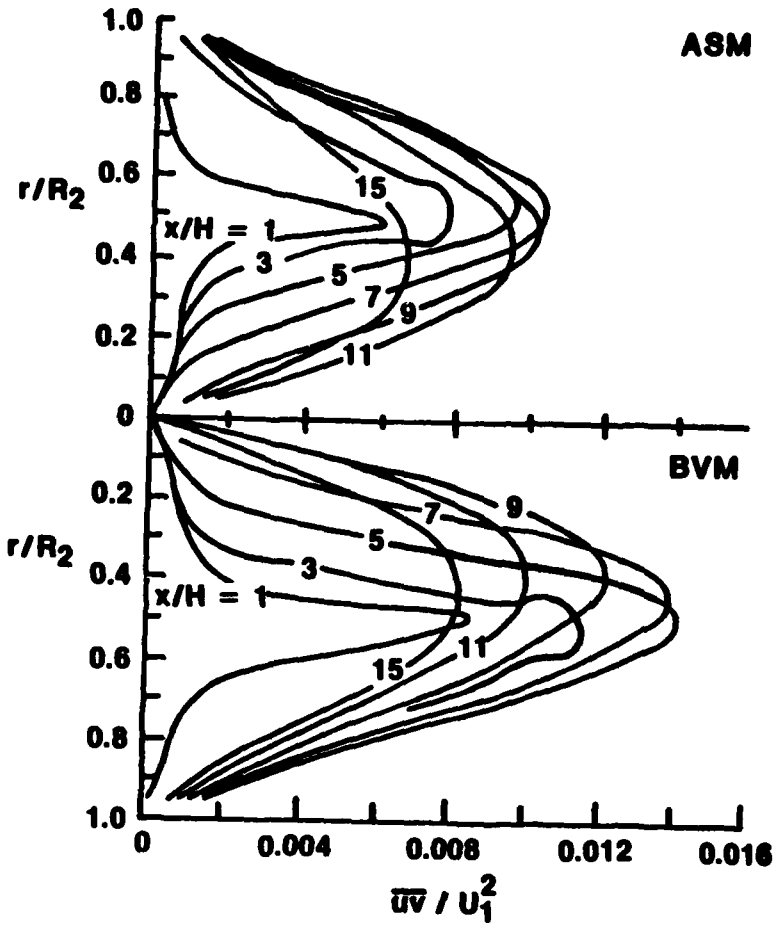

Fig. 5. BVM and ASM results for the distribution of Reynolds shear stress

As shown in Fig. 1, the most important feature of the flow in an sudden axisymmetric expansion is the recirculation region bounded by the dividing streamline and the confining wall. An accurate prediction of reattachment length depends, among other things, on the ability of the turbulence model to simulate the entrainment rate (or the growth rate of the shear layer). The BVM, with its simple eddy viscosity hypothesis, is found to be deficient in this respect, predicting a higher growth rate for the shear layer.

The streamlines in the recirculation region possess a stabilizing curvature resulting in the suppression of both turbulent shear stress and intensity. The BVM, using the model variables k and ε is unable to accurately simulate this vital flow physics. This is because, the Reynolds stress transport equations upon contraction yield the equation for k; the pressure-strain term becomes identically zero. In addition, with the eddy-viscosity assumption, the production term for k involves only the mean-strain terms. Thus, the BVM does not contain any term representing a direct interaction of turbulence with the mean flow. In this respect an important role is played by the "rapid" part $(\phi_{ij})_2$ in the ASM. The results for turbulent kinetic energy (Fig. 4) and turbulent shear stress (Fig. 5) for the two models clearly bring out the superiority of ASM over BVM in successfully predicting the suppression of turbulence by the stabilizing curvature in recirculation region.

6. Concluding Remarks

Two sudden expansion pipe flows with inlet Reynolds numbers of 60,000 and 110,000 are found to be well predited by the ASM in both their recirculation and redevelopment regions. The agreement with the data for these flows represents a significant improvement over the present BVM calculations and an earlier computation of one of the flows using the CHAMPION 2/E/FIX code. A comparison of results for the turbulence field using both the BVM and ASM demonstrates the ability of the latter to simulate the stabilizing effects of streamline curvature in the recirculation region which results in relative suppression of turbulence. It is believed that modeling of the pressure-strain redistribution term in the Reynolds-stress transport equation is accountable for this mechanism which correctly simulates the shear-layer growth and hence the reattachment length.

Acknowledgement

This work was sponsored by the Office of Naval Research under Contract No. N00014-81-K-0428.

References

1. Dellenback, P. A. (1985), Heat Transfer and Velocity Measurements in Swirling Flows through an Abrupt Axisymmetric Expansion, Ph.D. Thesis, Arizona State University, Tempe.

2. Gould, R. D., Stevenson, W. H. and Thompson. H. D. (1983), "Laser Velocimeter Measurements in a Dump Combustor", ASME Paper No. 83-HT-47.

3. Kline, S. J., Cantwell, B. J. and Lilley, G. M. (1981), The 1980-81 AFOSR-HTTM Stanford Conference on Complex Turbulent Flows: Comparison of Computation and Experiment I, II, III, Thermoscience Division, Mechanical Engineering Department, Stanford University, Stanford, California.

4. Laufer, J. (1954), The Structure of Turbulence in Fully Developed Pipe Flow, NACA Tech. Report 1174.

5. Launder, B. E. and Spalding, D. B. (1974), "The Numerical Calculation of Turbulent Flow", Computer Methods in Applied Mechanics and Engineering, Vol. 3, pp. 269-289.

6. Launder, B. E., Reece, G. J. and Rodi, W. (1975), "Progress in the Development of a Reynolds-Stress Turbulence Closure", Journal of Fluid Mechanics, Vol. 68, pp. 537-566.

7. Patankar, S. V. (1980), Numerical Heat Transfer and Fluid Flow, Hemisphere Publication Corporation, New York.

8. Patankar, S. V. and Spalding, D. B. (1974), "A Calculation Procedure for Heat, Mass and Momentum Transfer in Three-Dimensional Parabolic Flows", International Journal of Heat and Mass Transfer, Vol. 15, pp. 1787-1806.

9. Pun, W. M. and Spalding, D. B. (1976), A General Computer Program for Two-Dimensional Elliptic Flows, No. HTS/76/2, Mechanical Engineering Department, Imperial College, London.

10. Rodi, W. (1976), "A New Algebraic Relation for Calculating the Reynolds Stresses", ZAMM, Vol. 56, pp. 219-221.

11. Rotta, J. C. (1951), "Statistische Theorie Nchthomogener Turbulence", Z. F. Physik, Vol. 129, pp. 547-572, Vol. 131, pp. 51-77.

12. Schlichting, H. (1979), Boundary-Layer Theory, McGraw-Hill Book Company, New York.

13. Sultanian, B. K. and Neitzel, G. P. (1984), An Alternate Convergence Criterion for Internal Elliptic Flow Computations, Report No. CR-R-8409, Mechanical and Aerospace Engineering, Arizona State University, Tempe.

14. Sultanian, B. K. (1984), Numerical Modeling of Turbulent Swirling Flow Downstream of an Abrupt Pipe Expansion, Ph.D. Thesis, Arizona State University, Tempe.

Heat Transfer to Turbulent Swirling Flow Through a Sudden Axisymmetric Expansion

P.A. Dellenback, D.E. Metzger, and G.P. Neitzel

to appear, *Journal of Heat Transfer, Trans. ASME.*

Also to be presented at the 1987 ASME/AIChE National Heat Transfer Conference, Pittsburgh, August, 1987

HEAT TRANSFER TO TURBULENT SWIRLING FLOW THROUGH A SUDDEN AXISYMMETRIC EXPANSION

P.A. Dellenback, D.E. Metzger, and G.P. Neitzel
Arizona State University

Experimental data are presented for local heat transfer rates in the tube downstream of an abrupt 2:1 expansion. Water, with a nominal inlet Prandtl number of 6, was used as the working fluid. In the upstream tube, the Reynolds number was varied from 30,000 to 100,000 and the swirl number was varied from zero to 1.2. A uniform wall heat flux boundary condition was employed, which resulted in wall-to-bulk fluid temperatures ranging from 14°C to 50°C. Plots of local Nusselt numbers show a sharply peaked behavior at the point of maximum heat transfer, with increasing swirl greatly exaggerating the peaking. As swirl increased from zero to its maximum value, the location of peak Nusselt numbers was observed to shift from 8.0 to 1.5 step heights downstream of the expansion. This upstream movement of the maximum Nusselt number was accompanied by an increase in its magnitude from 3 to 9.5 times larger than fully developed tube flow values. For all cases, the location of maximum heat transfer occurred upstream of the flow reattachment point.

NOMENCLATURE

D	Diameter of upstream tube
D_2	Diameter of downstream tube
h	Local heat transfer coefficient
H	Step height; $(D_2 - D)/2$
I	Current in tube wall
k	Thermal conductivity of water
m	Mass flow rate
Nu	Nusselt number
Nu_{fd}	Fully developed Nusselt number for turbulent pipe flow represented by Dittus-Boelter or Sieder-Tate equations
Nu_m	Maximum or peak Nusselt number
q	Local heat flux
Q	Total heat input
r	Radial position relative to tube centerline
R	Resistance of tube wall
Re	Reynolds number in upstream tube; Ud/ν
R_1	Upstream tube inside radius
S	Swirl number in upstream tube as defined by

$$S = \frac{1}{R_1} \frac{\int_0^R r^2 \, U \, V \, dr}{\int_0^R r \, U^2 \, dr}$$

T_b	Bulk fluid temperature
T_o	Outside tube wall temperature
T_w	Inside tube wall temperature
U	Local mean axial velocity
U	Axial velocity averaged over cross section
U_1	Maximum axial velocity in upstream tube
V	Local mean tangential velocity
x	Axial distance from expansion face
x_r	Reattachment length
$x/H)_{Nu_m}$	Axial location of peak Nusselt no.

INTRODUCTION

Turbulent swirling flow through an abrupt axisymmetric expansion is a complex flow possessing several distinctly different flow regimes, either one or two recirculation regions, extremely high levels of turbulence, and periodic asymmetries under some conditions. An accompanying elevation of heat transfer rates is a principal motivation for application of these flow configurations in dump combustors of gas turbine engines and in solid fuel ramjet combustors. These applications also take advantage of the flow recirculation regions for flameholding, and of the high mixing rates for enhanced combustion efficiency.

Without swirl, flow through a sudden expansion produces mixing rates, and subsequently, heat transfer coefficients which are substantially higher downstream of the expansion than those which would be obtained at the same Reynolds number in the entrance region of a pipe. This enhancement in diffusion rates occurs in spite of a recirculation region extending about nine step heights downstream from the expansion. In this recirculation region, mean velocities are typically only ten percent as high as those found in the core flow, suggesting that the principle mechanism for heat transfer augmentation is the high turbulence levels which are present. In fact, very high levels of turbulence kinetic energy are generated by shearing as the core flow issues into the larger pipe. Because length scales are large in the shear layer, the

turbulent kinetic energy generated there dissipates relatively slowly maintaining much larger levels than would be found in ordinary pipe flow where no such internal shear layer exists. With high levels of turbulence kinetic energy, diffusion rates are elevated and the thickness of the viscosity dominated sublayer is reduced, resulting in high rates of heat transfer between the tube wall and mean flow.

Several interesting effects appear in the flowfield with the introduction of swirl (Gupta et al., 1984). Among these is an increase in growth rate, entrainment, and decay of the core flow just downstream of the expansion. Consequently, the flow reattachment zone moves upstream as swirl strength is increased. Swirl is also responsible for increased shear rates, greater turbulence production, and longer path lengths for a particular fluid particle so that the effect of swirl, like the effect of the sudden expansion, is also to significantly increase heat transfer rates over those found in purely axial pipe flow (Hay and West, 1975).

A further complex phenomenon which frequently occurs in swirling flows is the development of an unsteady (although usually periodic) asymmetry in the flowfield. These asymmetries are not fully understood, but it is known that they may assume many different forms depending on flow geometry and swirl strength (Dellenback, 1986; Leibovich, 1984; Hallett and Gunther, 1984). At low swirl levels in

the present study, the core flow departed from axial symmetry in the neighborhood of the expansion and then proceeded to precess about the tube centerline (Dellenback). This flow feature is referred to here as the precessing vortex core (PVC) after Gupta et al. (1984). In most geometries the PVC is only seen for swirl strengths large enough to produce a 'bubble' of on-axis recirculating fluid, known as vortex breakdown. However, in the present investigation (and in the work of Hallett and Gunther), oscillatory flow asymmetries were only detected at swirl numbers less than those associated with vortex breakdown. Specifically, the PVC was only present at the lowest non-zero swirl number for each of the three Reynolds numbers examined in this study. Flowfields at higher swirl numbers were symmetric with no apparent PVC (Dellenback).

Present computational capabilities are only able to successfully treat some of the simpler limiting cases of the present problem (Sultanian et al., 1985). Thus the purpose of the present investigation was to measure heat transfer characteristics throughout the separation, reattachment, and redevelopment regions in the downstream tube for a variety of flow conditions.

The present study began with an extensive characterization of the turbulent flowfield throughout the downstream tube and at two locations upstream of the expansion. A laser Doppler anemometer (LDA) was used to determine axial and tangential mean velocities in

conjunction with the two associated normal stresses for nine of the twelve flow conditions reported herein. Upstream profiles for the other three cases were measured so that the present heat transfer data could be correlated with swirl number. Because the swirl number was determined from integration of velocity profiles, it was essentially a dependent variable in these experiments and this accounts for its variability between Reynolds numbers in the following data. Only a summary of the mean velocity field is included in the present paper because of space limitations. Tabular data and additional details, including PVC observations, are described by Dellenback (1986).

PREVIOUS INVESTIGATIONS

A number of experiments have been reported which examine heat transfer to purely axial flows through a sudden pipe expansion (Ede et al., 1956; Ede et al., 1962; Krall and Sparrow, 1966; Zemanick and Dougall, 1970; and Baughn et al., 1984). However, there have apparently been no heat transfer investigations that incorporated swirl in the sudden expansion geometry. Thus the prior unswirled investigations are important to the present study as a limiting case which can be compared to the present data. Important conclusions from the extensive measurements of Krall and Sparrow (1966) and Zemanick and Dougall (1970) can be summarized as follows:

a) Nu/Nu_{fd} is a weak function of Reynolds number for air, but is a strong function of Reynolds number for water.

b) Maximum Nusselt numbers are well correlated by $Nu_m = C\ Re_d^{2/3}$, where C = 0.20 for air and 0.40 for water.

c) Locations of peak Nusselt numbers move slightly upstream with increasing expansion ratio, but show little dependence on Reynolds number.

Recently, Baughn et al. (1984) reported an extension to Zemanick and Dougall's (1970) work. In previous experiments, the region just downstream of the expansion has been subject to relatively high rates of heat conduction in the tube wall with consequently high uncertainty in the heat transfer coefficients. Baughn et al. (1984) devised a test section specifically to minimize the axial conduction problem, thus defeating an effect which they suggest introduced error into Zemanick and Dougall's data. For several expansion ratios, a minimum in the Nusselt number was observed at about one step height downstream and the authors suggest that this is possible evidence for a very small, counter-rotating corner-eddy.

Habib and McEligot (1982) reported an ambitious calculation of the flowfield and related heat transfer behavior for the present problem, including swirl. Their published results appear to underpredict the peak Nusselt number which is interpolated from the data of Zemanick and Dougall (1970) by about 50% for an unswirled flow with

Re = 50,000, β = 0.5, and Pr = 0.7. However, they did find the reattachment zone for unswirled flow to be centered at a generally accepted value of 8.2 step heights, while the corresponding location of peak Nusselt number occurred at 6.5 step heights.

EXPERIMENTAL APPARATUS

A stainless steel water flow loop comprised the main element of the test facility. Swirl was generated by tangential slots as shown in Figure 1. Inside diameters of the axial inlet tube, the swirler insert, and the upstream test section were 5.08 cm. The sudden expansion was 12 diameters downstream of the swirl generator and the axial inlet tube was 31 diameters long to allow axial flow development. Flowrates to the slots and the axial inlet tube could be controlled independently, thus giving capability for a continuously variable swirl strength. Flowrates of the tap water used in the loop were measured with turbine-type flowmeters. The flow loop included an on-line deaerator for removing air which tended to leave solution as a result of elevated water temperatures near the tube wall.

The axial and tangential components of mean and RMS velocities were measured, one at a time, with a single-component LDA. The profiles were taken at locations both upstream and downstream of the expansion using Plexiglas

test sections. Details of the optical system, data analysis, and procedures are described by Dellenback (1986).

Following the flowfield measurements, heat transfer tests were performed in a horizontal stainless steel tube by passing direct current in the tube wall. The steel heat transfer test section was of the same dimensions as the acrylic test section used for the velocity measurements. Heating began at, but did not include, the face of the sudden expansion, as shown in Figure 2. The unheated upstream tube (inside diameter of 5.08 cm) and the expansion face were the same Plexiglas components used in the flowfield measurements. The tube downstream of the expansion was a commercially available stainless steel tube with an inside diameter of 9.98 cm, a wall thickness of 0.89 mm, and a length of 1.04 m. Consequently, the expansion ratio was 1.97:1. Stainless steel flanges were carefully attached to each end of the tube by very shallow welds at the extreme ends of the tube. Although the flange-to-tube fit was snug, it was assumed that all of the electrical current passed through the weld and thus power was dissipated over the full 1.04 m length of the tube. This assumption was important to the computation of heat flux and to determining the location of the point of maximum heat transfer since the flanges were relatively thick at 1.27 cm or 0.5 step heights.

Conduction losses from the heated test section to the upstream tube and expansion face were minimal since the

thermal conductivity of Plexiglas is relatively low. Heat transfer to the mixing plenum immediately downstream of the test section was minimized by a 1.27 cm-thick spacer made from a machinable dielectric (Melamine) which was placed between the test section's flange and the plenum. Finally, nylon bolts were used to secure the test section to the plenum to further minimize conduction heat losses.

Copper electrical busses consisting of an inner ring and an outer ring connected by six spokes were machined from a single plate 1.27 cm-thick. The busses joined current carrying cables to the stainless steel flanges of the test section. Experience showed that a liberally applied film of copper-based anti-seize compound between the bus and flange would decrease electrical contact resistance and consequent heat generation. A dedicated 108 kW direct current power supply was coupled via seven 2.5 cm-diameter cables to the outer rims of each bus. Two water-carrying copper tubes were soldered around the periphery of the busses' outer rim for the purpose of guard heating or cooling. Each bus had two pairs of thermocouples imbedded in such a way that temperature gradients across the spokes could be monitored. Due to the large power levels employed in these experiments (22 kW at 8.5 V and 2600 A), ohmic heating in the cables proved to be the dominant heat source in the power connection scheme. Hence, guard cooling was always performed to minimize temperature gradients in the spokes of

the bus and heat conduction from the cables to the bus, and in turn, to the test section.

The tube-wall temperature distributions were measured with commercially available copper-constantan thermocouples mounted on the outside of the tube. The junction of each thermocouple was sandwiched between two 51 μm-thick glass-reinforced polymer-laminate films to provide electrical insulation from the test section. A high thermal conductivity paste was applied between the thermocouples and the test section. Flat, well insulated steel bands encircling the test section held the thermocouples tightly in place. Nineteen thermocouples were employed, spaced at smaller intervals near the upstream end of the test section to provide high resolution in the region of rapidly changing heat transfer coefficients. Four inches of fiberglass insulation surrounded the test section and flanges, and all but the outer rim of the electrical busses.

Power input levels to the working fluid were deduced in two ways. In the first, power was taken as the current-voltage product after measuring the voltage drop across both a shunt and the test section. A thermocouple was affixed to the copper shunt to correct for temperature dependent resistivity. Input power was also determined from the measured fluid enthalpy rise through the test section. To this end, bulk fluid temperatures were measured at the inlet and outlet of the test section with immersion thermocouples.

Over the range of test conditions, wall-to-bulk fluid temperatures ranged from 14°C to 50°C.

PROCEDURES AND DATA REDUCTION

The 22 kW power levels produced heat fluxes on the order of 6.7 W/cm^2. After applying power to the test section, the time required for the loop to reach steady state was between 30 and 60 minutes.

For most trials, the wall-temperature measuring thermocouples were located along the top of the tube. However, in order to examine the influence of natural convection on the present problem, for at least one of the multiple trials at each flow condition the entire test section (with thermocouples still attached) was removed, rotated 180° about the tube axis, and reinstalled so that the temperature measurements could be made along the bottom of the tube.

Local heat transfer results are presented in terms of Nusselt numbers normalized with those for fully developed non-swirling flow, where

$$Nu = \frac{h\ D_2}{k} \quad . \tag{1}$$

Here, D_2 is the downstream tube diameter, k is the thermal conductivity of water evaluated at the local film temperature, and h is the local heat transfer coefficient defined as

$$h = \frac{q}{T_w - T_b} \quad . \tag{2}$$

The local heat flux is designated by q, the local wall temperature by T_w, and the local bulk temperature by T_b. Because wall-to-bulk fluid temperature differences were moderate-to-large, and hence property variations appreciable, the Sieder-Tate correlation (Kern, 1950) was used to evaluate reference Nusselt numbers for the corresponding fully-developed flow without swirl:

$$Nu_{fd} = 0.027\ Re^{.8}\ Pr^{1/3}\ (\mu/\mu_w)^{0.14} \quad . \tag{3}$$

All fluid properties used in eqn. (3) were evaluated at the local bulk temperature except μ_w, which was evaluated at the local wall temperature.

Although the present experiments have a nominally uniform heat flux boundary condition, the local heat fluxes are not strictly uniform due to both the temperature dependence of tube material properties and axial heat conduction in the tube wall. The procedure used for finding the local heat fluxes began by dividing the wall into 19 control volumes corresponding to the 19 wall-temperature thermocouples. The magnitude of Joule heating in each volume was determined from I^2R, where a linear curve fit of the temperature dependent resistivity of the stainless steel (Touloukian, 1967) test section was used. Heat loss from the outside of the tube wall through the fiberglass insulation which surrounded the test section was assumed negligible. This loss was eventually calculated to be no more than 0.05% of the total power input in a worst case

analysis of the data. The wall temperature (T_w) in eqn. (2) is the temperature of the inside surface of the test section wall. Because exterior surface temperatures were actually measured, the interior surface temperatures were determined from the solution of the one-dimensional heat conduction equation for a cylindrical shell. This procedure assumes that only radial conduction is important, an assumption that must be justified since natural convection may cause slight asymmetry in circumferential temperature profiles. Also, the axial variation in heat transfer coefficients gives rise to axial temperature gradients and conduction in the tube wall. However, both circumferential (discussed below) and axial temperature gradients were examined and found to be small compared to those in the radial direction. A worst case computation of axial heat flux for the present results showed that, at most, the net heat conducted out of a tube wall element to an adjacent element was about 1% of the Joule heat generated in that element, even near the test section flanges.

Determining the local heat flux and inside wall temperature is inherently an iterative process, but one which converges suitably in one iteration because the temperature differences across the tube wall are small (typically on the order of 2°C). The maximum variation in local heat flux between any two locations on the tube was eventually calculated to be less than 1.5%. Finally, to be consistent in methodology, local water enthalpies and bulk

temperatures were computed from an energy balance which considered the local, slightly non-uniform, heat input.

The methods of Kline and McClintock (1953) were employed to determine that the largest uncertainties are about 2% in upstream Reynolds number and 8% in swirl number. The highest uncertainties in Nusselt numbers were computed to be about 9%, with these occurring near the location of peak Nusselt number where wall-to-bulk temperature differences were smallest. Details of the analysis and tabular data are given in the dissertation by Dellenback (1986).

RESULTS AND DISCUSSION

In the figures which follow, the axial coordinate is non-dimensionalized with the upstream tube diameter (D). The swirl numbers shown on the plots were evaluated from velocity profiles measured two diameters upstream of the expansion. Similarly, Reynolds numbers are based on properties and mean velocities in the upstream tube.

Summary of the Flowfield. Figures 3 and 4 show typical mean velocity profiles for various swirl levels at Re = 100,000. All mean velocities (and the turbulence intensities referred to below) were normalized using the maximum axial velocity in the upstream tube. Data for unswirled flows agreed very well with the recent LDA data of Stevenson et al. (1983), but flow predictions of Habib and

McEligot (1982) for strongly swirled flows are in only fair agreement as to locations of peak velocities near the expansion and extents of recirculation regions.

Flow conditions upstream of the expansion varied greatly with swirl number. Upstream velocity profiles for the lowest swirl case at each Reynolds number closely approximated solid body rotation plug-flow. Figure 3 shows that with increasing swirl number the highest axial velocities move toward the tube wall. Near the tube centerline, large gradients in the mean tangential velocity are responsible for turbulence intensities on the order of 30%. Turbulence diffuses away from the tube's axis with both the axial and tangential turbulence intensities decreasing rapidly to about 12% between r/R = 0.2 and the wall.

Prandtl numbers of the fluid entering the heated test section were 5.1 at Re = 100,000; 5.8 at Re = 60,000; and from 5.9 to 6.7 for Re = 30,000. This variation in Prandtl number is probably insignificant when examining the present results, as suggested by the near congruence of Krall and Sparrow's (1966) data for Prandtl numbers of 3 and 6.

Axial Heat Transfer Variations. Figures 5-7 show the measured axial variations in normalized Nusselt number as a function of swirl for nominal Reynolds numbers of 30,000, 60,000, and 100,000, respectively. The peak Nusselt numbers increase consistently in magnitude and move upstream with increasing swirl strength. This upstream migration of Nu_a

is a direct result of the shortening reattachment length discussed previously. The shortening of the recirculation region causes shear rates and hence production of turbulence kinetic energy to increase with consequently higher heat transfer rates. This enhancement is also promoted by higher local mean velocities as the tangential velocity component increases at nominally constant values of mean axial velocity.

Comparison of the unswirled flow results from Figures 5-7 demonstrate that larger enhancements in heat transfer rates over straight pipe flow occur at lower Reynolds numbers. This feature is simply rationalized by the observation that convection heat transfer behavior in separated flow is commonly found to depend on $Re^{2/3}$ (Krall and Sparrow, 1966; Zemanick and Dougall, 1970), so that when Nusselt numbers are normalized with a fully-developed tube-flow value which depends on $Re^{0.8}$, the ratio depends on $Re^{-0.13}$. For zero swirl, the recovery to fully-developed flow Nusselt numbers occurs faster with increasing Reynolds number. Nusselt numbers are strongly influenced by turbulence intensity, which velocity field measurements gave as $\approx$ 8% for Re = 30,000 and $\approx$ 3% for Re = 100,000 at the end of the test section. The turbulence intensities have relaxed more quickly in the latter case due to higher rates of dissipation at the larger Reynolds numbers (Laufer, 1954).

Table 1 gives a summary of peak Nusselt numbers (Nu_m), locations of Nu_m (x/H_{Nu}), and reattachment lengths (x_r/H) for the flows examined in this study. Because there was an inevitable limit to the spatial resolution of the temperatures which could be attained, magnitudes and locations of the maximum Nusselt numbers which are tabulated in Table 1 were determined by interpolation of expanded scale plots of local Nusselt numbers in this region. The tabular results show that the locations of maximum Nusselt number are largely Reynolds number independent, consistent with the unswirled results of investigations discussed previously.

Maximum Nusselt numbers are shown for the present data and five other investigations in Figure 8. The present unswirled data for Nu_m fit comfortably among similar water data which show the $Re^{2/3}$ dependence mentioned above. However, at the larger swirl numbers there is a slight, but noticeable decrease in the slope of the curves. Although the swirl number is not a fixed value at each Reynolds number, we may tentatively infer from Figure 8 that Nu_m depends approximately on $Re^{0.46}$ for a fixed swirl number in the range, $0.60 < S < 1.23$. Thus it appears that heat transfer enhancement due to swirl alone does contain some Reynolds number dependence.

Figure 9 contrasts the locations of maximum Nusselt number with the flow reattachment points determined from LDA measurements. Although it is often assumed that the peak

Nusselt number occurs at the reattachment point (Krall and Sparrow, 1966; Zemanick and Dougall, 1970), for this work it fell consistently upstream of the reattachment point for all swirl numbers. The axial distance is non-dimensionalized with the step height (H) of the expansion in Figure 9 since reattachment lengths have been frequently shown to correlate well with this length scale.

Maximum Nusselt numbers display a consistent behavior as swirl number is varied at constant Reynolds number, as shown in Figure 10. These curves lead to speculation that swirl influence on heat transfer may be expressible as a power law, as for example in the work of Hay and West (1975), where $Nu/Nu_{fd} = (S + 1)^{1.75}$ for free swirling flow in a constant diameter pipe. However, an indirect influence of the sudden expansion is that it causes the swirl number to change dramatically just downstream of the expansion (Gupta et al., 1984; Dellenback, 1986), and this feature, along with the difficult-to-specify relationship between Nu_m and Reynolds number, have thus far defeated efforts to separate quantitatively the effects of separation and swirl in the present results.

Computed differences between the two methods which are available for determining energy balances are also shown in Table 1 (as '% difference in Q'). Incomplete mixing in the downstream plenum is believed to be largely responsible for the discrepancies by giving larger than actual downstream bulk temperatures. This hypothesis is consistent with the

downstream thermocouple's location which would be within the wall boundary layer if the test section extended approximately 30 cm into the plenum. In almost every case, $\Sigma(I^2R)$ was smaller than $mC_p\Delta T_b$, which is also supportive of the present hypothesis but contrary to normal expectation, where heat losses usually cause the fluid enthalpy rise to be less than the power input.

Rapidly fluctuating wall temperatures were observed at low Reynolds and swirl number combinations, indicating a random unsteadiness at these flow conditions. For example, at Re = 30,000 (for both S = 0 and 0.14) wall temperatures were repeatedly observed to fluctuate by as much as ±4°C over a short time interval of about two seconds, but these fluctuations were not periodic. Similarly, for Re = 60,000 (both S = 0 and 0.18), fluctuations were on the order of ±2°C for the same time frame. When these fluctuations occurred at the lowest swirl strength, there was no apparent correlation with the PVC previously mentioned. Also, because the unsteadiness was apparent for the unswirled flow as well as the weakly swirled flow, it is plausible that the fluctuations are a consequence of slight shifts of the reattachment point within a small, but finite, zone of reattachment. At higher Reynolds and swirl numbers (for which the reattachment zone is narrower), these large fluctuations disappeared.

Impact of Free Convection. The influence of free convection on heat transfer in these experiments was

believed to be minimal, especially for the swirled flows since swirl tends to overpower secondary flow generated by buoyancy forces. Hence, temperature asymmetry was not expected, and indeed, none was found in any of the tests where swirl was present.

The measured wall-to-fluid temperature differences were used to compute the largest possible Rayleigh numbers (based on tube diameter) for each flow case. The extreme Rayleigh numbers were found to range from $1.2 - 3 \times 10^9$ and reference to the maps of free, mixed, and forced convection regimes compiled by Metais and Eckert (1964) suggest free convection should have little or no impact on the overall heat transfer for these Rayleigh numbers, even without the presence of swirl. It is only for Re = 30,000, where temperature differences were large, that the Rayleigh numbers indicate a proximity to the mixed convection regime where temperature asymmetries might be expected in the absence of swirl.

Further indication that free convection did not make a significant contribution to the overall heat transfer in these experiments may be deduced by comparing Nusselt numbers for runs where the thermocouples were fixed along the top of the tube to those runs where temperatures were measured along the bottom of the tube. Inspection of the results showed that, for all swirled flows, local Nusselt numbers deduced from these two orientations were indistinguishable. For unswirled flows, the only clear

contribution by free convection occurred at the last four downstream measurement stations for Re = 30,000. For consistency in comparing low swirl and low Reynolds number cases, only runs where all temperature measurements were made using the bottom-mounted thermocouples have been used in this presentation.

Comparison with Previous Investigations. Comparison of the present results with those of other investigations is limited to the case of unswirled flows for which data are readily available. Figure 11 shows one such comparison for 86,400 < Re < 101,000. The comparison is based on normalized Nusselt numbers, but since fully-developed Nusselt numbers used for normalization were obtained in a different manner for each study, this can present problems when comparing results. For example, if the present results had been normalized using the Dittus-Boelter relation rather than the Sieder-Tate correlation, then peak values of Nu/Nu_{fd} would have been 8% larger for Re = 100,000 (and about 11% larger for Re = 30,000) than the values shown in Figures 5-7 and 11. However, a study by Malina and Sparrow (1964) concluded that the Sieder-Tate relation over-predicts variable-property enhancement of heat transfer by about 4% while the Dittus-Boelter relation under-predicts fully-developed tube flow Nusselt numbers by 6-11% in the Reynolds and Prandtl number ranges of the present data. Thus the results of Malina and Sparrow suggest that the apparent 10% difference in Nu/Nu_{fd}, which is due to the choice of a

correlation for normalization, may in fact be much smaller. For the work of Krall and Sparrow (1966), the data of Malina and Sparrow were used to obtain fully-developed Nusselt numbers, but the effect of employing the Dittus-Boelter relation would be to increase the peak Nu/Nu_{fd} ratio by 5-10% over their values shown in Figure 11. To complicate the comparison further, Zemanick and Dougall (1970) used their own downstream data for normalization, while the data of Baughn et al. (1984) and Ede et al. (1956, 1962) are normalized with the Dittus-Boelter relation. In any event, the Nusselt numbers of Krall and Sparrow's appear somewhat high at several Reynolds numbers. It seems reasonable to conclude that the vena-contracta produced by their orifice makes the effective expansion ratio larger than 2:1, and it has been clearly demonstrated (Krall and Sparrow; Zemanick and Dougall; Baughn et al.) that peak Nusselt numbers increase with increasing expansion ratio. The present results exhibit very good agreement with the recent results of Baughn et al., particularly at small x/D. This provides confidence in the present results since the principle motivation for the work of Baughn et al. was to minimize axial heat conduction, especially in the near expansion region where measurement inaccuracies are usually largest.

CLOSURE

The principal contribution of the present results is to specify the quantitative effect of swirl on the heat transfer enhancement for the flow downstream of a sudden axisymmetric expansion. Local heat transfer rates have been shown to increase dramatically in the separated flow region and to peak just upstream of the flow reattachment point. The results also show that the location of peak Nusselt number is a strong function of swirl number. However, the locations of maximum heat transfer rate are found to be largely Reynolds number independent, particularly at higher swirl numbers.

ACKNOWLEDGEMENTS

The work reported here was supported by the Office of Naval Research.

REFERENCES

Baughn, J.W., Hoffman, M.A., Takahashi, R.K. and Launder, B.E., 1984, "Local Heat Transfer Downstream of an Abrupt Expansion in a Circular Channel with Constant Wall Heat Flux," *ASME Trans.-J. of Heat Transfer*, Vol. 106, pp. 789-796.

Dellenback, P.A., 1986, "Heat Transfer and Velocity Measurements in Turbulent Swirling Flow Downstream of an Abrupt Axisymmetric Expansion," Ph.D. Dissertation, Arizona State Univ.

Ede, A.J., Morris, R. and Birch, E.S., 1962, "The Effect of Abrupt Changes of Diameter on Heat Transfer in Pipes," *Nat. Eng. Lab. Report no. 73,* East Kilbride, Glasgow, Scotland.

Ede, A.J., Hilsop, C.J. and Morris, R., 1956, "Effect on the Local Heat Transfer Coefficient in a Pipe of an Abrupt Disturbance of the Fluid Flow: Abrupt Convergence and Divergence of Diameter Ratio 2/1," *Inst. of Mech. Engs. (London)*, Proc. 170, no. 38, pp. 1113-1126.

Gupta, A.K. Lilley, D.G. and Syred, N., 1984, *Swirl Flows*, Abacus Press, Tunbridge Wells, Kent.

Habib, M.A. and McEligot, D.M., 1982, "Turbulent Heat Transfer in a Swirl Flow Downstream of an Abrupt Pipe Expansion," *Proc. of the 7th Int. Heat Transfer Conf.*, Washington, D.C., pp. 159-165.

Hallett, W.L.H. and Gunther, R., 1984, "Flow and Mixing in Swirling Flow in a Sudden Expansion," *Canadian J. of Chem. Eng.*, Vol. 62, pp. 149-155.

Hay, N. and West, P.D., 1975, "Heat Transfer in Free Swirling Flow in a Pipe," *ASME Trans.-J. of Heat Transfer*, Vol. 97, pp. 411-416.

Kern, D.Q., 1950, *Process Heat Transfer*, McGraw-Hill, New York.

Kline, S.J. and McClintock, F.A., 1953, "Describing Uncertainties in Single-sample Experiments," *Mechanical Engineering*, Vol. 75, no. 1, pp. 3-8.

Krall, K.M. and Sparrow, E.M., 1966, "Turbulent Heat Transfer in the Separated, Reattached, and Redevelopment Regions of a Circular Tube," *ASME Trans.-J. of Heat Transfer* Vol. 88, pp. 131-136.

Laufer, J., 1954, "The Structure of Turbulence in Fully Developed Pipe Flow," *NACA Tech Report 1174.*

Leibovich, S., 1984, "Vortex Stability and Breakdown: Survey and Extension," *AIAA J.*, Vol. 22, pp. 1192-1206.

Malina, J.A. and Sparrow, E.M., 1964, "Variable-property, Constant-property, and Entrance-region Heat Transfer Results for Turbulent Flow of Water and Oil in a Circular Tube," *Chem. Eng. Sci.*, Vol. 19, pp. 953-962.

Metais, B. and Eckert, E.R.G., 1964, "Forced, Mixed and Free Convection Regimes," *ASME Trans.-J. of Heat Transfer*, Vol. 86, pp. 295-296.

Stevenson, W.H., Thompson, H.D. and Gould, R.D., 1983, "Laser Velocimeter Measurements and Analysis in Turbulent Flows with Combustion, part II," AFWAL-TR-82-2076.

Sultanian, B.K., Neitzel, G.P., and Metzger, D.E., 1985, "Turbulent Flow Predictions in a Sudden Axisymmetric Expansion," *Proc., Int. Symp. on Refined Flow Modeling and Turbulence Measurements*, B22.

Touloukian, Y.S. (editor), 1967, *Thermophysical Properties of High Temperature Solid Materials, Vol. 3: Ferrous Alloys*, Thermophysical Properties Research Center, Purdue Univ., McMillan.

Zemanick, P.P. and Dougall, R.S., 1970, "Local Heat Transfer Downstream of Abrupt Circular Channel Expansion," *ASME Trans.-J. of Heat Transfer*, Vol. 92, pp. 53-60.

Reynolds Number	Swirl Number	T/C loc	% diff in Q[1]	Nu_m	$\frac{Nu_m}{Nu_{fd}}$	$\frac{x^{(2)}}{H_{Nu_m}}$	$\frac{x_r}{H}$
30,200	0	Bot	+1.4	430	3.7	7.7	9.1
29,800	.14	Bot	-1.8	550	4.8	3.8	-
30,600	.60	Top	-1.8	960	8.1	2.0	2.4
30,800	.98	Top	-1.3	1130	9.5	1.5	1.9
61,100	0	Bot	-12.3	610	3.0	8.0	9.0
60,600	.18	Bot	-0.5	960	4.9	3.4	-
61,600	.77	Top	-0.5	1280	6.5	1.9	2.2
60,800	1.16	Top	-1.4	1540	8.0	1.4	1.8
101,400	0	Top	-9.6	850	3.1	8.5	9.0
100,300	.17	Top	-4.9	1230	4.4	2.8	-
100,000	.74	Top	-2.3	1670	6.0	2.0	2.2
99,800	1.23	Top	-4.1	1970	7.1	1.4	1.8

[1] % difference in Q employs $\dot{m}C_p\Delta T$ as the reference value
[2] Locations of Nu_m determined from average of several runs

Table 1

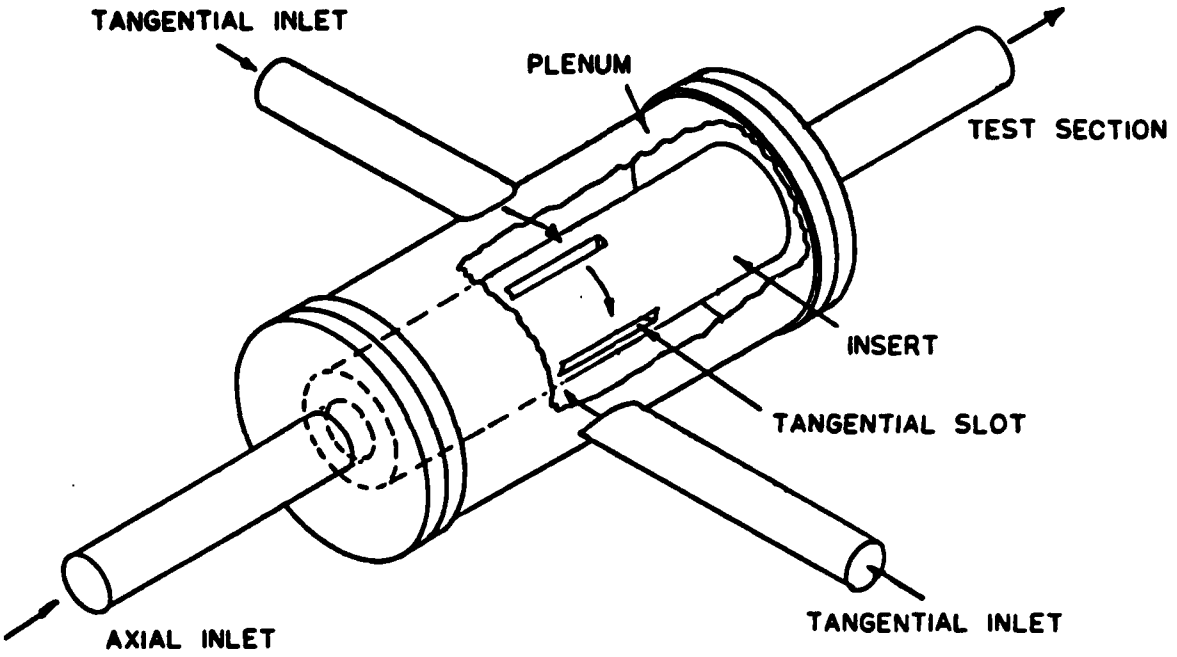

Fig. 1 Detail of the swirl generator

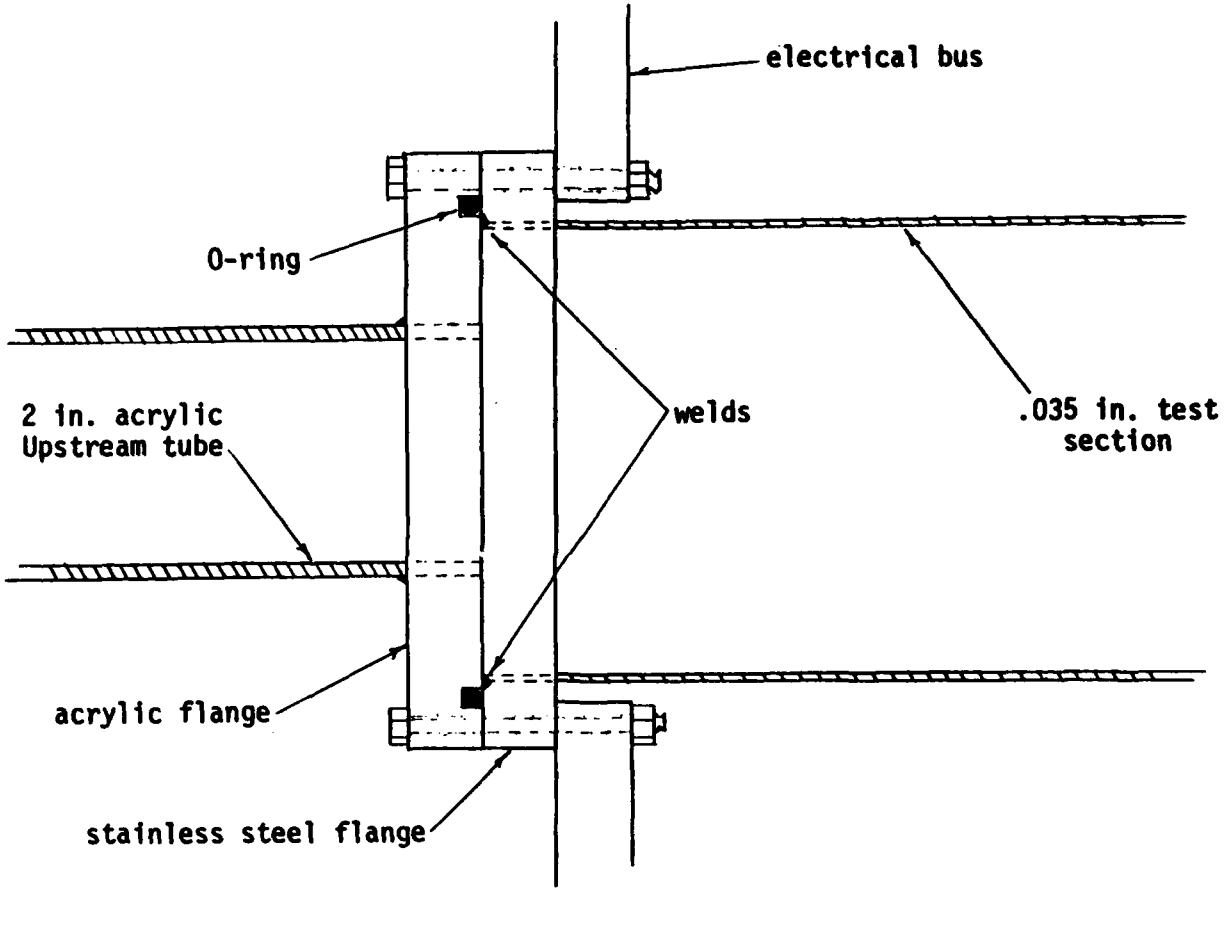

Fig. 2 Detail of the test section near the expansion

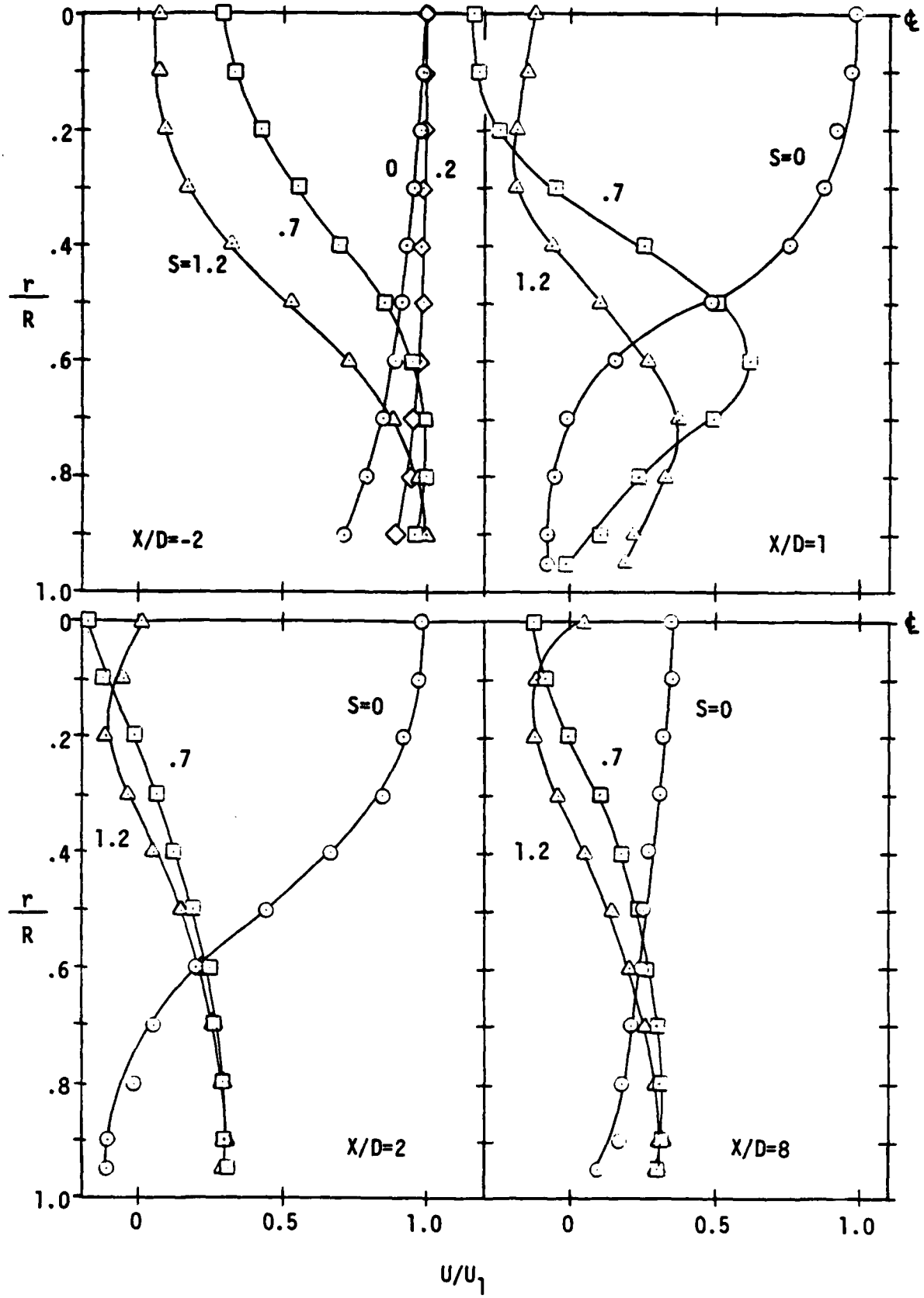

Fig. 3 Axial velocity profiles for Re = 100,000

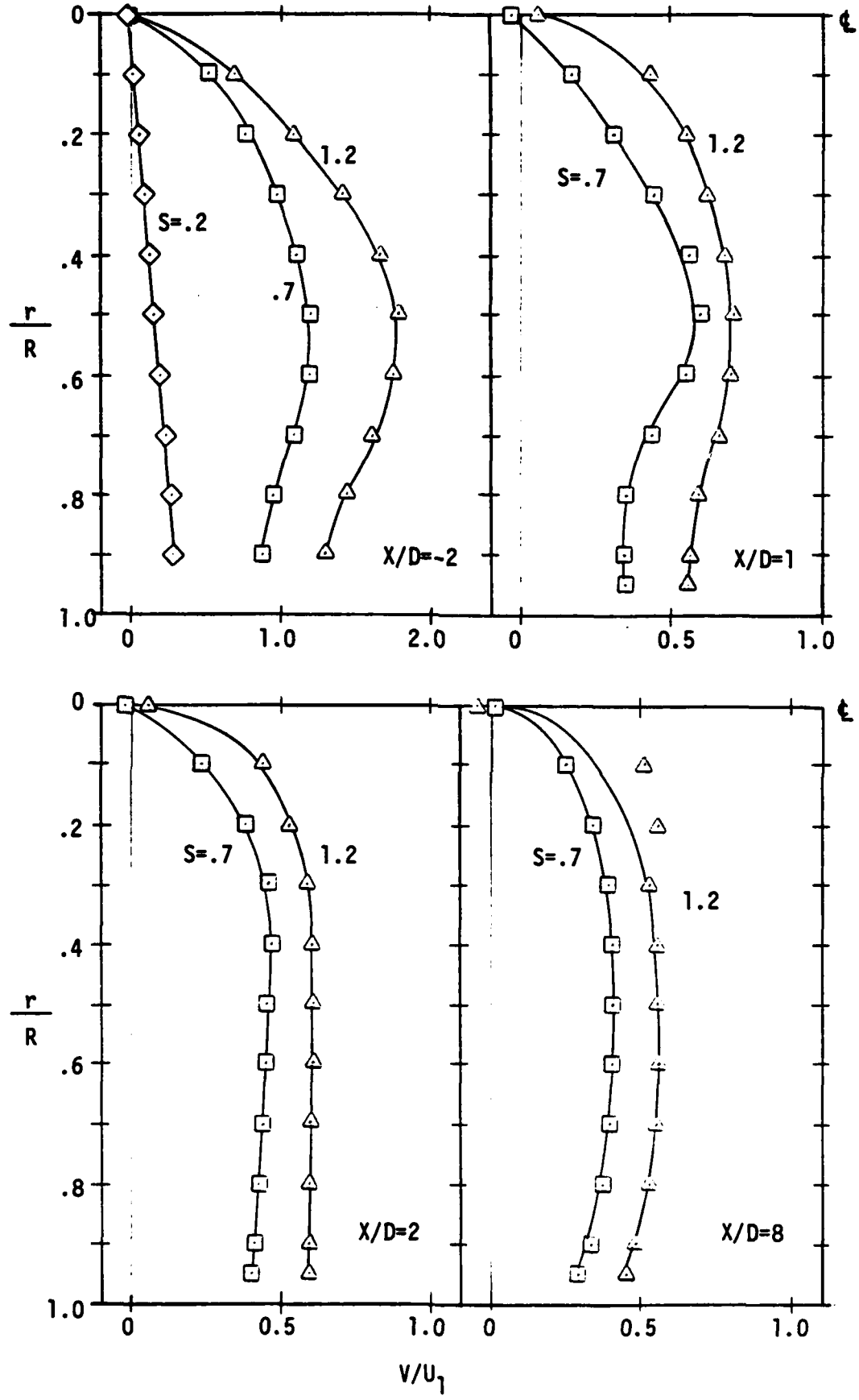

Fig. 4 Tangential velocity profiles for Re = 100,000

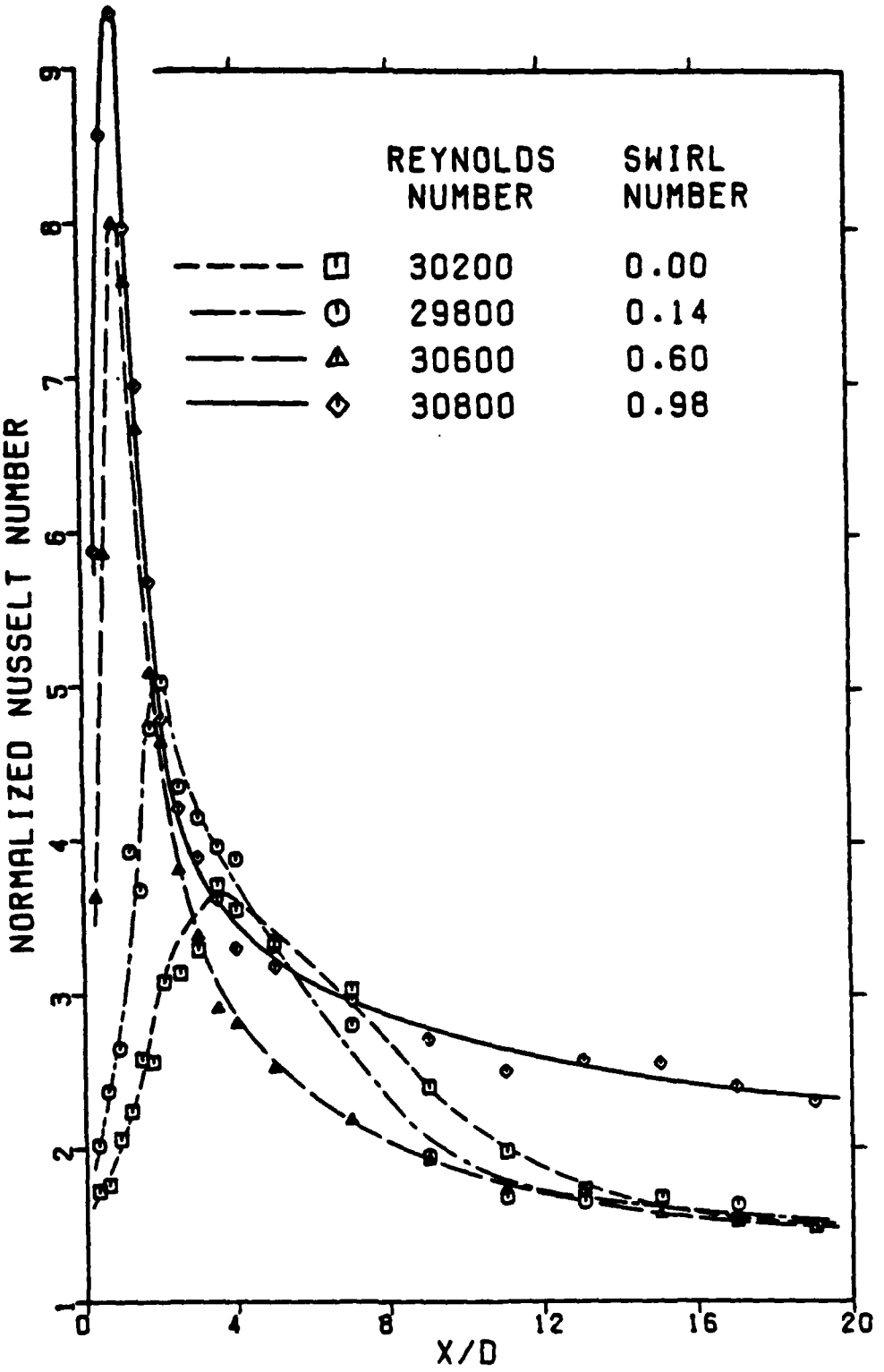

Fig. 5 Local heat transfer results; Re = 30,000

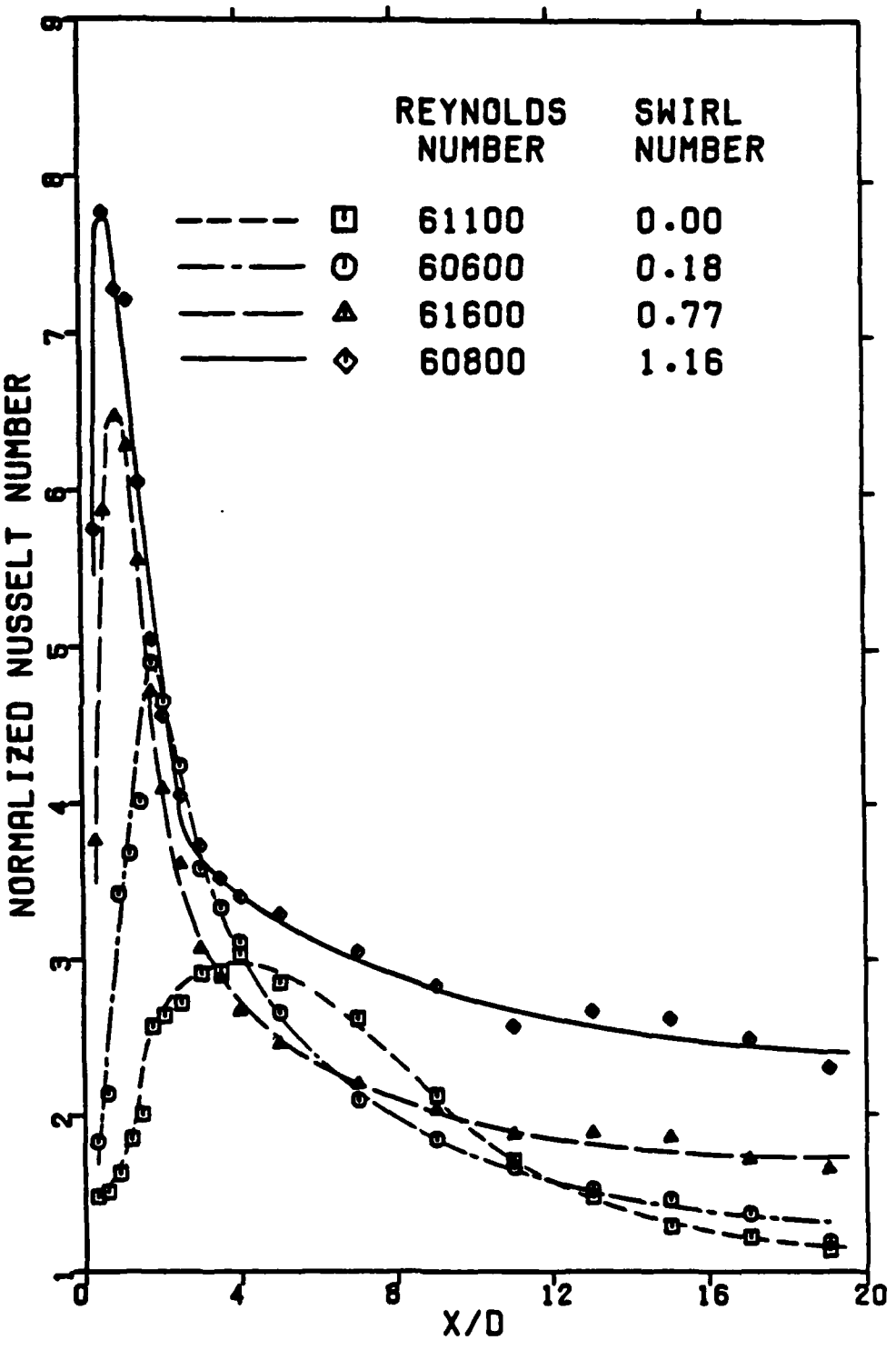

Fig. 6 Local heat transfer results; Re = 60,000

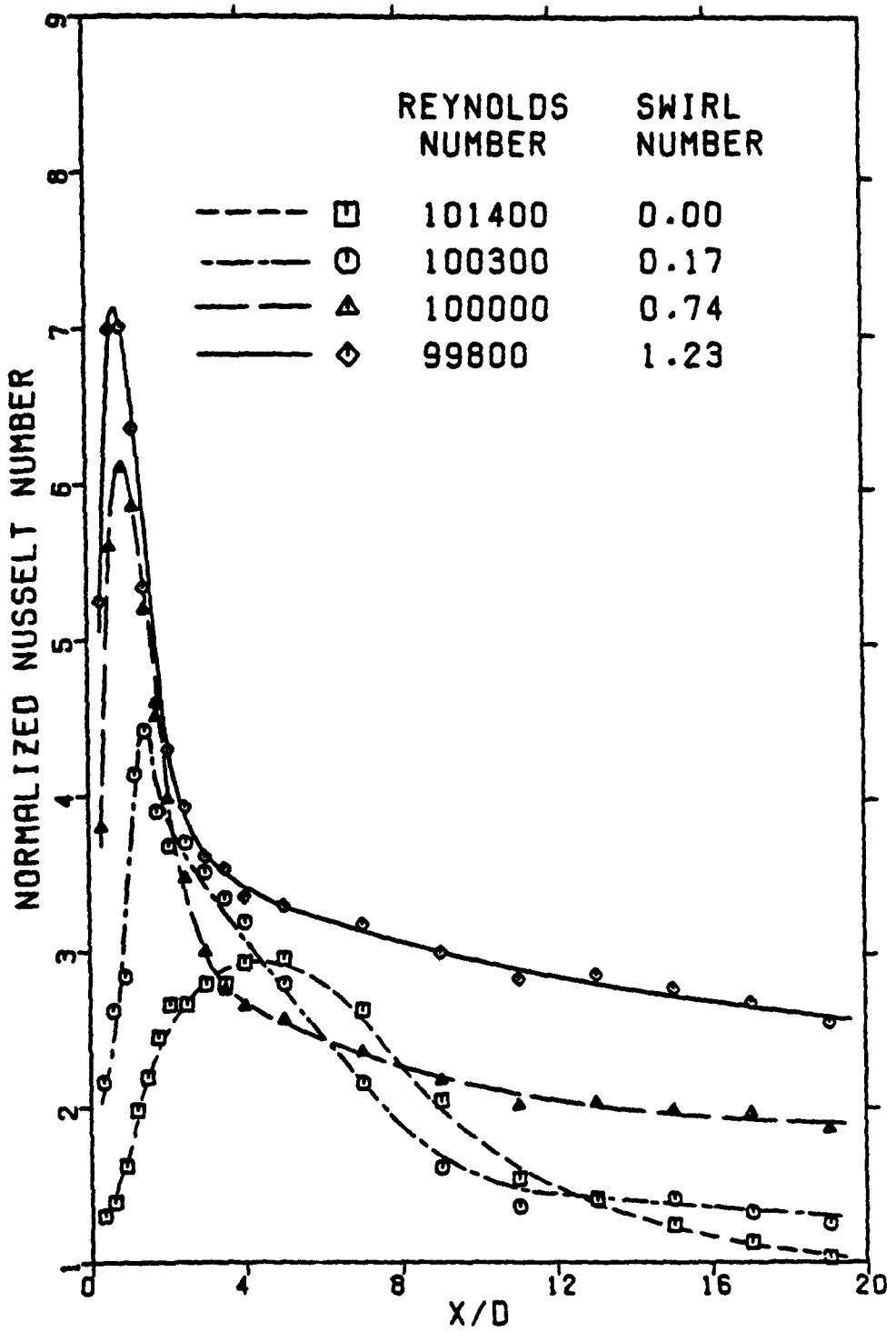

Fig. 7 Local heat transfer results; Re = 100,000

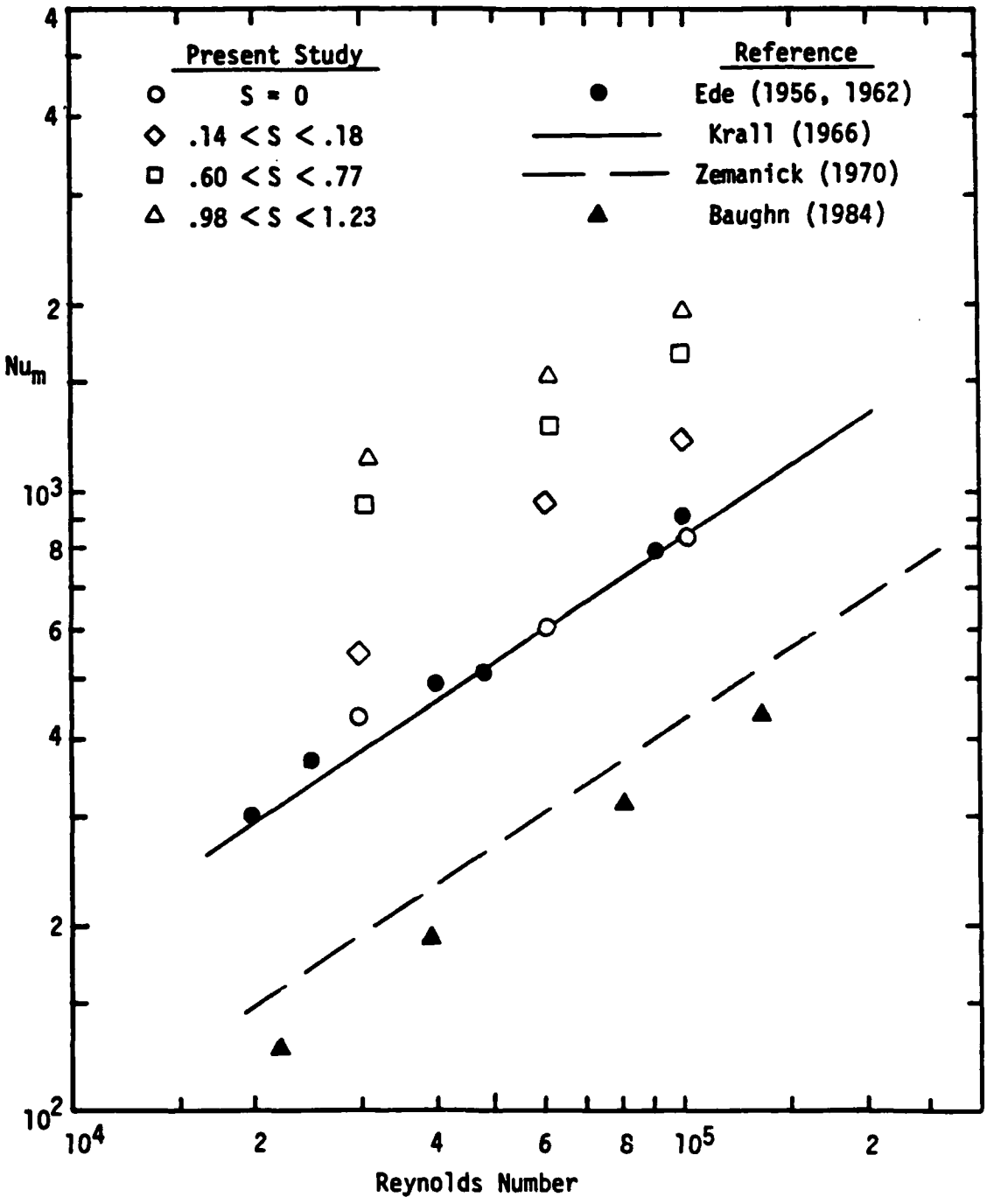

Fig. 8 Comparison of maximum Nusselt numbers between various investigations

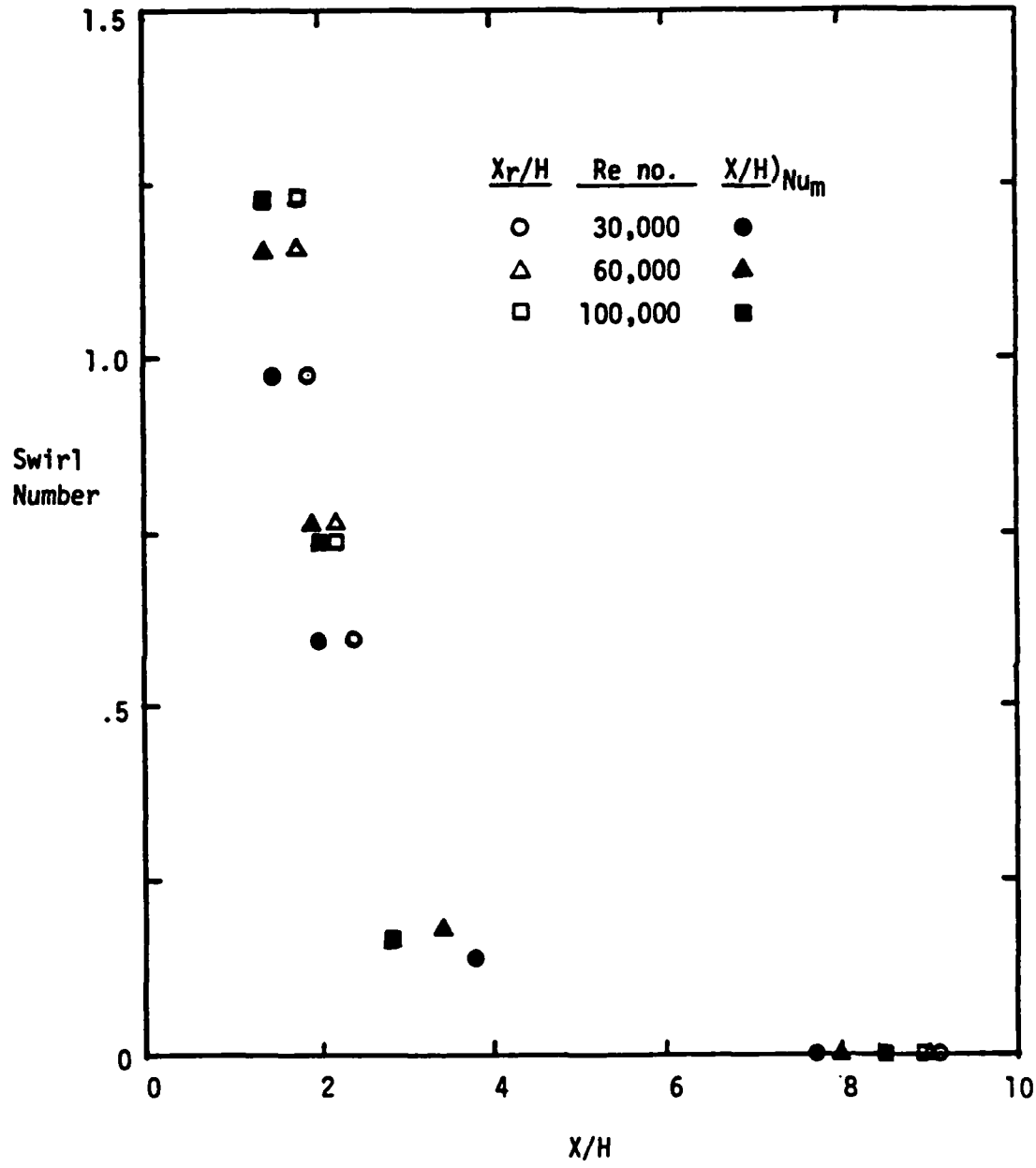

Fig. 9 Comparison of maximum Nusselt number locations with flow reattachment lengths

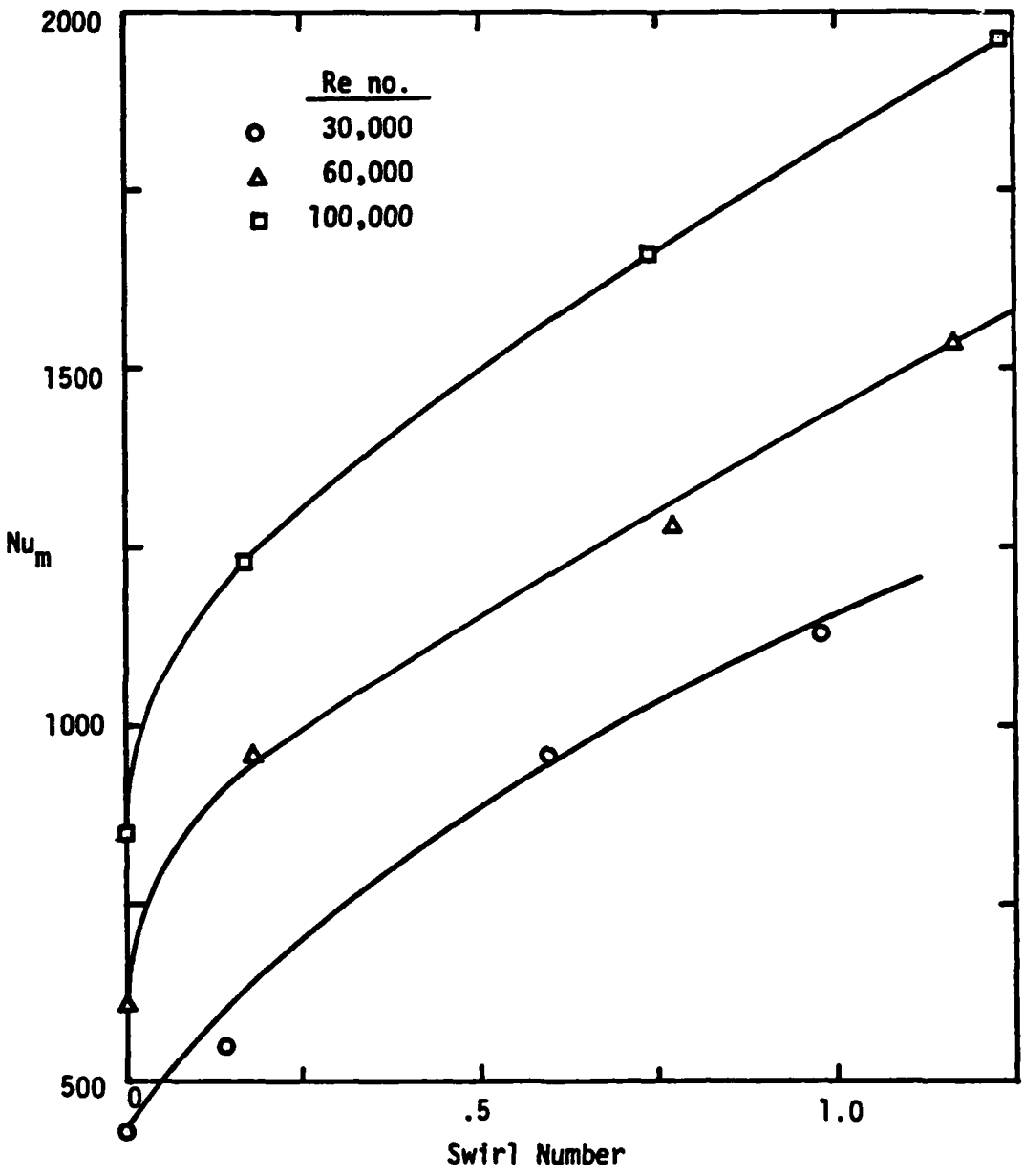

Fig. 10 Relationship between maximum Nusselt number and Swirl number

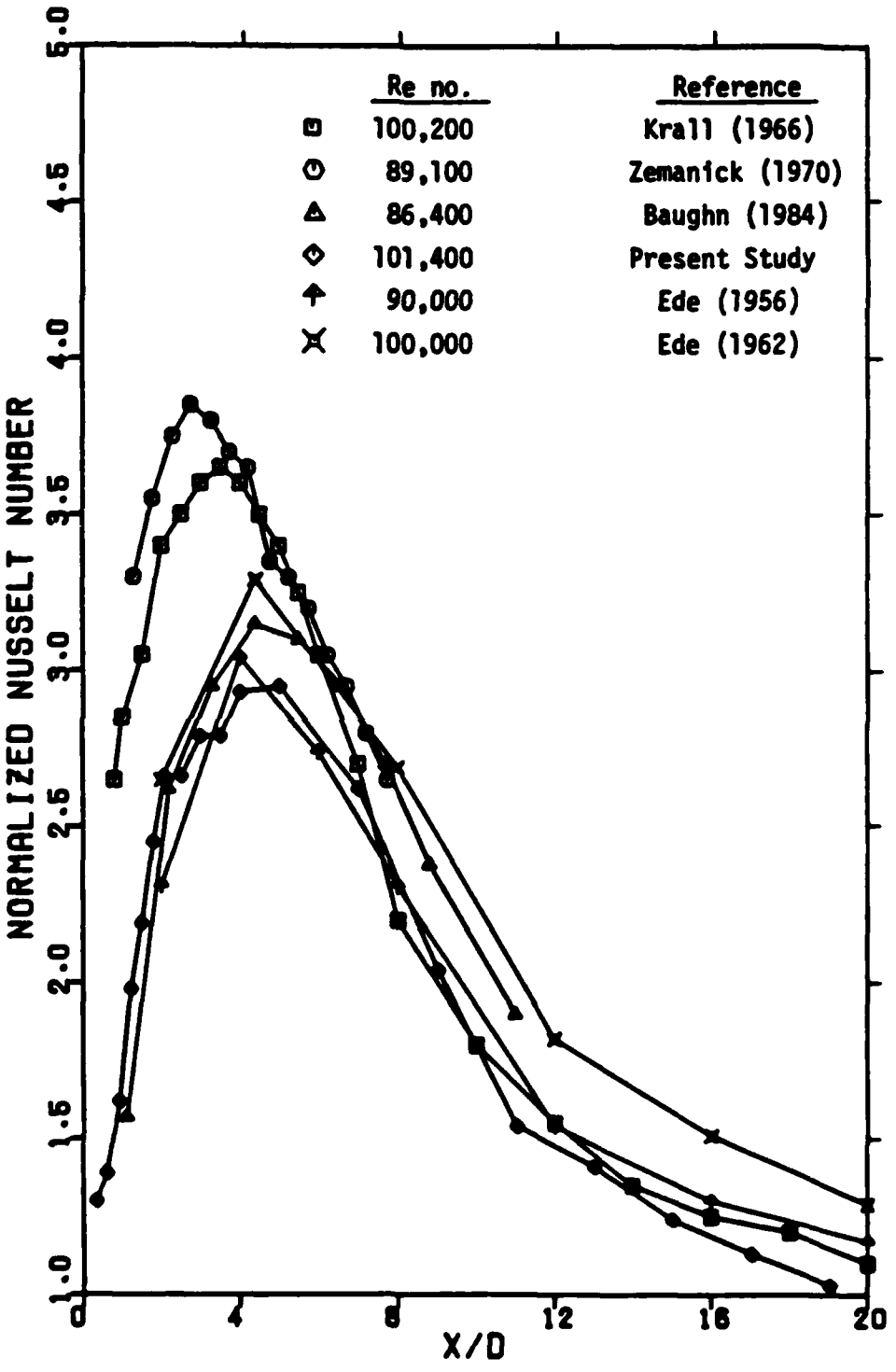

Fig. 11 Comparison of results with other investigations

Measurements in Turbulent Swirling Flow Through an Abrupt Axisymmetric Expansion

P.A. Dellenback, D.E. Metzger, and G.P. Neitzel

submitted to *AIAA Journal*

MEASUREMENTS IN TURBULENT SWIRLING FLOW THROUGH AN ABRUPT AXISYMMETRIC EXPANSION

P.A. Dellenback, D.E. Metzger, and G.P. Neitzel
Arizona State University

Experimental data are presented for both axial and tangential velocity components in turbulent swirling flow downstream of an abrupt 1:2 expansion. Measurements of mean and RMS velocities were performed in a water flow with a laser-Doppler anemometer. In the upstream tube, the Reynolds number was varied from 30,000 to 100,000 and the swirl number was varied from zero to 1.2. For low swirl levels, as the core flow passed through the expansion, it departed the axis of symmetry and precessed about that axis at frequencies on the order of 1 Hz. As swirl was increased to moderate levels, the flow became axisymmetric with on-axis recirculation marking the onset of vortex breakdown. At the highest swirl levels, flow on the tube centerline was in the same direction as the mean flow, with reverse flow occurring just off-axis. Turbulence intensities at the highest swirl levels were found to reach 60%. As the swirl was increased from zero to its maximum value, the flow reattachment point moved upstream from 9 to 2 step heights.

NOMENCLATURE

D	Diameter of upstream tube
D_2	Diameter of downstream tube
f	Precession frequency of PVC
h	Step height; $(D_2 - D)/2$
k	Turbulence kinetic energy
PVC	Precessing Vortex Core
Q	Volumetric flow rate
r	Radial coordinate
R	Radius of upstream tube
R_2	Radius of downstream tube
Re	Reynolds number in upstream tube; $\bar{U}D/\nu$
S	Swirl number in upstream tube, see equation (1)
TI	RMS velocity normalized with U_1 (* 100)
U	Local mean axial velocity
$\bar{U}$	Axial velocity averaged over cross section
U_1	Maximum axial velocity in upstream tube
V	Local mean tangential velocity
x	Axial distance from expansion face
x_r	Reattachment length
y	Thickness of viscous sublayer
β	Ratio of D/D_2
ν	Molecular viscosity of fluid

INTRODUCTION

Turbulent swirling flow through an abrupt axisymmetric expansion is a complex flow possessing several distinctly different flow regimes, either one or two recirculation regions, extremely high levels of turbulence, and periodic asymmetries under some conditions. An accompanying elevation of heat transfer rates is a principle motivation for the addition of swirl to flows in dump combustors of gas turbine engines and in solid fuel ramjet combustors. The objective of the present investigation was to experimentally examine these flowfields in some detail.

The sudden-expansion geometry produces mixing rates downstream of the expansion which are substantially higher than those which would be obtained at the same Reynolds number in the entrance region of a pipe. This enhancement in mixing occurs in spite of a recirculation region extending about nine step heights downstream from the expansion. In this recirculation region, mean velocities are typically only ten percent as high as those found in the core flow. The elevated mixing rates are due to very high levels of turbulence kinetic energy generated by shearing as the core flow issues into the larger pipe. Near the tube wall, where length scales are small, dissipation dominates since the dissipation is inversely proportional to the length scale. But in the high-shear regions away from the wall, length scales are large and dissipation rates consequently low. Thus, turbulence kinetic energy generated

in the shear layer dissipates relatively slowly and its levels are much higher than would be found in ordinary pipe flow where no such internal shear layer exists. High turbulence kinetic energy levels also cause the thickness of the (molecular) viscosity-dominated sublayer to be reduced. Specifically, for flows where the principle energy generation is not at the wall, but rather removed from it as in the sudden-expansion flowfield, Spalding[1] suggested that the viscous sublayer thickness (y) changes with the turbulence kinetic energy (k) so that the sublayer Reynolds number ($yk^{1/2}/\nu$) is a universal constant. Hence, the sublayer will become thinner with increasing levels of turbulence kinetic energy.

There has been speculation (Johnston[2]) that a small, counter-rotating corner eddy lies very close to the face of the expansion. Mean velocities in the corner eddy are of the order $0.01U_1$ according to Johnston, but there are apparently no velocity measurements or flow visualization results in the literature which either confirm this value, or support the existence of this feature in the axisymmetric-expansion flowfield. However, in a series of heat transfer measurements, Baughn, Hoffman, Takahashi, and Launder[3] speculated that small and consistent minima in Nusselt numbers near the face of the expansion were possible evidence for the presence of a corner eddy. The hypothesized corner eddy is likely to continue to defy direct velocity measurement since the available

instrumentation consists of comparatively large probes or probe volumes for detection of such a small feature in this restrictive geometry.

Adding swirl to the sudden-expansion flowfield causes an increase in the width, growth rate, entrainment, and decay of the core flow emanating from the upstream tube. It is also found that on-axis recirculation (known as vortex breakdown[4]) may occur for sufficiently high swirl strengths. This recirculation is driven by an adverse pressure-gradient on the tube centerline which results from the viscous dissipation of the tangential velocity component as the flow proceeds downstream. As swirl strength is increased from zero, the vortex breakdown may first be seen as an on-axis ellipsoid of recirculating fluid. As the degree of swirl is further increased, the ellipsoid may stretch in the downstream direction and form a tube of recirculating fluid, at least in the sudden-expansion geometry.

A further complex and little-understood phenomenon which frequently occurs in swirling flows is the existence of an unsteady (although usually periodic) asymmetry in the flowfield. These asymmetries are usually associated with the vortex breakdown phenomenon and on-axis recirculation[4]. Consequently, they are usually observed at moderate-to-large swirl strengths. However, the present investigation documents an asymmetry like that observed by Hallett and Gunther[5], which occurs at low swirl strengths in the absence of on-axis recirculation. This latter flow asymmetry is

characterized by the vortex emanating from the upstream tube departing the axis of symmetry and then precessing about that axis. This feature will be referred to here as the precessing vortex core (PVC) after Gupta, et al[6].

Analytical prediction of the present flowfield is sufficiently complex that it is manageable only if the flow is assumed to be steady and axisymmetric. With these simplifications there is no potential for predicting the unsteady three-dimensional asymmetry which occurs. Furthermore, Sultanian's[7] recent computations of this flow had difficulty in accurately predicting the extent of the on-axis recirculation zone and turbulence intensities downstream of the expansion. Sultanian also found his model to be quite sensitive to the inlet conditions, especially turbulence intensity. With this in mind, we present measurements upstream of the sudden expansion to facilitate subsequent modeling efforts.

At this point, it is convenient to define several scales and independent variables which will be used in the following discussion. There are two length scales required in the axisymmetric sudden-expansion problem. The first is the step height (h) which experience has shown to be reasonably well suited for correlation of reattachment lengths. A second necessary length scale is either the upstream or the downstream tube diameter. Here, the upstream tube diameter (D) is employed. The Reynolds number is based on the diameter of the upstream tube and the

average velocity in the upstream tube. Swirling flows are commonly characterized by the following definition for a device-independent swirl number:

$$S = \frac{1}{R} \frac{\int_0^R r^2\ U\ V\ dr}{\int_0^R r\ U^2\ dr} = \frac{\int_0^1 (r/R)^2\ U\ V\ d(r/R)}{\int_0^1 (r/R)\ U^2\ d(r/R)} \qquad (1)$$

The swirl number may be physically interpreted as the ratio of axial fluxes of swirl and linear momentum, divided by a characteristic radius.

PREVIOUS INVESTIGATIONS

Sudden Expansion Flow without Swirl. Axial flow through a sudden axisymmetric expansion is a fairly well studied problem[8-13] which represents the limiting case of zero swirl against which current results can be compared. The widely referenced set of data by Chaturvedi[8] includes mean velocities and turbulence quantities measured with a hot wire anemometer. However, a check of Chaturvedi's mass balances yields profile-to-profile variations as high as 30%. Chaturvedi attempted to smooth the data, but the arbitrary nature of this correction reduces one's confidence in it. Freeman[9] used a laser-Doppler anemometer (LDA) to measure axial mean velocity and turbulence intensity while Moon and Rudinger[10] report only an axial mean velocity from their LDA measurements. Yang and Yu[11] report turbulence quantities and mean velocities, also obtained with an LDA,

but the validity of their data has been called into question recently[14] due to significant mass balance discrepancies which are actually higher than those quoted in the paper. Among the various studies, the measurements of Gould, Stevenson & Thompson[12] and Stevenson, Thompson & Gould[13] appear to be the most complete and most closely related to the present work.

The present state of the art of computational flow modeling is such that the sudden-expansion problem (purely axial flow) is now fairly well handled by various schemes. The reader is referred to Gosman, Khalil, and Whitelaw[15] and Stevenson, Thompson, and Gould[13] for discussions of k-ε modeling, and to Minh and Chassaing[16] and Sultanian[7] for application of Reynolds stress modeling to this problem.

Axisymmetric Expansion with Swirl. There have been several recent investigations reporting measurements in swirled flows through sudden expansions[17-20], but all have used intrusive probes, even though it is known that such probes can significantly alter flowfields with recirculation. In fact, these studies are concerned primarily with the development of measurement techniques using five-hole pitot tubes and hot wire anemometry for application in multi-dimensional complex flows. Consequently, these four papers might be considered work in progress on the development of measurement techniques rather than a collection of results available for comparison purposes.

Vortex Breakdown and the PVC. There have been a number of analytical investigations of vortex breakdown (see reviews by Hall[21] and Leibovich[22]) but the asymmetries in swirled flows are so complex and irregular that these analytical treatments have been mostly unsuccessful. Thus the primary body of information about unsteady asymmetries in swirling flows has been gathered in experimental studies[4,23-26]. The flow geometries in these experiments are all axisymmetric, but a wide variety of configurations are represented. These include straight tubes[23], diffusers[4,25,26], sudden contractions[23], and unconfined swirling jets[24]. Although the geometries are diverse, the nature of the asymmetrical flows observed in the various experiments is remarkably similar. The single feature common to all of these flows is a precession of the flow about the tube axis in conjunction with vortex breakdown.

All of the prior vortex breakdown experiments were essentially flow visualization studies. In those cases where hot wire and laser-Doppler anemometry were employed[4,23,24], they were used to look for a sinusoidal variation in mean velocity as the asymmetry swept past the point of measurement. Cassidy and Falvey[23] noted that the precession frequency was independent of Reynolds number for $Re \geq 10^5$. In very careful flow visualization studies, Faler and Leibovich[4] identified six distinct disturbance modes whose flow regimes could be characterized by Reynolds and swirl numbers. The experiments of Faler and Leibovich led

them to conclude that there are no truly axisymmetric disturbance patterns in these flows.

There is an important distinction between the papers mentioned above and the work of Hallett and Gunther[5]. In the previously mentioned studies, the flow asymmetries occur only in conjunction with vortex breakdown, but Hallett and Gunther's PVC in a sudden expansion occurs only for swirl strengths below those associated with vortex breakdown. In fact, with increasing swirl, the periodicity of the PVC became weaker and less distinct until just before onset of vortex breakdown, it disappeared altogether. Also, they noted that precession was strongest and most regular at low swirl, while at higher swirl the motion became increasingly irregular. Hallett and Gunther observed that the amplitude of the PVC dissipated with increasing downstream distance as the PVC became more coincident with the tube axis. Finally, they report no evidence of flow asymmetry upstream of the expansion in velocity measurements made with a five-hole pitot probe.

EXPERIMENTAL APPARATUS

A water flow loop, constructed of stainless steel, and shown schematically in Figure 1, comprised the main element of the test facility. Swirl was generated by supplying a variable portion of the flow through tangential slots as indicated by Figure 2. Inside diameters of the axial inlet

tube, the swirler insert, and the upstream test section were 5.08 cm. The axial inlet tube was 31 diameters long to allow axial flow development, and the sudden expansion was 15 diameters downstream of the swirl generator. Flow rates to the slots and the axial inlet tube could be controlled independently, thus providing the capability to continuously vary swirl strength. Flow rates were measured with turbine-type flowmeters. An in-line filter was used to remove particles nominally larger than 1 μm from the water.

The tube upstream of the expansion was made of Plexiglas which was bored, honed, and polished to a final ID of 5.078 ±.008 cm. To allow LDA measurements close to the expansion, the tube and attached expansion face extended into the downstream tube so that structural flanges and bolts did not interfere with the laser beams. Measurements were thus possible 1 cm downstream of the expansion. The downstream tube was not machined or honed due to complications associated with its relatively large size. Consequently, it was very slightly oval with an ID of 9.850 ±.020 cm and OD of 10.767 ±.003 cm. Thus the expansion ratio was 1:1.94. The length of the downstream tube was 1.04 m.

The LDA Optical System. The laser-Doppler anemometer was a conventional, single-component system operated in the dual-beam mode. The system included a 15 mW He-Ne laser, a Bragg cell for frequency shifting of one beam, and beam-expansion optics to minimize probe volume size. The optical

components produced an ellipsoidal probe volume whose nominal $1/e^2$ extent was .91 mm long and .09 mm in diameter.

Both transmitting and forward-scatter receiving optics were mounted on a single aluminum channel which in turn was rigidly affixed to the table of a three-axis milling machine. To obtain the desired 1 m travel in the axial direction, the milling table was permanently fastened to four precision linear bearings which rode on two parallel steel shafts. A dial indicator was used to monitor the radial position of the probe volume.

EXPERIMENTAL PROCEDURES

Artificial seeding of the flow was not required. The test loop was filled with tap water having a relatively high mineral and particulate content. The water was filtered briefly after each filling of the loop to remove particles nominally larger than 1 μm. Filtering to this size was consistent with the Melling and Whitelaw[27] suggestion that particulates smaller than 10 μm will adequately follow the flow up to frequencies of 500 Hz. For most water flows, the bulk of the energy-containing eddies have frequencies in this range.

Both axial and tangential components of mean velocity and RMS turbulence levels were measured on a dense grid of points lying in a horizontal plane through the tube centerline. Included in the grid of measurement stations

were two upstream locations at X/D = -2.0 and -0.5. Locations for profiles in the downstream tube were chosen to optimize resolution in the near-expansion region where velocity and turbulence levels change rapidly with X/D. Corrections for optical refraction of the laser beams at the air-Plexiglas and Plexiglas-water interfaces[28] were employed to locate the probe volume at even intervals in the radial direction. For most cases with swirl, profiles were made across the entire tube to check for flow asymmetry even though asymmetry was only found in the subcritical-swirl flows.

Measurements at radius ratios ±0.95 were attempted for all profiles. However, measurement close to walls is generally difficult since scattered light from the walls results in poor signal-to-noise ratios. In the present work, spurious wall reflections were largely overcome by collecting scattered light at about 5 degrees off the forward scatter axis, thus truncating the probe volume slightly and keeping the light-collection optics out of the horizontal plane which contains most of the disruptive stray light. Using this technique, results at r/R_2 = ±.95 in the downstream tube were consistent and credible. In the upstream tube, because of its smaller size, the same degree of credibility extended only to r/R = ±.90.

Velocity biasing was eliminated by random sampling in the present experiments. Dureo, Laker, and Whitelaw[29] suggest that, for data collection percentages of less than

40%, the average velocity obtained will be less than 2% higher than the true mean velocity. Stevenson, et al.[13] suggest that the velocity bias will be effectively eliminated for collection percentages on the order of 1%. For this work, a computer sampled the output from a counter processing device at a rate of 130 Hz. Data rates often fell to about 4000 Hz at the near-wall grid points of $r/R_2 = \pm.95$, but usually ranged from 8000 to 40,000 Hz elsewhere. Hence the worst-case collection percentages were about 3% near the tube walls. The waiting period also minimizes the potential bias caused by a single particle generating multiple measurements before leaving the probe volume.

Mean and RMS velocities were determined from sample sizes of 4000 data points. The statistical error[30] associated with this sample size is ±1% in the mean-velocity measurement for a local turbulence intensity (TI) of 70% and about ±2% in the measurement of TI. A worst-case computation of the spatial velocity biasing due to the finite probe-volume size[31] suggests that the spatially averaged TI is only 0.6% higher than the TI at the probe volume's center.

Investigation of the PVC. The experimental examination of the precessing vortex core and the vortex-breakdown bubble consisted of both flow visualization and selective probing with the LDA. Some modest success in visualizing the flow was obtained using air bubbles and

high-intensity lighting in two different procedures. The first and more useful method was to introduce approximately one liter of air into the 250 liter capacity of the test loop. The air and water were then mixed by operating the loop for a short time. The ensuing air bubbles were so small as to be almost invisible to the eye with ordinary room lighting, but with the use of a high intensity photographic light source, a "mist" of bubbles could be seen well enough to perceive qualitative details of the flow. These bubbles were sufficiently small that they showed no discernible tendency to either rise to the top of the tube or collect on the tube centerline, but rather seemed to follow the flow. When the flow field was visualized in this fashion it was often difficult to determine what was happening in the tube. In particular, while it was clear that the vortex from the upstream tube was entering the downstream tube asymmetrically and precessing, vigorous activity in the near-wall recirculation zone complicated the examination so that the direction of precession at very low swirl numbers ($S \leq .15$) could not be determined. To aid in the resolution of this dilemma, air was injected through a small total-pressure probe on the centerline of the upstream tube. The air-injecting probe was located just downstream of the swirl generator. As the larger bubbles which were produced in this way moved downstream, they were pinned on the tube centerline by centrifugal forces. As they passed

through the expansion, they marked the vortex axis and thus revealed the direction of vortex precession.

Precession frequency information was gathered by monitoring the counter-processor's analog output on both a strip-chart recorder and a spectrum analyzer to obtain a real-time variation of mean velocity. An RMS voltmeter with adjustable time constant was connected between the counter's output and the recorder or analyzer so that the higher frequencies associated with turbulent fluctuations could be filtered out.

The methods of Kline and McClintock[32] were employed to determine that the largest uncertainties were about 2% in Reynolds number, 8% in swirl number, 10% in Strouhal number, and 1% in probe volume positioning. Uncertainties in mean and RMS velocities due to the many possible biases and broadening errors are estimated to be about ±3% and ±10%, respectively.

RESULTS AND DISCUSSION

Velocity and TI Distributions. The results for U, u', and v' for unswirled flow at Reynolds numbers of 30,000, 60,000, and 100,000 are shown in Figure 3. The mean and fluctuating velocities in Figure 3 have been normalized with the axial centerline velocity occurring in the upstream tube. Mean velocities for the three Reynolds numbers collapse to single curves, but when examining the regions

far downstream (X/D = 18) it can be seen that the turbulent fluctuations have apparently dissipated faster for larger Reynolds numbers (the TI for Re = 60,000 and Re = 100,000 were virtually identical). Figure 3 indicates that the axial TI has decreased to a nominal background level of about 2.5% for Re = 100,000 while it remains near 8% for Re = 30,000. The difference in TI's is due to higher rates of dissipation at the larger Reynolds numbers. Dissipation usually scales as u'^3/ℓ, or $(u'/U)^3/(\ell/U^3)$, so that for length scales (ℓ) and turbulence intensities (u'/U * 100) of the same order, dissipation increases with increasing U, or increasing Reynolds number.

For unswirled flows, we see that a state of near-isotropy in u' and v' exists at X/D = -2.0, and then again far downstream after the flow has redeveloped. However, throughout much of the intermediate region the axial TI is approximately 30% greater than the tangential TI. The peak values for both of these quantities are generally coincident and lie in the region bounded by the edge of the shear layer and the tube centerline. For each Reynolds number, these maximum values are on the order of 20 - 22% for axial TI and about 15% for tangential TI. This maximum value (and the distributions of U and u') compare very favorably with the work of Stevenson, Thompson, and Gould[13] who report a maximum axial TI of 22%.

Swirled-flow data for five supercritical-swirl cases are shown in Figures 4-8. For these highly swirled flows,

the maximum axial velocity in the upstream tube (U_1) occurred near $r/R \approx .8$, and it is this value which is used for the normalization of mean and RMS velocities. Figures 4-8 demonstrate a large influence of the downstream flow on the X/D = -0.5 profiles for all supercritical-swirl cases. The influence is especially strong on the TI's whose magnitudes and distributions are changed dramatically from the X/D = -2.0 station. The turbulence intensities continue to be highly non-isotropic in the downstream tube for all the supercritical-swirl flows. These results have important ramifications on modeling of this flow since they imply the frequently used k-ε model, with its assumption of isotropy, will be unable to accurately predict the observed features of highly swirled flows.

The highest swirl strength achieved in this set of experiments is shown in Figure 8, where we see two features not present in the flows with lower swirl numbers. The first is that, as the flow development proceeds downstream from X/D = 4, the centerline velocity is positive with recirculation just off-axis. We also find that the on-axis tangential velocity gradient is steepening throughout the downstream tube, consequently producing greater shearing and ever-increasing turbulence intensities. Both of these trends continued through X/D = 18. These two features cannot be wholly discerned from the data presented for Re = 60,000, S = 1.16, but from Figure 6 and measurements made further downstream (those for X/D > 10 not shown here),

the trends toward positive centerline velocity and continuously increasing TI do seem to be present and hence consistent with the Re = 100,000, S = 1.23 data. That centerline TI's continue to increase to the end of the test section is a limitation of the test section's length. In a longer tube the decay of swirl would give rise to a maximum in TI at some axial location. However it is perhaps surprising that this flow condition with its high diffusion rates and relatively short wall recirculation zone is still evolving so far downstream at X/D = 18.

For the swirled flows in general, the peak value for axial TI always occurs in the shear layer near $r/R_2 = 0.5$, and the maximum value of tangential TI is always found along the tube centerline. For the swirled flows there is a considerable divergence in the behaviors of axial and tangential turbulence intensities for X/D = -0.5 and throughout the downstream tube. It can be seen from Figures 4-8 that, along the tube centerline, the tangential TI is typically twice the axial TI. At the same time in the shear layer around $r/R_2 = 0.5$, the axial TI is commonly twice the tangential TI. The largest axial TI are on the order of 45% for moderate swirl ($.60 < S < .77$) and 58 - 65% for high swirl ($.98 < S < 1.23$). In each case the corresponding maximum tangential TI is always several percent less than the axial value. For the swirled flows these maximum values were found near X/D = 0.5, while for the unswirled flows, they were found between $3 < X/D < 6$.

A composite of axial centerline velocities is shown in Figure 9. For the unswirled flows, the flat portion of the curve for X/D > 12 indicates that the velocity profile has redeveloped. From an area-ratio argument, one would anticipate that for the present expansion ratio of 0.51 that the normalized centerline velocity would achieve a downstream value of $(0.51)^2$ or 0.265. The actual value reached was a consistent 0.24, which suggests that downstream profiles are flatter and more developed than those upstream of the expansion. That this is true can be seen in the velocity profile plots of Figure 3. It is hypothesized that the profile upstream of the expansion is not quite fully developed due to slight tube-wall irregularities associated with the swirl generator's slots, pipe joints located at the swirl generator, and a flanged pipe connection approximately four diameters upstream of the X/D = -2.0 measuring station.

The normalized centerline velocity has no Reynolds-number dependence for the unswirled flows. If we assume this also to be true for swirled flows, then Figure 9 suggests that there is a swirl number between 0.74 and 0.98 which gives a maximum reverse velocity. Further, the maximum reverse velocity, which is seen to occur between X/D = 0.5 and X/D = 1.3, decreases in magnitude as swirl number is increased beyond S = .98. This suggests that there may be swirl numbers greater than 1.23 for which the centerline velocity may always be positive, as for the

unswirled flows. Unfortunately, S = 1.23 was the upper limit on swirl strength available from the equipment used in this study, so that this hypothesis could not be investigated further.

For the present work, the position of U = 0 points at radial locations of r/R_2 = .8, .9, and .95, was determined by linear interpolation between adjacent grid points for which U had opposite signs. The U = 0 points from the three radial locations were then fitted with a spline and the resulting curve extrapolated to the wall to find the reattachment "point". Reattachment lengths obtained in this fashion for the present data are shown in Table 1. For the three unswirled cases, the reattachment lengths agree well with those reported for unswirled flows in the previously mentioned investigations (also shown in Table 1). We know of no existing data which can be used for comparison of reattachment lengths in swirled flows. When reattachment lengths are plotted against swirl number, the resulting curve is independent of Reynolds number and appears to be asymptotic to $x_r/h \approx 1.7$ as swirl number increases beyond 1.2. The reattachment lengths given here are actually average values determined from four to eight sets of velocity data obtained in the region of reattachment. The slight variations found in these velocities were sufficient to appreciably alter the computed lengths, this being especially true for the unswirled flows where variations in reattachment length of ±0.5 step heights were not uncommon

between individual data sets. The variation in reattachment length for the swirled cases was a more modest ±0.1 step heights for individual data trials. It is probably reasonable to consider these variations as representative of random fluctuations in the reattachment zone's width rather than as an uncertainty in the measurement, but it is difficult to separate these two effects.

Mass balances obtained from integration of velocity profiles have become a commonly used standard for appraising the credibility of internal-flow velocity data. For a particular flow condition in the present work, the largest differences between the mass flux at any one profile and the average mass flux for all profiles (at that flow condition) were between 3% and 5%. The locations of poorest agreement were randomly scattered in the axial direction. Tabular velocity data and further details are available in the dissertation by Dellenback[33].

The PVC and Vortex Breakdown. Information which can be generalized about swirling-flow asymmetries and the PVC from previous studies is very sparse, largely due to the complexity of the flow's structure. Historically, the most easily and commonly measured feature of these asymmetries has been the relationship between the swirl number and precession frequency. This relationship also constitutes the principle result of the present study of the PVC. While the computation of swirl number requires knowledge of the mean velocity profiles, which are not known a priori, the

swirl number can also be related to the ratio of mass fluxes entering the swirl generator. For weakly swirled flows ($S < .15$), the swirl number was obtained from an algebraic relationship[6] between the axial and tangential mass fluxes which results from assuming plug flow with superimposed solid-body rotation. A second, experimentally determined relationship between the mass-flow ratio and the swirl number (from integrated velocity profiles) was deduced for higher swirl numbers. Precession frequencies were examined only at the two limiting Reynolds numbers of 30,000 and 100,000.

Precession-frequency data are combined with flow-visualization observations to summarize vortex breakdown and the PVC's swirl-dependent behavior in Table 2. Previous investigations have found that swirling flow asymmetries usually precess in the same direction as the mean swirl for confined flows, and in the opposite direction for free jets. However, Escudier[25] reports that his sudden expansion data contradict this general rule. In the present experiments, the PVC precessed with the mean swirl for larger swirl numbers, and against the mean swirl for low swirl numbers. Table 2 shows that, while results for the two Reynolds numbers are similar, specific events occur at slightly different swirl numbers. Two regions were especially difficult to resolve. These were the precession frequencies for very low swirl ($S < .1$) and the swirl number at which the direction of precession changes. On the other hand, two

points which had very sharp transitions as the swirl number was changed were the transition from PVC to vortex breakdown, and the transition from a bubble-like vortex breakdown to a full-length tube of recirculating fluid on the tube centerline. Throughout the regime of swirl numbers for which the vortex-breakdown bubble exists, considerable unsteadiness of the bubble's location was noted in both the flow visualization and LDA data. This unsteadiness made it impossible to accurately measure either the velocities inside the bubble or the bubble's dimensions, but it was noted that the bubble extended to about 2-1/4 D downstream of the expansion. Downstream of the bubble, it was observed that, while fluid on the tube axis was mostly stagnant in the mean, it was also quite unsteady, sometimes showing a tendency to drift randomly either upstream or downstream. When the PVC was present, flow oscillations could be detected at the upstream station of X/D = -0.5, but not further upstream at X/D = -2.0. Although several of the investigations cited previously observed the PVC at supercritical-swirl numbers, the PVC in the present study could only be detected at subcritical-swirl numbers. Finally, none of the results shown in Table 2 displayed any apparent hysteresis in swirl number.

Frequency information taken from the stripcharts (or spectrum analyzer, which agreed closely) was converted to Strouhal numbers[23] (fD^3/Q, where f is the precession frequency and Q the volumetric flow rate) and used to

generate Figure 10. The scarcity of data points for S < .1 and near the zero-frequency crossovers is illustrative of the previously mentioned inability to resolve frequencies at these transitory swirl numbers. Away from these swirl numbers, smooth curves drawn through the available data points fit well and thus give confidence in extrapolating the swirl number for the zero frequency crossovers. Figure 10 also shows clearly the dependency of the precession frequency on Reynolds number.

The frequencies of precession seem to follow a trend consistent with other investigations of asymmetries in swirling flows as shown by Figures 11 and 12. Although Syred and Beer's[24], and Cassidy and Falvey's[23] experiments were in dissimilar geometries (free jet; straight tube and sudden contraction, respectively) and the PVC occurred in conjunction with vortex breakdown, there is a noticeable congruence of results in Figure 12. In particular, the Strouhal number appears to be independent of Reynolds number for Re > 10^5, but a slowly decreasing function of Reynolds number at lower values of this parameter.

CLOSURE

The principle contribution of the present study has been to quantify the magnitudes of mean and fluctuating velocities as a function of swirl and Reynolds numbers in an abrupt axisymmetric-expansion flow. In addition, a number

AD-A183 674 MODELING AND MEASUREMENT OF TURBULENT SWIRLING FLOWS THROUGH ABRUPT EXPAN..(U) ARIZONA STATE UNIV TEMPE DEPT OF MECHANICAL AND AEROSPACE ENG.. G P NEITZEL ET AL. 2/2

UNCLASSIFIED MAR 87 ASU-TR-ERC-R-86104 N00014-81-K-0428 F/G 20/4 NL

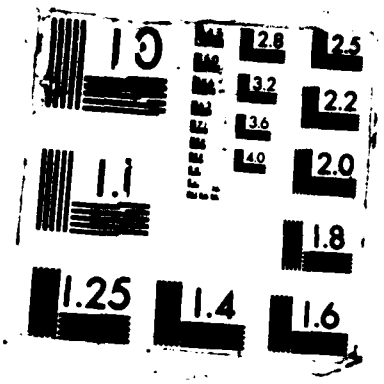
2.8
2.5
3.2
2.2
3.6
4.0
2.0
1.8
1.25
1.4
1.6
1.1

of qualitative trends and features have been observed which may contribute in a general way to the understanding of complex shear flows. Documentation of the velocity field in the upstream tube should be helpful to computational flow modelers, and of general interest in light of how vastly the upstream flow changes just before reaching the expansion. For low swirl levels, an unsteady, three-dimensional flow asymmetry has been observed. The asymmetry is such a complex flow structure that only a limited number of useful measurements can be obtained which help to specify its structure. At the higher swirl levels, the flow becomes symmetric and extraordinarily high levels of turbulence are produced. The on-axis recirculation normally associated with highly swirled flows changes such that the on-axis flow is in the downstream direction with recirculation just off-axis.

ACKNOWLEDGEMENT

This research was supported by the Office of Naval Research.

REFERENCES

1) Spalding, D.B., "Heat Transfer from Turbulent Separated Flows," *J. of Fluid Mechanics* Vol. 27, 1967, pp. 97-109.

2) Johnston, J.P., "Internal Flows," *Turbulence: Topics in Applied Physics*, 12th Ed., Springer-Verlag, 1978, pp. 144-152.

3) Baughn, J.W., Hoffman, M.A., Takahashi, R.K. and Launder, B.E., "Local Heat Transfer Downstream of an Abrupt Expansion in a Circular Channel with Constant Wall Heat Flux," *ASME Trans.-J. of Heat Transfer*, Vol. 106, 1984, pp. 789-796.

4) Faler, J.H., and Leibovich, S., "Disrupted States of Vortex Flow and Vortex Breakdown," *The Physics of Fluids*, Vol. 20, no. 9, 1977, pp. 1385-1400.

5) Hallett, W.L.H., and Gunther, R., "Flow and Mixing in Swirling Flow in a Sudden Expansion," *Canadian J. of Chem. Eng.*, Vol. 62, 1984, pp. 149-155.

6) Gupta, A.K., Lilley, D.G., and Syred, N., *Swirl Flows*, Abacus Press, Turnbridge Wells, Kent, 1984.

7) Sultanian, B.K., Neitzel, G.P., and Metzger, D.E., "Turbulent Flow Predictions in a Sudden Axisymmetric Expansion," *Proceedings of the International Symposium on Refined Flow Modeling and Turbulence Measurements*, 1985, paper B22.

8) Chaturvedi, M.C., "Flow Characteristics of Axisymmetric Expansions," *J. of the Hydraulics Div. - Proc. of the ASCE*, Vol. HY 3, 1963, pp. 61-92.

9) Freeman, A.R., "Laser Anemometer Measurements in the Recirculating Region Downstream of a Sudden Pipe Expansion," *Accuracy of Flow Measurements by Laser Doppler Methods - Proc. of the LDA Symposium, Copenhagen*, 1975, pp. 704-709.

10) Moon, L.F., and Rudinger, G., "Velocity Distribution in an Abruptly Expanding Circular Duct," *ASME Trans-J. of Fluids Eng.*, Vol. 99, 1977, pp. 226-230.

11) Yang, B.T., and Yu, M.H., "The Flowfield in a Suddenly Enlarged Combustion Chamber," *AIAA J.*, Vol. 21, no. 1, 1983, pp. 92-97.

12) Gould, R.D., Stevenson, W.H., and Thompson, H.D., "Laser Velocimeter Measurements in a Dump Combustor," ASME Paper No. 83-HT-47, 1983.

13) Stevenson, W.H., Thompson, H.D., and Gould, R.D., "Laser Velocimeter Measurements and Analysis in Turbulent Flows with Combustion, Part II," AFWAL-TR-82-2076, 1983.

14) Sultanian, B.K., "Numerical Modeling of Turbulent Swirling Flow Downstream of an Abrupt Pipe Expansion," Ph.D. Dissertation, Arizona State University, 1984.

15) Gosman, A.D., Khalil, E.E., and Whitelaw, J.H., "The Calculation of Two-dimensional Recirculating Flows," *Turbulent Shear Flows,* Vol. 1, Springer-Verlag, 1977, pp. 237-254.

16) Minh, H.H., and Chassaing, P., "Perturbations of Turbulent Pipe Flow," *Turbulent Shear Flows,* Vol. 1, Springer-Verlag, 1977, pp. 178-197.

17) Jackson, T.W., and Lilley, D.G., "Single-wire Swirl Flow Turbulence Measurements," AIAA Paper No. AIAA-83-1202, 1983.

18) Janjua, S.I., Mclaughlin, D.K., Jackson, T.W., and Lilley, D.G., "Turbulence Measurements in Confined Jets Using a Rotating Single-wire Probe Technique," *AIAA J.*, Vol. 21, no. 12, 1983, pp. 1609-1610.

19) Rhode, D.L., Lilley, D.G., and McLaughlin, D.K., "Mean Flowfields in Axisymmetric Combustor Geometries with Swirl," *AIAA J.*, Vol. 21, no. 4, 1983, pp. 593-600.

20) Abujelala, M.T., Jackson, T.W., and Lilley, D.G., "Swirl Flow Turbulence Modeling," AIAA Paper No. AIAA-84-1376, 1984.

21) Hall, M.G., "Vortex Breakdown," *Ann. Rev. of Fluid Mechanics*, Vol. 4, 1972, pp. 195-218.

22) Leibovich, S., "Vortex Stability and Breakdown: Survey and Extension," *AIAA J.*, Vol. 22, no. 9, 1984, pp. 1192-1206.

23) Cassidy, J.J. and Falvey, H.T., "Observations of Unsteady Flow Arising After Vortex Breakdown," *J. of Fluid Mechanics*, Vol. 41, pt. 4, 1970, pp. 727-736.

24) Syred, B., and Beer, J.M., "Combustion in Swirling Flows: A Review," *Combustion and Flame*, Vol. 23, 1974, pp. 143-201.

25) Escudier, M.P., "Observations of Confined Vortices," *Flow Visualization,* Vol. II, 1980, pp. 379-383.

26) Sarpkaya, T., "On Stationary and Travelling Vortex Breakdowns," *J. of Fluid Mechanics*, Vol. 45, 1971, pp. 545-559.

27) Melling, A., and Whitelaw, J.H., "Optical and Flow Aspects of Particles," *Accuracy of Flow Measurements by Laser Doppler Methods - Proceedings of the LDA Symposium, Copenhagen*, 1975, pp. 382-392.

28) Boadway, J.D., and Karahan, E., "Correction of Laser Doppler Anemometer Readings for Refraction at Cylindrical Interfaces," *DISA Information* No. 26, 1981, pp. 4-6.

29) Durao, D.F.G., Laker, J., and Whitelaw, J.H., "Bias Effects in Laser Doppler Anemometry," *J. Physics E: Scientific Instruments*, Vol. 13, 1980, pp. 442-445.

30) Bates, C.J., and Hughes, T.D.R., "The Effect of Both Sample Size and Sampling Rate on the Statistical Fluid Flow Parameters in a High Reynolds Number, Low Turbulence Intensity Flow," *Symposium on Turbulence*, University of Missouri, Rolla, 1977, pp. 125-131.

31) Karpuk, M.E., and Tiederman, W.G., "Effect of Finite-size Probe Volume Upon LDA Measurements," *AIAA J.*, Vol. 14, no. 8, 1976, pp. 1099-1105.

32) Kline, S.J., and McClintock, F.A., "Describing Uncertainties in Single-sample Experiments," *Mechanical Engineering*, Vol. 75, no. 1, 1953, pp. 3-8.

33) Dellenback, P.A., "Heat Transfer and Velocity Measurements in Turbulent Swirling Flow Downstream of an Abrupt Axisymmetric Expansion," Ph.D. Dissertation, Arizona State University, 1986.

Present Investigation

Reynolds no.	Swirl no.	x_r/h
30,000	0	9.3
	.60	2.5
	.98	1.9
60,000	0	9.2
	.77	2.2
	1.16	1.8
100,000	0	9.0
	.74	2.2
	1.23	1.8

Investigator	method	media	β	Re (UD/ν)	$\frac{x_r}{h}$
Chaturvedi[3]	hot wire	air	.50	200,000	9.2
Freeman[9]	LDA	water	.48	63,000	8.8
Moon & Rudinger[14]	LDA	air	.70	280,000	8.8
Gould[12], Stevenson[13]	LDA	air	.50	90,000	8.6
Yang and Yu[11]	LDA	air	.37	53,000	9.2

TABLE 1. Reattachment Lengths

Re=30,000		Re=100,000
0 < S < .18	Vortex precesses in direction opposite to the mean swirl	0 < S < .12
S ≈ .18	Precession frequency goes to zero	S ≈ .12
.18 < S < .37	Vortex precesses in same direction as mean swirl	.12 < S < .40
S ≈ .37	The PVC vanishes	S ≈ .40
.37 < S < .50	Bubble-type vortex breakdown	.40 < S < .57
S ≈ .50	Transition from recirculating bubble to strong on-axis tube of recirculating flow	S ≈ .57
S > .50	Strong on-axis recirculation	S > .57

Table 2. Summary of Flow Regions

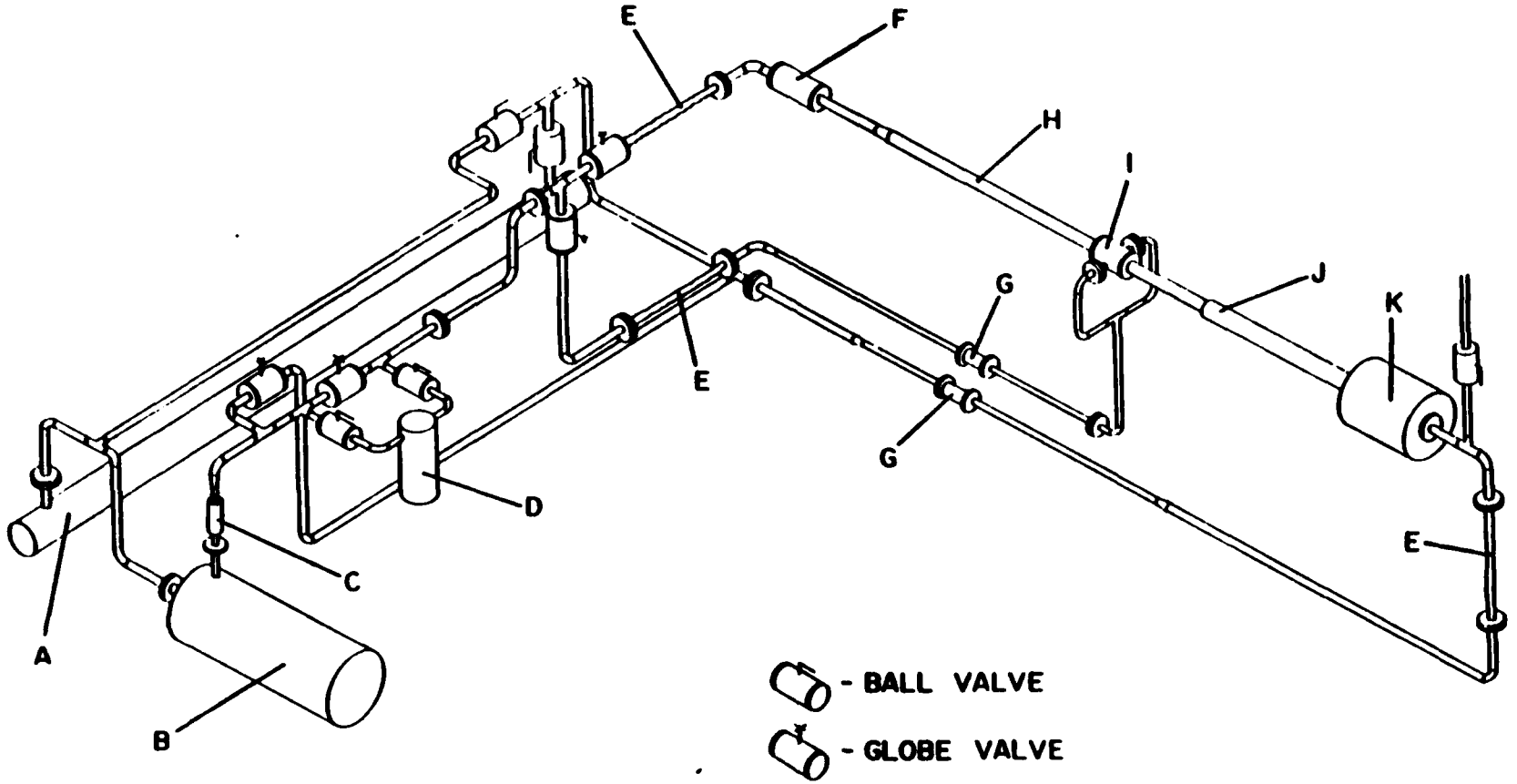

A- HEAT EXCHANGER
B- PUMP
C- CHECK VALVE
D- FILTER
E- FLEXIBLE PIPE
F- FLOW STRAIGHTENER
G- TURBINE FLOWMETER
H- DEVELOPING TUBE
I- SWIRL GENERATOR
J- TEST SECTION
K- MIXING CHAMBER

Figure 1. Schematic of Flow Loop

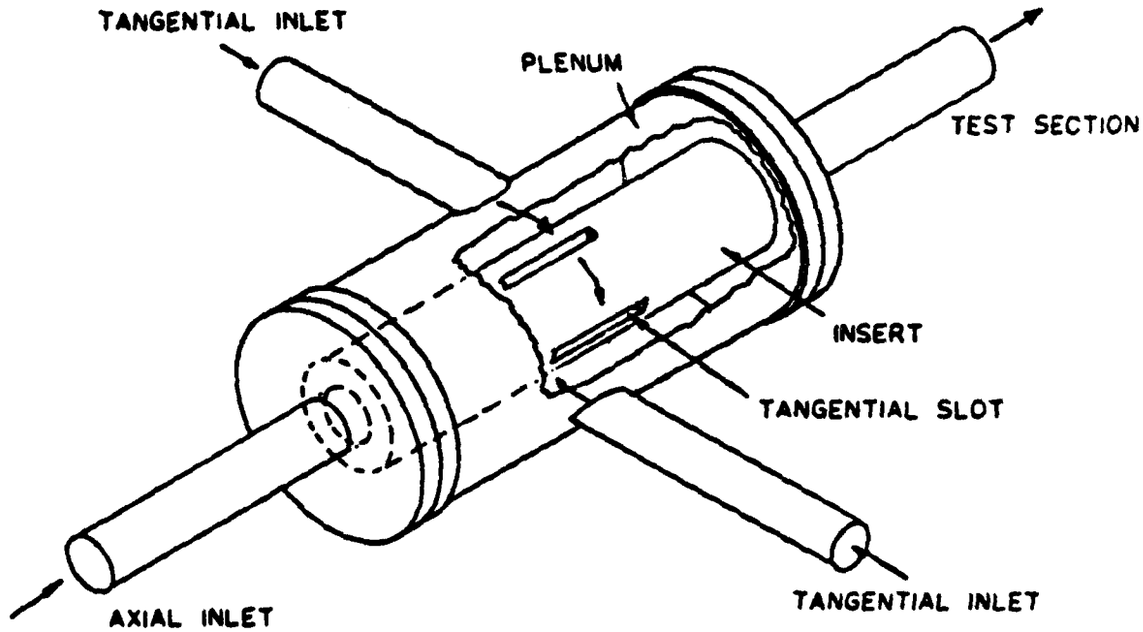

Figure 2. Detail of Swirl Generator

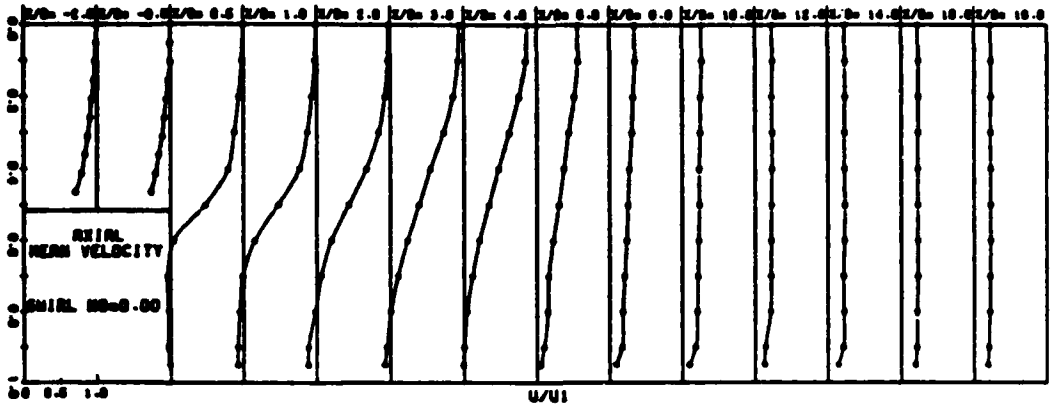

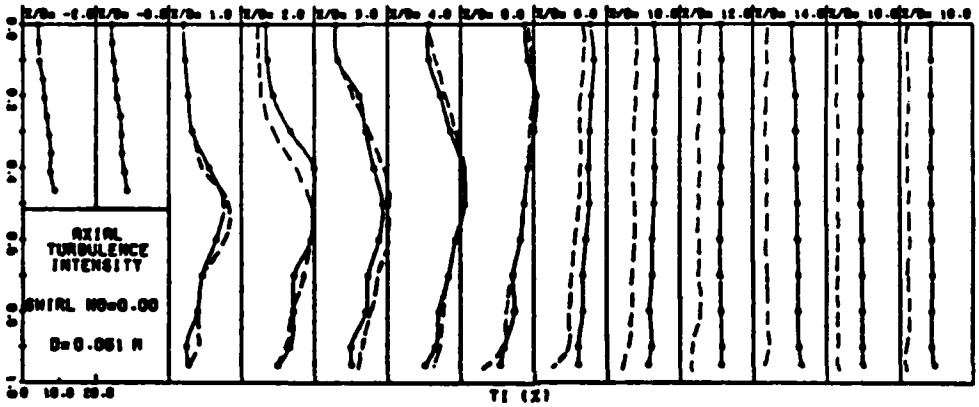

Re=30,000 Re=60,000 & 100,000

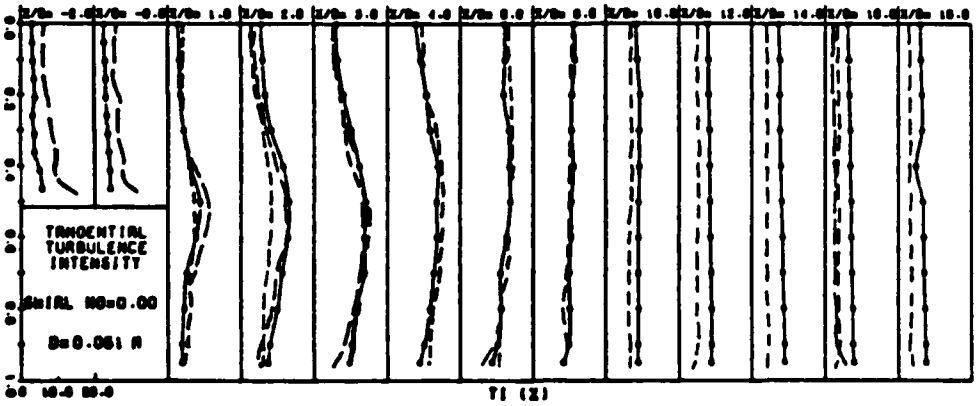

Re=30,000 Re=60,000 Re=100,000

Figure 3. Velocity Field; S = 0

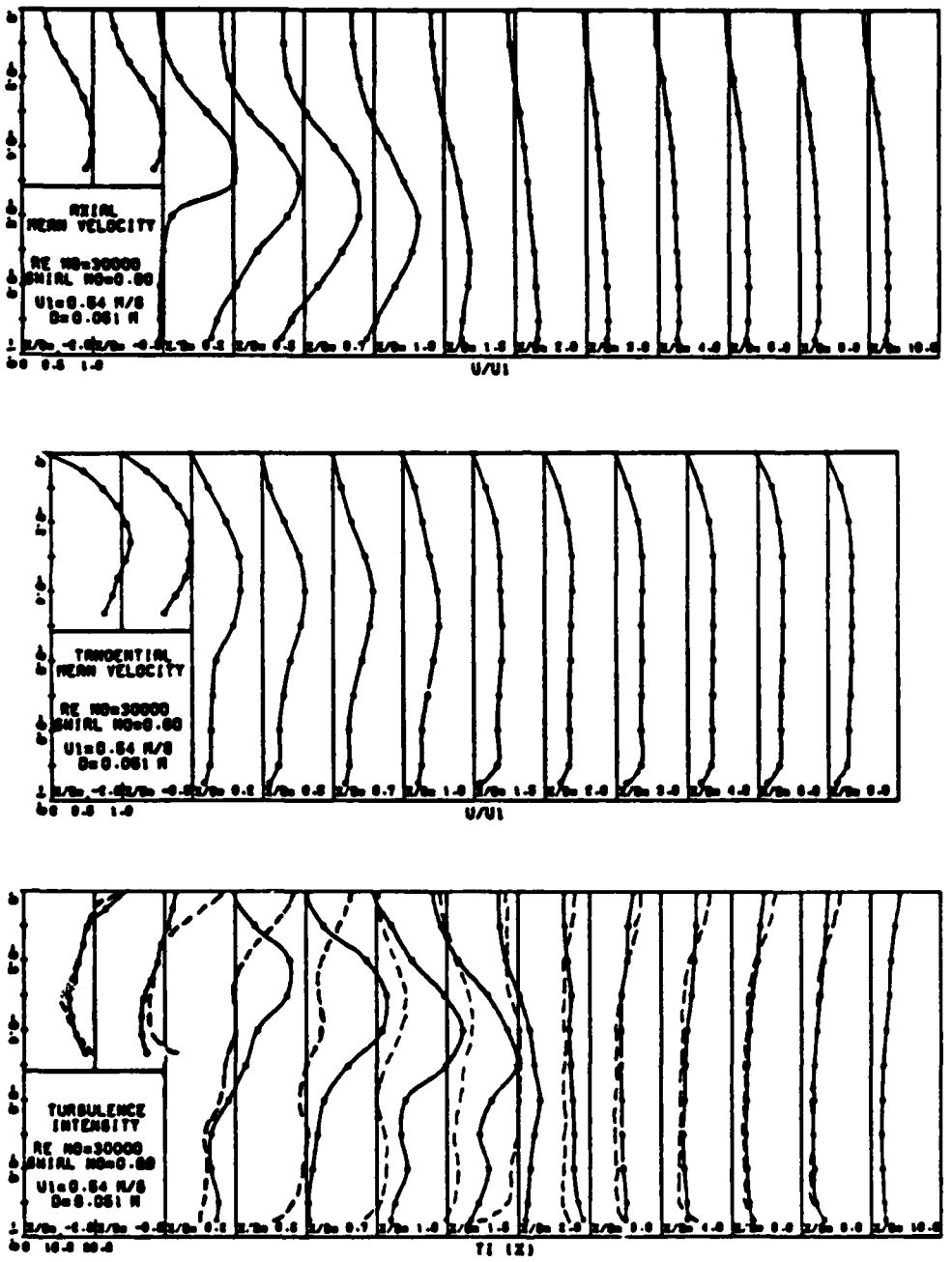

Figure 4. Velocity Field; Re = 30,000, S = .60

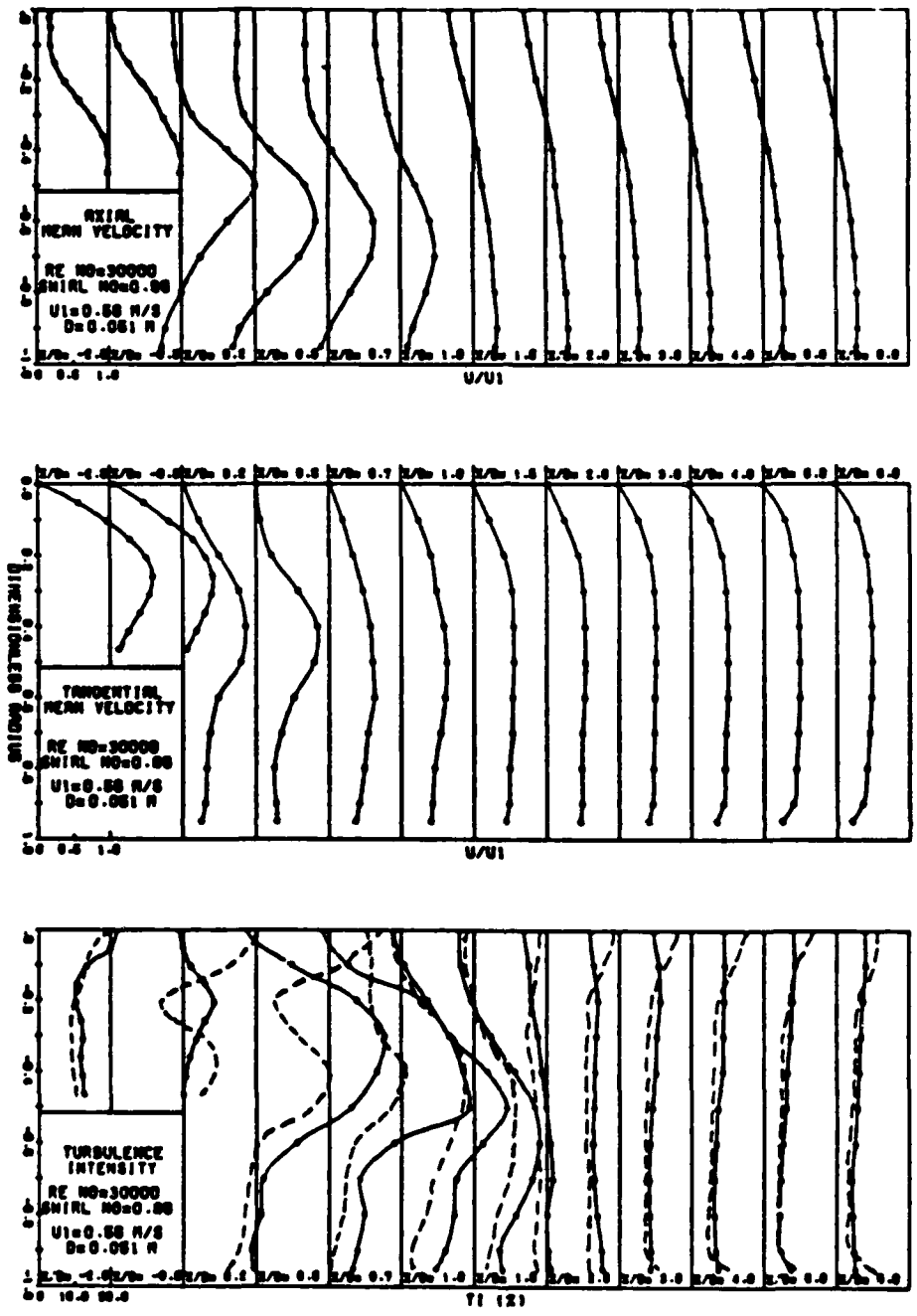

Figure 5. Velocity Field; Re = 30,000, S = .98

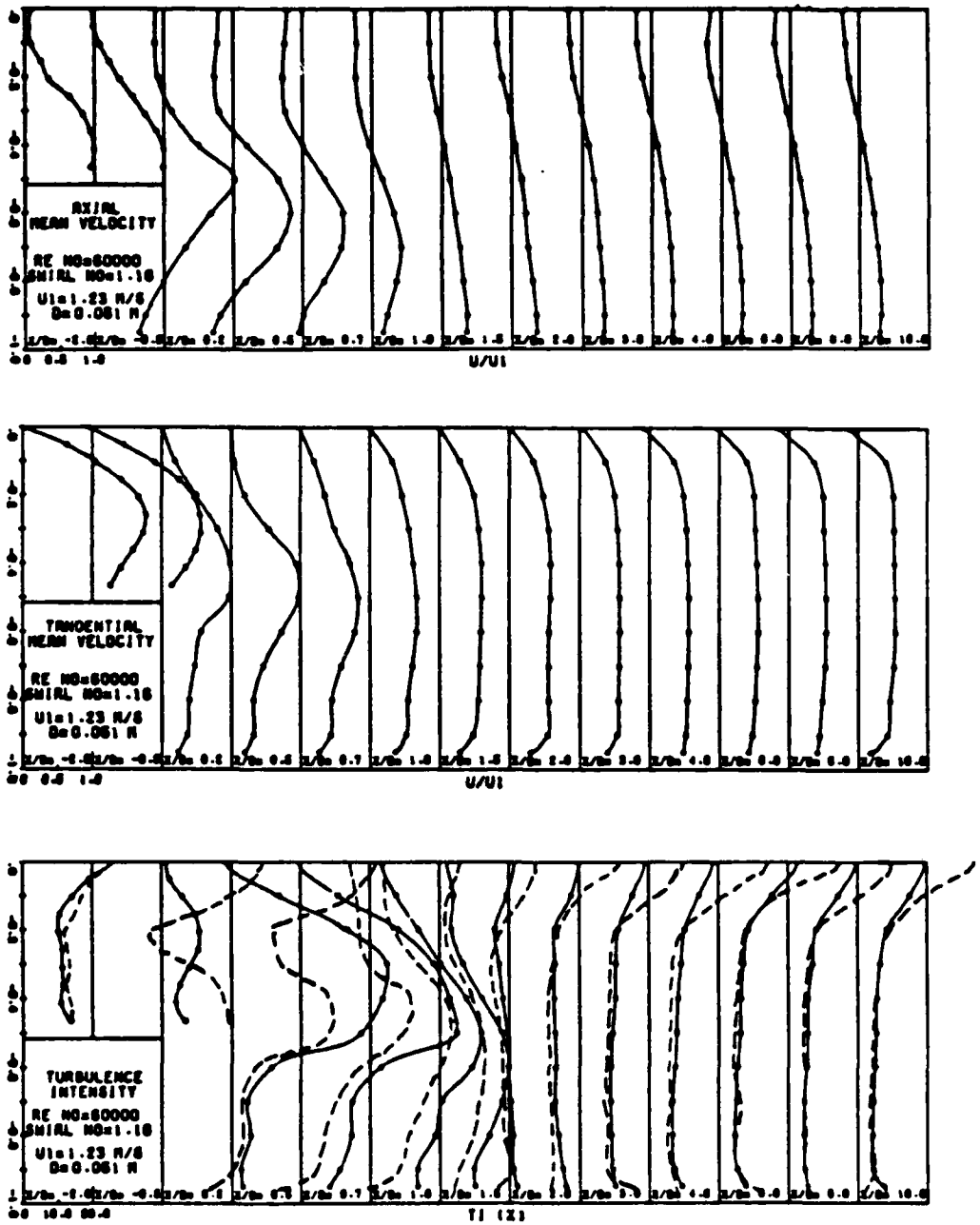

Figure 6. Velocity Field; Re = 60,000, S = 1.16

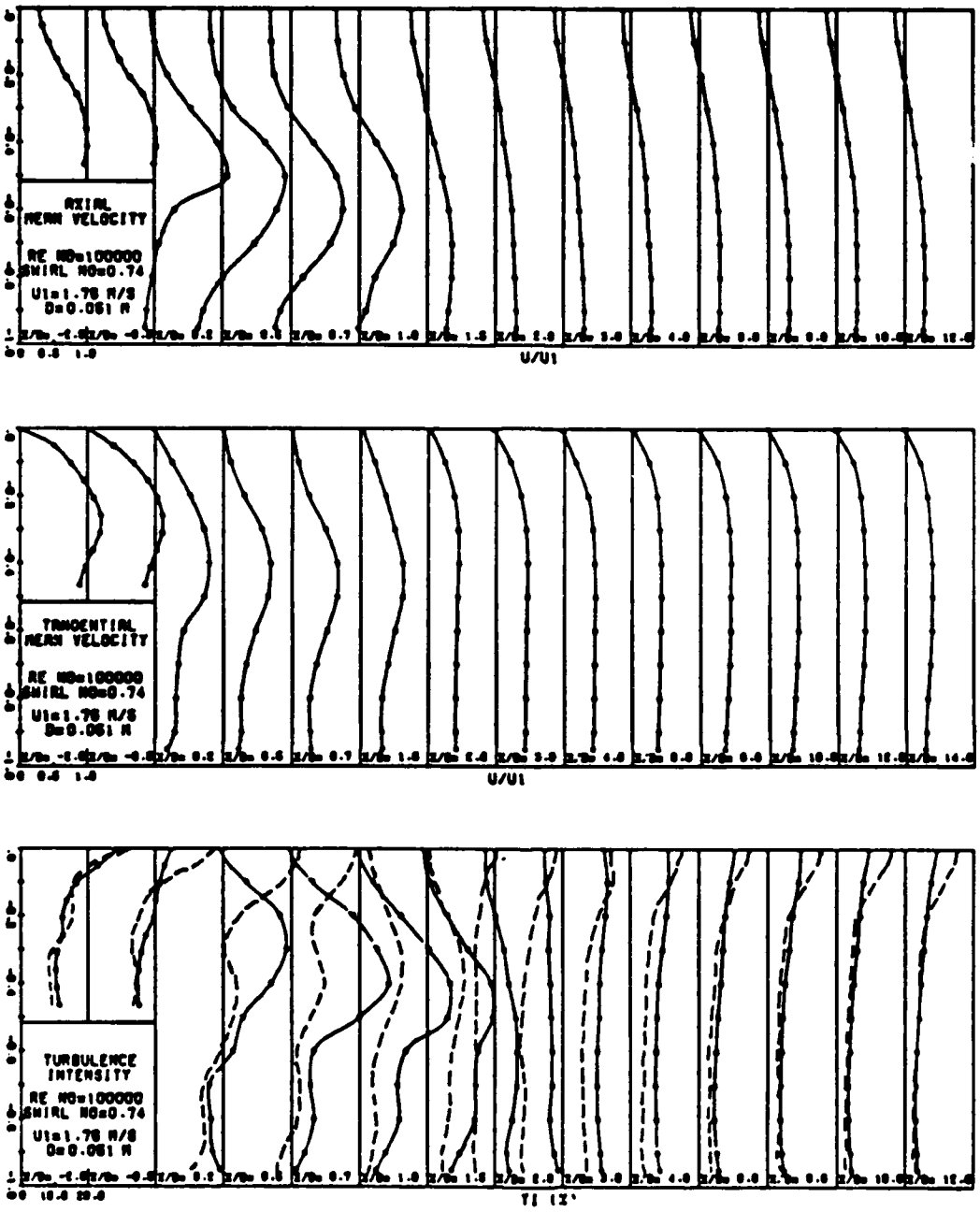

Figure 7. Velocity Field; Re = 100,000, S = .74

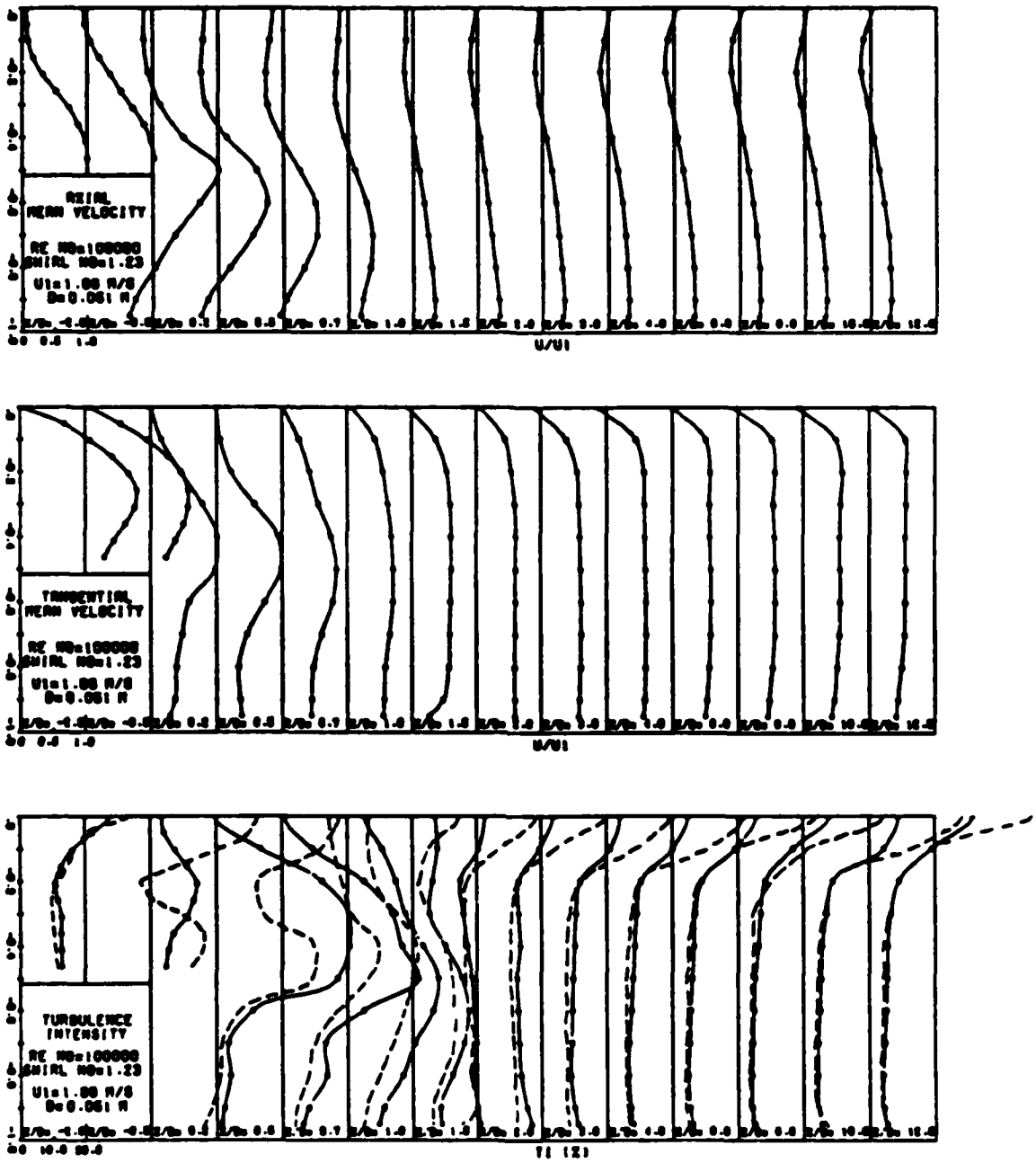

Figure 8. Velocity Field; Re = 100,000, S = 1.23

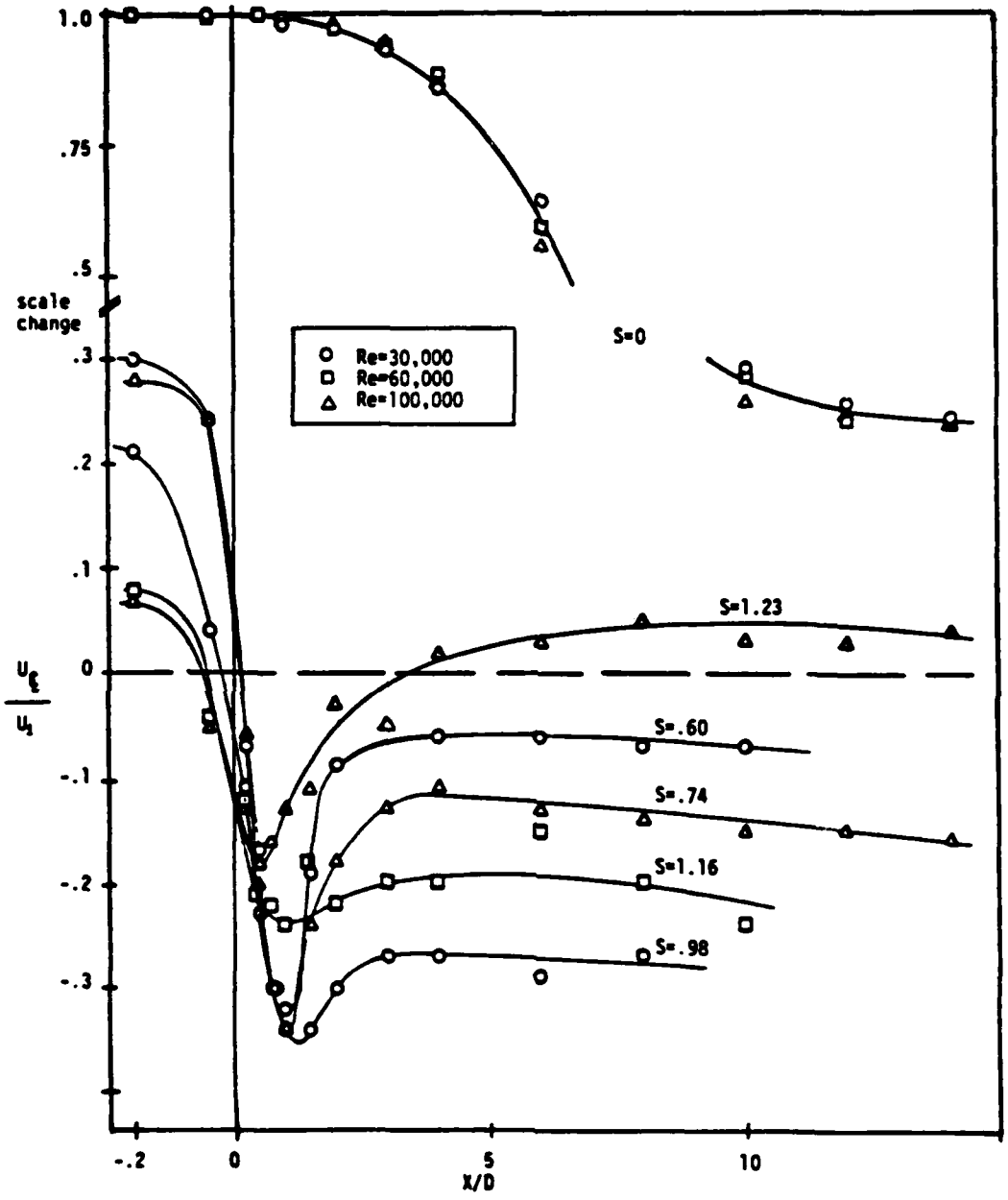

Figure 9. Centerline Velocities.

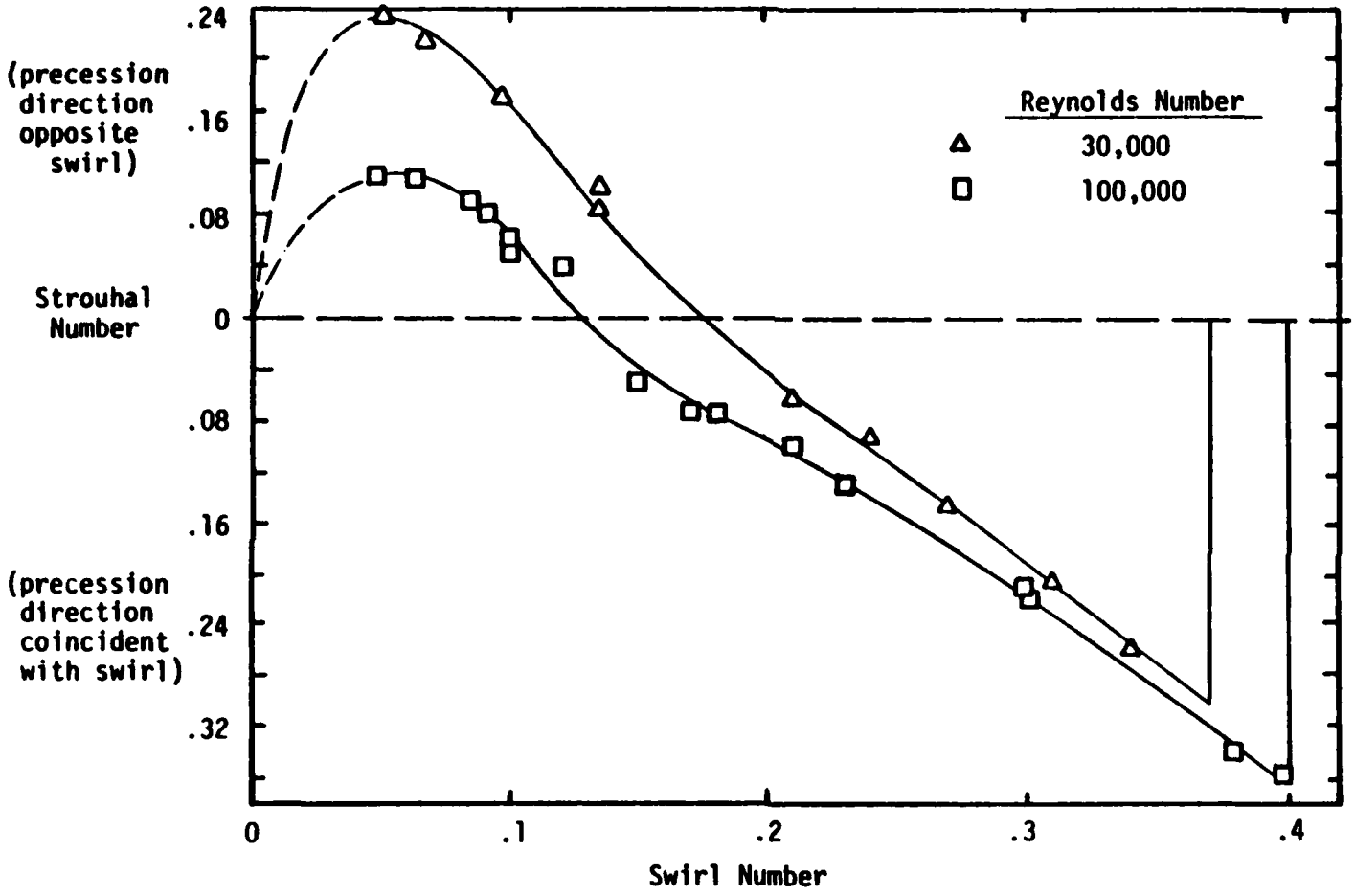

Figure 10. Variation of Strouhal Number with Swirl Number.

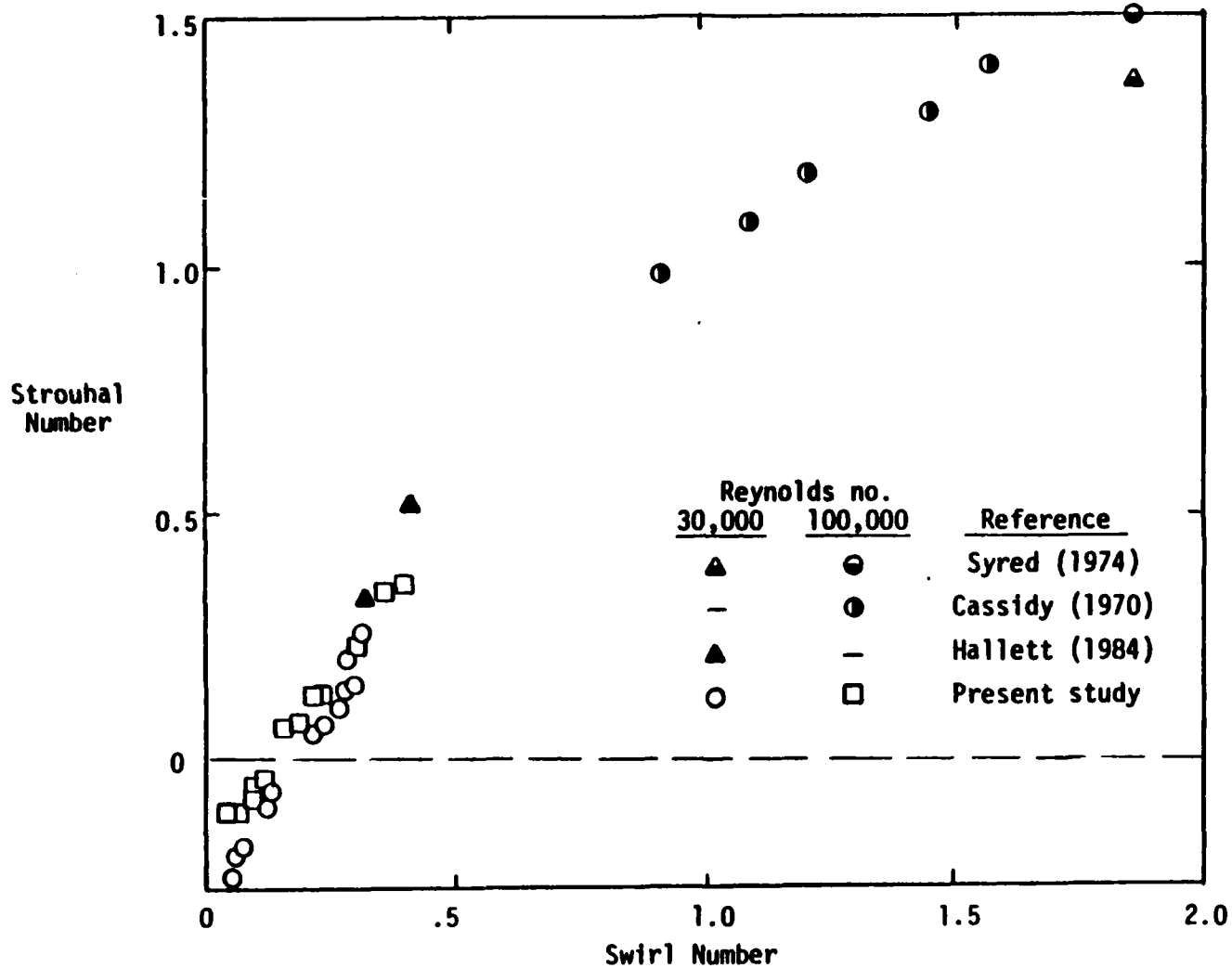

Figure 11. Relationship between Strouhal Number and Swirl Number (Various Experiments).

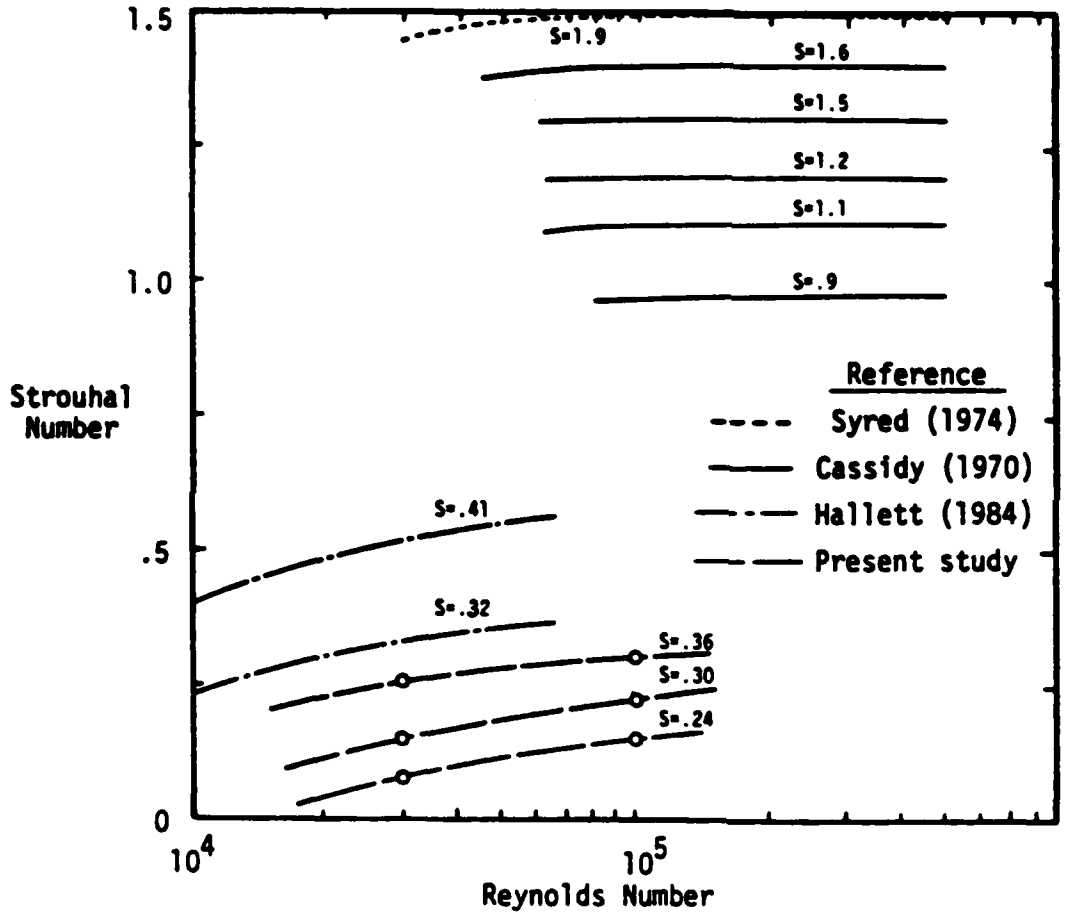

Figure 12. Relationship between Strouhal Number and Reynolds Number (Various Experiments).

END

9-87

DTIC